Magnetostrictie in elektrisch staal: numerieke modellering en ontwikkeling van een optische meetmethode

Magnetostriction in electrical steel: numerical modelling and development of an optical measurement method

Setareh Gorji Ghalamestani

Promotoren: Prof. dr. ir. Lieven Vandevelde, Prof. dr. ir. Jan Melkebeek en Prof. dr. Joris Dirckx
Proefschrift ingediend tot het behalen van de graad van
Doctor in de Ingenieurswetenschappen: Werktuigkunde-Elektrotechniek (UGent) en Doctor in de Wetenschappen (Universiteit Antwerpen)

Vakgroep Elektrische Energie, Systemen en Automatisering
Voorzitter: Prof. dr. ir. J. Melkebeek
Faculteit Ingenieurswetenschappen en Architectuur
Academiejaar 2013 – 2014

UNIVERSITEIT GENT

Magnetostriction in electrical steel: numerical modelling and development of an optical measurement method

Setareh Gorji Ghalamestani

Dissertation submitted to obtain the academic degree of
Doctor of Electromechanical Engineering and Doctor of Science

Publicly defended at Ghent University on December 19, 2013

Supervisors:

Prof. dr. ir. Lieven Vandevelde
Electrical Energy Laboratory, Department of Electrical Energy, Systems and Automation
Faculty of Engineering and Architecture, Ghent University
St.-Pietersnieuwstraat 41, B-9000 Ghent, Belgium

Prof. dr. ir. Jan Melkebeek
Electrical Energy Laboratory, Department of Electrical Energy, Systems and Automation
Faculty of Engineering and Architecture, Ghent University
St.-Pietersnieuwstraat 41, B-9000 Ghent, Belgium

Prof. dr. Joris Dirckx
Laboratory of Biomedical Physics
Faculty of Sciences, University of Antwerp
Groenenborgerlaan 171, B-2020 Antwerp, Belgium

Members of the examining board:

Prof. dr. ir. Rik Van de Walle (chairman)	Ghent University, Belgium
Prof. dr. ir. Patricia Verleysen (secretary)	Ghent University, Belgium
Prof. dr. ir. Lieven Vandevelde (supervisor)	Ghent University, Belgium
Prof. dr. ir. Jan Melkebeek (supervisor)	Ghent University, Belgium
Prof. dr. Joris Dirckx (supervisor)	University of Antwerp, Belgium
Prof. dr. Anouar Belahcen	Aalto University, Finland
Prof. Dr. -Ing. habil. Dr. h. c. Kay Hameyer	RWTH Aachen University, Germany
Prof. dr. ir. Johan Gyselinck	Université Libre de Bruxelles, Belgium

EELAB

ENGINEERING ARCHITECTURE

UNIVERSITEIT GENT

Universiteit Antwerpen

Acknowledgement

First of all, I wish to express my sincere gratitude to the promoters of my PhD Prof. Lieven Vandevelde and Prof. Jan Melkebeek. I would like to thank them for giving me the opportunity to do a PhD in the Electrical Energy Laboratory (EELAB). I always think of PhD as a "learning path". Their guidance helped me all the way through the accomplishment of this work, while I was given the freedom and the support to find my own way.

Prof. Lieven Vandevelde, I would like to thank you for all the discussions about the research and finite element calculations, which I learnt a lot from them. You always solved my computer problems with your magic commands, many thanks for that.

Prof. Jan Melkebeek, I am grateful for your scientific input and proofreading my articles and my PhD thesis. I wish to thank you for all your support to help me settle down in Belgium.

Many thanks to my promoter Prof. Joris Dirckx from the Laboratory of Biomedical Physics of University of Antwerp, who helped me with the development of the measurement setup with respect to the laser technique. Thank you for the quick answers to my questions.

The first four years, my research was funded with FWO (Research Foundation - Flanders, Project G.0011.08) in collaboration with the University of Antwerp and I gratefully acknowledge the financial support. I would like to thank again Prof. Jan Melkebeek for granting me the assistant position, which provided me the financial support during the last year of my PhD.

Furthermore, I wish to thank all the members of the examination board of my PhD: Prof. Rik Van de Walle, Prof. Patricia Verleysen, Prof. Anouar Belahcen, Prof. Johan Gyselinck and Prof. Kay Hameyer. Their valuable comments and suggestions improved the quality of this work.

The vibration measurements were performed at Vrije Universiteit Brussel (VUB). For that, I would like to deeply thank Prof. Patrick Guillaume from the Department of Mechanical Engineering.

I will not forget all my colleagues in EELAB during all these years. Thank you for the nice work atmosphere. I wish to thank Prof. Luc Dupre and Prof. Alex Van den Bossche for answering my questions when it crossed their field of expertise. Many thanks to dr. Tom Hilgert who shared with me his experience in the field of magnetostriction and magnetic measurements and helped me to start my PhD with building a new measurement setup. My research was a continuation of his PhD work. I really appreciate that he was always ready to help me with my questions and problems, even

after he left EELAB. I should also thank dr. Bart Meersman who helped me to prepare my transformer test setup and dr. Lode Vandenbossche and dr. Ben Van de Wiele who presented my work in the conferences when I could not attend. Special thanks to my officemates: dr. Ahmed Abdallh, dr. Damian Kowal, ir. Ahmed Hemeida and dr. Bertrand Itembe for all the technical discussions and experience sharing we had.

I am thankful to Stefaan Dhondt and Tony Boone for their assistance regarding the measurement setup and Nic Vermeulen for helping me with the computer problems. I would like to especially thank Ingrid Dubois and also Marilyn Van den Bossche for the administrative works.

I am grateful to my friends and I would like to thank them for all the good times we had together.

Last but certainly not the least, my deepest gratitude goes to my family for their unconditional support without which this work would not be possible. Many thanks to my mother Safoora, who has always been a constant source of love and energy. Special thanks to my sisters, my brothers in law and my nieces. My twin sister and my best friend Sepideh, although we are in two different countries, the distance could never make us apart. I wish you and Omid a lot of success in your PhDs. Akram, Elaheh, Raheleh, Hassan and Mahmoud many thanks for all your support and encouragement for all the years of my studies. Akram and Hassan, I will never forget your care, support and hospitality during my study in Norway.

Setareh Gorji Ghalamestani
Ghent, November 2013

Contents

Samenvatting

De geluidsproductie van transformatoren en elektrische machines is een vrij complexe materie. De diverse bronnen van dit geluid zijn het onderwerp geweest van talrijke studies. In dit werk wordt enkel de bijdrage van de magnetische kern tot de geluidsproductie behandeld. Meer bepaald worden de vervormingen en de trillingen van de kernen als gevolg van magnetische oorzaken bestudeerd. De berekening van het voorgebrachte geluid door deze trillingen valt niet meer binnen het bereik van dit werk.
De vervorming van een magnetische kern is te wijten aan twee verschijnselen die samen optreden: magnetische krachten en magnetostrictie. De bijdrage van de magnetische krachten wordt vaak uitgedrukt als het effect van een "externe" magnetische kracht op het magnetische materiaal. Anderzijds is de vervorming door magnetostrictie het gevolg van interatomaire interacties van het materiaal zelf door de aanwezigheid van een magnetisch veld.

Het uiteindelijke doel van het onderzoek is het beperken van de geluidsproductie van transformatoren en elektrische machines door middel van een optimalisatieprocedure. Er werd reeds een eindige-elemententechniek (EE) ontwikkeld voor tweedimensionale berekeningen van de vervorming van de magnetische kern, wat de focus is van dit werk. De ontwikkelde EE-techniek maakt gebruik van een continuumbeschrijving van het magnetische materiaal waarin zowel de lange-afstands magnetische krachtwerking als magnetostrictie in rekening worden gebracht. Hierbij worden "magnetostrictiekrachten" ingevoerd om de vervorming (rek) ten gevolge van magnetostrictie weer te geven. De methode maakt verder gebruik van de klassieke elastische vergelijkingen en voor de magnetische verschijnselen worden de Chu-formuleringen gebruikt. Terwijl het effect van de magnetische krachten analytisch kan berekend worden op basis van de magnetische velden, is er voor de bijdrage van magnetostrictie een model nodig voor het magnetostrictief gedrag van het materiaal dat experimenteel moet bepaald worden.

Voor de identificatie van het magnetostrictief gedrag van het kernmateriaal werd er een meetopstelling ontwikkeld tijdens dit werk. Hierbij wordt de tweedimensionale vervorming van een staal opgemeten in een Single Sheet Tester (SST). De focus van dit doctoraatsonderzoek ligt op transformatoren, waarvan de kernen bestaan uit

lamellen van elektrisch staal. De gebruikte materialen vertonen magnetostrictie in de grootte-orde van micrometer per meter. De meetopstelling meet de trillingssnelheid van een sample van een lamel door middel van laser-vibrometers. Na de signaalverwerking wordt de rek ten gevolge van magnetostrictie, d.i. de relatieve lengteverandering van het staal, berekend. De resultaten bekomen met deze opstelling worden vergeleken met deze bekomen met een eerder ontwikkelde opstelling met rekstrookjes. De laseropstelling levert een aantal voordelen op, zoals een hogere nauwkeurigheid, een eenvoudige voorbehandeling van het staal en de mogelijkheid om stalen met coating op te meten.

Voor wat gegevens over magnetostrictie in de literatuur betreft, wordt meestal een zuivere sinusodale magnetisatie verondersteld. Gezien de toepassing op transformatoren, is het nuttig de netspanningsgolfvorm in acht te nemen, die meestal hogere harmonischen bevat, voornamelijk als gevolg van niet-lineaire belastingen. Hierdoor is het noodzakelijk de invloed van deze harmonischen in de magnetisatie op het magnetostrictief gedrag te bestuderen. In dit werk tonen experimentele gegevens over het effect van de derde harmonische bij verschillende elektrische staalsoorten (georinteerde en niet-georinteerde) aan dat zowel de amplitude als de faseverschuiving van de hogere harmonische ten opzichte van de grondgolf een significante invloed hebben op de harmonischen in de magnetostrictie. Daarom moeten de harmonischen in de magnetisatie in rekening worden gebracht bij de identificatie van het magnetostrictief gedrag van de materialen. Daartoe werden de magnetostrictiemodellen die aangewend worden in de EE-berekeningen, die vroeger enkel magnetisatie met een grondgolf beschouwden, verbeterd om ook de effecten van de hogere harmonischen in de spanning (en dus in de magnetisatie) in rekening te brengen.

Aangezien er een model van het magnetostrictief gedrag van het materiaal nodig is in de EE-berekening, werd een dergelijk model gemaakt op basis van de metingen met de laseropstelling voor elk van de richtingen in het vlak van de lamellen. De modellering van de data wordt uitgevoerd met behulp van een artificieel neuraal netwerk (ANN). De inputs van het netwerk zijn de amplitude en de frequentie van de magnetische inductie B in het materiaal. Als er hogere harmonischen aanwezig zijn in de magnetische inductie, worden de amplitudes en de faseverschuivingen van deze hogere harmonische, ten opzichte van de grondgolf, hieraan toegevoegd als input. Het netwerk genereert de amplitude en de fase van de harmonischen van de magnetostrictieve rek. Eens het ANN is ontworpen, dient het getraind te worden met de opgemeten data van het beschouwde kernmateriaal.

De berekeningsmethode werd voorheen reeds toegepast om de vervorming van een driefasige transformatorkern te valideren gebaseerd op een magnetostrictiemodel bekomen met de meetresultaten van de opstelling met rekstrookjes. De vergelijking van de opgemeten en de berekende vervormingen leverde een onvoldoende overeenstemming op, te wijten aan de assemblage van de transformatorkern en de aanwezigheid van andere trillingsbronnen.
In dit werk wordt er een validering van een nfasige transformatorkern uitgevoerd bij

een puur sinusodale magnetisatie. De kern werd specifiek ontworpen om toe te laten enkel de magnetostrictieve rek te kunnen evalueren. De vervorming van de kern wordt berekend met de EE-methode en de resultaten worden vergeleken met die bekomen aan de hand van trillingsmetingen. De trillings- en vervormingsmetingen op de transformatorkern werden uitgevoerd met een laser-scanning vibrometer. De vergelijking tussen de berekende en de opgemeten data toont een relatief goede overeenkomst. De mogelijke oorzaak van bepaalde verschillen is te wijten aan het feit dat een tweedimensionale berekeningsmethode wordt gebruikt, waarbij de derde dimensie (loodrecht op het vlak van de lamellen) niet in rekening wordt gebracht. Het uitbreiden van de EE-techniek van een twee- naar een driedimensionale aanpak is n van de suggesties voor verder onderzoek.

Als een toepassing van de EE-berekeningsmethode, wordt het effect van de hogere harmonischen in de netspanning op de vervorming van een driefasige transformatorkern berekend. De berekeningen worden uitgevoerd met een 50Hz-grondgolf en een vijfde harmonische, aangezien deze vijfde harmonische de belangrijkste is in de netspanning van (Europese) netten. De modale trillingen bij verschillende vijfde harmonische componenten in de magnetisatie worden vergeleken met deze bekomen bij puur sinusodale magnetisatie. Hierbij is het verschil voor de 100Hz-component van de trillingen gering. De harmonische 200Hz-component toont echter een significante toename in het geval een vijfde harmonische aanwezig is in de aangelegde spanning. De aanwezigheid van zowel een 50Hz-grondgolf als een vijfde harmonische (250 Hz) genereert immers een 200Hz-harmonische in de magnetostrictieve rek (en in de magnetische krachtwerking).

Summary

The noise generation in transformers and electrical machines is a rather complex topic. There are different sources of this noise which have been the focus of many studies. In this work only the contribution of the noise generated in the magnetic core of the device is treated. More specifically, the vibrations and the deformation of the cores as a result of the magnetic noise sources are studied. The calculation of the ensued noise is not within the scope of this work. The deformation of a magnetic core is due to two phenomena: electromagnetic forces and magnetostriction, which occur together. The contribution of the electromagnetic forces is often expressed as the effect of an external magnetic source on the magnetic material. However, magnetostriction deformation is a result of the interatomic interaction of the core material itself in the presence of a magnetic field.

The final goal of this research is to reduce noise of transformers and electrical machines by means of an optimisation procedure. Focusing on the deformation of the magnetic cores, which is the scope of this work, a Finite Element (FE) technique has been developed in the past for a two-dimensional (2D) computation. Such technique considers a continuum description of the magnetic core material and takes into account both long-range magnetic forces and magnetostriction. A set of magnetostriction forces are introduced in order to generate the magnetostriction strains in the material. This method is mainly derived from basic elasticity equations and, for the magnetic phenomena, the Chu model formulations are applied. While the effect of the magnetic forces can be analytically computed, for the contribution of the magnetostriction strains a model of the magnetostrictive behaviour of the material is required, where the latter needs to be obtained experimentally.

To this end, for the identification of the magnetostrictive behaviour of the core material a measurement setup has been built during this work. The setup measures a 2D deformation of a sample in a Single Sheet Tester (SST) method. The focus of this PhD research is only on transformers, the cores of which consist of laminations of electrical steels. Such material shows magnetostrictive deformations in the order of micrometer per meter. The setup measures the vibrational velocity of a sample of electrical steel by means of laser vibrometers. After a signal post-processing the corresponding magnetostriction strains, i.e. the relative length change of the sample,

are calculated. The results obtained by this setup are compared with those obtained by a strain gauge setup which was developed in the past. The laser setup offers some advantages such as: higher accuracy, easy sample preparation and the possibility of measuring coated samples.

For the magnetostriction strains reported in the literature often a purely sinusoidal magnetisation is considered. Regarding the application in transformers, it is worthwile to consider the grid voltage which generally contains some higher harmonics, mainly due to nonlinear loads which are connected to it. Thus, information about the effect of such harmonics on the magnetostrictive behaviour is necessary. In this work, experimental data on the effect of the third harmonic on the magnetisation for different electrical steel materials, grain-oriented and nonoriented, showed that not only the amplitude but also the phase delay of the higher harmonic, with respect to that of the fundamental, can significantly change the harmonics of the magnetostriction strains. As a result, the harmonics on the magnetisation need to be taken into account for the identification of the magnetostriction strains. To this end, the FE method, which previously could only consider a magnetisation with a fundamental component only, has been improved to consider also the effects of the higher harmonics in the voltage (and thus in the magnetisation).

Since a model of the magnetostrictive behaviour of the core material is required for the FE computation, a model of the measurement results obtained by the laser measurement setup has been made for the magnetostriction strains in both directions in the plane of the sheets. The data modelling has been carried out with Artificial Neural Network (ANN). The network inputs are then the amplitude and frequency of the magnetic induction B in the material. If there are higher harmonics present on the magnetisation the amplitude and the phase delay of these higher harmonics, with respect to those of the fundamental harmonic, are the other inputs to the network. The network outputs are the magnitude and the phase of the harmonics of the magnetostriction strains. Once a network is designed it needs to be trained based on the measurement data of the given core material.

The computation technique was previously applied to validate the deformation of a three-phase transformer core based on a magnetostrictive model of the strain gauge setup measurement results. However, due to the assembly of the transformer core and the presence of other vibration sources the comparison of the measured and computed deformation did not show a satisfactory agreement.
In this work, a validation on a single-phase transformer core has been performed under a purely sinusoidal magnetisation. This core has a special design in order to make it possible to evaluate the magnetostrictive vibrations only. The core deformation has been computed by the FE technique and the results were compared with those obtained by the vibration measurements. The vibration and deformation measurements of the transformer core were performed by means of a laser scanning vibrometer. The comparison between the computed and experimental data showed quite good agreement. The possible reason for some differences is due to the 2D computational method,

which does not account for the third dimension of the core (perpendicular to the plane of the laminations). One of the suggested future works is improving the technique from a 2D to a three-dimensional (3D) approach.

As an application for the FE technique, the effect of the higher harmonics in the grid voltage on the deformation of a three-phase transformer core is computed. The calculations are performed for a sinusoidal voltage with a 50Hz frequency and a fifth harmonic component, since this fifth harmonic has the largest contribution in the European grid voltage. The modal vibrations under various magnetisations (viz with different fifth harmonic components) are compared with those obtained under a purely sinusoidal magnetisation and showed that the variations for the 100Hz harmonic of the vibrations are small. However, the 200Hz harmonic showed a significant increase when a fifth harmonic was present on the applied voltage. In fact, the presence of a fundamental component with 50Hz frequency and a fifth harmonic on the magnetisation signal generates a 200Hz harmonic on the magnetostriction strains (and the magnetic forces), and thus this harmonic increases significantly.

List of Abbreviations

2D	Two-Dimensional
3D	Three-Dimensional
ANN	Artificial Neural Network
BOP	biopolar
DAQ	Data-acquisition
DC	Direct Current
EDM	Electrical Discharges Machines
EELAB	Electrical Energy Laboratory (Ghent University)
FE	Finite Element
FFNN	Feed Forward Neural Network
FFT	Fast Fourier Transform
FM	Frequency Modulated
IEC	International Electrotechnical Comission
IFFT	Inverse Fast Fourier Transform
IVS	Industrial Vibrometer Sensor
LDV	Laser Doppler Vibrometer
SST	Single Sheet Tester
VUB	Free University of Brussels (Vrije Universiteit Brussel)

List of Symbols

General notations

- A: scalar
- $\overline{A}$: vector
- $\overline{\overline{A}}$: tensor
- $\langle 100 \rangle$: indices of family of crystallographic directions

Mathematical symbols

$.$	scalar product
$\times$	cross product
$\nabla .$	divergence
$\nabla \times$	curl
$:$	contracted product
$\ddot{x}$	second order derivative
$[\dots]$	matrix

List of symbols-Greek letter

α_i	direction cosines of magnetisation M, relative to the three cubic crystal axes (i=1,2,3) []
β_i	direction cosines of saturation magnetostriction λ_s, relative to the three cubic crystal axes (i=1,2,3) []
γ_i	direction cosines of uniform tensile stress σ, relative to the three cubic crystal axes (i=1,2,3) []
μ_0	magnetic permeability of vacuum [H/m]
ρ_{m}	magnetic charge density [Wb/m^3]
ρ	mass density [kg/m^3]
λ_{laser}	laser wavelength [m]
λ	magnetostriction strain []
λ_0	spontaneous magnetostriction []
λ_s	saturation magnetostriction []
λ_{100}	saturation magnetostriction of a cubic single crystal, magnetised along a $\langle 100 \rangle$ direction []
λ_{111}	saturation magnetostriction of a cubic single crystal, magnetised along a $\langle 111 \rangle$ direction []
$\lambda_{\parallel}$	magnetostriction strain in the direction parallel to the magnetisation direction []
$\lambda_{\perp}$	magnetostriction strain in the direction perpendicular to the magnetisation direction []
θ	angle [rad]
σ	stress [Pa]
ν	Poisson's ratio []
ε	strain []
ϕ	magnetic flux [Wb]
ω	angular velocity [rad/s]
Ψ	mode shape [m]

List of symbols-Roman letter

a	acceleration [m/s^2]
A	cross section area [m^2]
B	magnetic induction [T]
C	capacitance [F]
e	spontaneous strain []
E	Young's elasticity modulus [Pa]
$\overline{\overline{E}}$	elasticity tensor [Pa]
E_{ani}	anisotropy energy [J]
E_{exch}	exchange energy [J]
E_{MS}	magnetostatic energy [J]
E_{me}	magnetoelastic energy [J]
E_{a}	externally applied magnetic field (Zeeman) energy [J]
E_{G}	Gibbs free energy [J]
f	frequency [Hz]
$\overline{f}$	force density [N/m^3]
G	shear modulus [Pa]
H	magnetic field [A/m]
I	current [A]
J	current density [A/m^3]
k	stiffness [Nm^{-1}]
K_i	ith order anisotropy constant [J/m^3]
K_{GF}	gauge factor []
k_{p}	linear control variable []
l	geometrical quantity, length [m]
L	inductance [H]
M	mass [kg]
$\overline{M}$	magnetisation [A/m]
$\overline{n}$	normal vector []
N	torque [Nm]
r	position [m]
R	resistance [Ω]
t	time [s]
$\overline{\overline{T}}_{\mathrm{mf}}$	magnetic stress tensor [Pa]
$\overline{\overline{T}}_{\mathrm{ms}}$	magnetostriction stress tensor [Pa]
$\overline{\overline{T}}$	stress tensor []
u	displacement [m]
u_{f}	free energy density [J/m^3]

u_{mag}	magnetostatic energy density [J/m^3]
u_{mstr}	magnetostriction energy density [J/m^3]
u_{el}	magnetoelastic energy density [J/m^3]
v	velocity [m/s]
V	voltage [V]
W	work [J]
$w_{\mathrm{i,j}}$	weight factor of the ith neuron in the jth layer []

List of Publications

Articles in the Web of Science

1. S. Gorji Ghalamestani, T. Hilgert, L. Vandevelde, J. Dirckx, and J. Melkebeek "Magnetostriction measurement by using dual heterodyne interferometers," *IEEE Transactions on Magnetics*, vol. 46, no. 2, pp. 505-508, 2010.

2. S. Gorji Ghalamestani, L. Vandevelde, J. Dirckx, and J. Melkebeek "Magnetostriction and the influence of higher harmonics in the magnetic field," *IEEE Transactions on Magnetics*, vol. 48, no. 11, pp. 3981-3984, 2012.

3. S. Gorji Ghalamestani, L. Vandevelde, J. Dirckx, and J. Melkebeek "Magnetostrictive vibrations model of a three-phase transformer core and the contribution of the fifth harmonic in the grid voltage," *accepted for publication in the Journal of Applied Physics*.

4. S. Gorji Ghalamestani, L. Vandevelde, J. Dirckx, P. Guillaume and J. Melkebeek "Magnetostrictive Deformation of a Transformer: a Comparison Between Calculation and Measurement," *accepted for publication in the International Journal of Applied Electromagnetics and Mechanics*.

5. S. Gorji Ghalamestani, L. Vandevelde, J. Dirckx, and J. Melkebeek "Magnetostriction strain measurement and its application for the numerical deformation calculation of a transformer," *accepted for publication in the International Journal of Numerical Modelling: Electronic Networks, Devices and Fields*.

6. S. Gorji Ghalamestani, T. Hilgert, S. Billiet, L. Vandevelde, J. Melkebeek, and J. Dirckx "Measurement of magnetostriction using dual heterodyne interferometers: experimental challenges and preliminary results," *Optical Measurement Techniques for Systems & Structures*, J. Dirckx and J. Buytaert (Eds.), Shaker Publishing, ISBN 978-90-423-0366-9, 4th International conference on Optical Measurement Techniques for Systems and Structures (OPTIMESS 2009),

pp. 171-180, 2009.

7. S. Gorji Ghalamestani, L. Vandevelde, J. Dirckx, and J. Melkebeek "Magnetostriction and the advantages of using noncontact measurements," *AIP conference proceedings*, vol. 1253, 9th International ccnference on Vibration Measurements by Laser and Noncontact Techniques, pp. 171-175, 2010.

8. S. Gorji Ghalamestani, L. Vandevelde, J. Dirckx, and J. Melkebeek "Magnetostriction strain measurement: heterodyne laser interferometry versus strain gauge technique," *Optical Measurement Techniques for Systems & Structures*^{2}, J. Dirckx and J. Buytaert (Eds.), Shaker Publishing, ISBN 978-90-423-0419-2, 5th International conference on Optical Measurement Techniques for Systems and Structures (OPTIMESS 2012) pp. 167-174, 2013.

Articles in conference proceedings (not included in Web of Science)

1. S. Gorji Ghalamestani, L. Vandevelde, J. Dirckx, and J. Melkebeek "Magnetostriction measurement and the contribution of magnetostriction to the noise of a one-phase transformer," *5th International Conference on Magnetism and Metallurgy Proceedings*, pp. 272-276, Ghent, Belgium, 20-22th June, 2012.

Conference abstracts

1. S. Gorji Ghalamestani, L. Vandevelde, J. Dirckx, and J. Melkebeek "Magnetostriction measurements on electrical steel and the effect of coating," *11th International Workshop on 1&2 Dimensional Magnetic Measurements and Testing*, Oita, Japan, 3-6th November, 2010.

2. S. Gorji Ghalamestani, L. Vandevelde, J. Dirckx, and J. Melkebeek "Magnetostriction and the influence of higher harmonics in the electricity grid," *IEEE International Magnetics Conference*, p. 161, Vancouver, Canada, 7-11th May, 2012.

3. S. Gorji Ghalamestani, L. Vandevelde, J. Dirckx, and J. Melkebeek "Magnetostriction and its contribution to the noise of a one-phase transformer," *12th International Workshop on 1&2 Dimensional Magnetic Measurements and Testing*, pp. 43-44, Vienna, Austria, 3-6th September, 2012.

List of attended conferences/workshops with a presentation

1. OPTIMESS2009, 4th International Conference on Optical Measurement Techniques for Structures & Systems, Antwerp, Belgium, May 2009.

2. SMM19, Soft Magnetic Materials Conference, Torino, Italy, September 2009.

3. AIVELA, 9th International Conference on Vibration Measurements by Laser and Noncontact Techniques, Ancona, Italy, June 2010.

4. 1&2DM, 11th International Workshop on 1&2 Dimensional Magnetic Measurements and Testing, Oita, Japan, November 2010.

5. MMM, 55th Annual Magnetism and Magnetic Materials Conference, Atlanta, GA, November 2010.

6. OPTIMESS2012, 5th International Conference on Optical Measurement Techniques for Structures & Systems, Antwerp, Belgium, April 2012.

7. INTERMAG, International Magnetic Conference, Vancouver, Canada, May 2012.

8. WMM12, 5th International Conference Magnetism and Metallurgy, Ghent, Belgium, June 2012.

9. 1&2DM, 12th International Workshop on 1&2 Dimensional Magnetic Measurements and Testing, Vienna, Austria, September 2012.

10. EMF2013, 9th International Symposium on Electric and Magnetic Fields, Bruges, Belgium, April 2013.

MAGNETOSTRICTION IN ELECTRICAL STEEL: NUMERICAL MODELLING AND DEVELOPMENT OF AN OPTICAL MEASUREMENT METHOD

CHAPTER 1

Introduction

1.1. Rationale of the work

The growing world population and increased urbanisation have resulted in more concentrated living areas. The urbanisation growth has brought the industrial areas closer to the residential areas. As a result, everyday lives of people have been subject to many changes. One of the consequences is suffering the industrial noise, e.g. noise of electrical machines and transformers, which has gained more attention during the past years. Focusing on transformers, they are essential for the transmission and distribution of electricity to households. More transformers have been placed in the residential areas to provide them with electricity. However, the unwanted audible noise of transformers worsens the life quality of the neighbours. The generation of this noise and the contributing sources have been the focus of many studies, e.g. [1], [2], [3] and [4].

In essence, transformers consist of a wound core which is physically protected inside a tank. However, the transformer construction is an extensive topic e.g. with respect to the choice of the core material, the assembly of the core and the windings pattern [5]. This work only focuses on transformers the cores of which are stacks of laminations of ferromagnetic materials, specifically electrical steel. Further on in this chapter, only the noise sources of the aforementioned transformer type will be presented.

Transformer noise sources

Noise of a transformer is generated by different sources. A schematic depiction of the different noise sources is shown in Fig. 1.1. The total noise of a transformer is contributed by three main groups: aerodynamic, magnetic and winding noise.

- The **aerodynamic noise** originates from the cooling system of the device. In large transformers the installation of a fan is required which generates a low frequency noise.

- The **windings noise** is a result of the Lorentz force acting on the winding conductors which is proportional to the vector product of the magnetic induction B and the current I in the winding conductors.

- The **magnetic noise** refers to the noise generated in the ferromagnetic core of the transformer. The noise in the core is itself produced as a result of the electromagnetic forces and magnetostriction, which will be described in chapter 2.

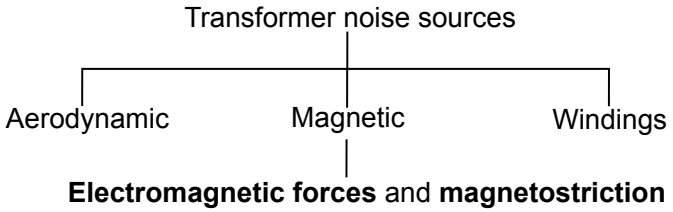

Figure 1.1: A schematic of the noise sources in a transformer.

The noise generation in a transformer is in reality more complicated. The aforementioned noise sources cause a force which results in pulsating vibrations of the core. Based on the mechanical structure of the core, these vibrations result in the deformation and ensue audible acoustic noise. Regarding the mechanical structure of the core, for instance the total generated noise can be amplified by the transformer tank. If the dominant frequency of the vibrations of the core of the transformer coincides with the natural frequencies of the metal plates of the tank, the noise radiation will be considerably increased. In the construction of transformers, the transformer designers attempt to decrease the noise in different ways, e.g. the followings

- Lowering the magnetic induction B (1.2T instead of 1.7T-1.85T) decreases the generated magnetic noise. Once the transformer works at a lower magnetic induction B (1.2T instead of 1.7T-1.85T) the noise generation decreases.

- The geometry and the dimensions of the core may activate the natural frequencies of the core. A suitable geometry can lower the noise significantly.

- If the core design is strong and stiff, the noise radiation may decrease.

- To lower the noise of the tank, a damping pad is inserted between the core of the transformer and the tank bottom [5].

The magnetic noise of transformers is of interest to us. Since the electromagnetic forces can be calculated, the magnetostriction of electrical steels and its consequences do interest us. Magnetostriction refers to the change in the dimensions of ferromagnetic alloys due to a change in their magnetisation. As a result of the magnetostriction, the core of a transformer is subjected to pulsating distortions, which cause noise. Several studies have focused on the magnetostriction noise of transformers and electrical machines, as it is one of the main noise sources e.g. [6], [7], [8] and [9].

1.2. Motivations and goals

The ultimate goal of this research is to reduce noise of transformers. In order to do so, an optimization procedure is required to modify transformers to reach an optimal design. To this end, first different noise sources and their contributions to the total noise should be well identified. Regarding the deformation of transformer cores, which results in vibrations and the magnetic noise, a computation technique has been developed in the past at the Electrical Energy Laboratory (EELAB) of Ghent University. Such technique needs a model of the magnetostrictive behaviour of the transformer core material. This model is based on the results of the magnetostriction strain measurements of the samples of the core material.

To this ends, a magnetostriction strain measurement setup has been developed in the past which was based on strain gauge technique. To overcome the limitation of this strain gauge setup, i.e. inability to measure the behaviour of coated samples, and achieve a higher measurement accuracy there was a motivation for a new measurement setup. This new setup, which has been developed during this PhD work, is based on laser technique.

The computation technique has been validated for a test transformer core. In the past, the technique could only calculate the deformations under a magnetisation with a fundamental harmonic component. The method has been improved in order to calculate deformations under a magnetisation with higher harmonic components.

1.3. Overview of the work done

Here a short overview of the content of the following chapters will be presented.

In chapter 2, first the magnetisation process of ferromagnetic materials is presented. Different energy terms and the equilibrium state based on the minimisation of the free energy are discussed. Further on, the magnetostriction phenomenon is explained both from the microscopic and macroscopic point of view. For the computation of the deformation of the magnetic cores due to the magnetic sources, the formulation based on the Chu model is applied. Thus, this model is further described in this chapter.

The model description requires a model of the magnetostrictive behaviour of the core material. Such behaviour is experimentally obtained by means of measurement

techniques. In chapter 3, first a short literature overview of the existing magnetostriction measurement setups is presented. Thereafter, the magnetostriction strain measurement setups which have been developed at EELAB will be presented. The strain gauge setup, which was developed in the past, and its advantages and drawbacks will be explained. After that, the new magnetostriction strain measurement setup, which is based on the laser technique, will be concisely presented. The development of this new setup and programming the controlling software have been all carried out during this PhD work.

In chapter 4 first the measurement results obtained by the new setup on samples of grain-oriented and nonoriented electrical steel under a purely sinusoidal magnetisation will be presented. Next, a comparison between the measured results obtained by the laser setup and those with the strain gauge setup will be made. Since in reality some higher harmonics are present on the electricity grid, the effect of of such harmonics on the magnetostrictive deformation needs to be identified. To this end, measurements are performed under a sinusoidal magnetisation once with a third and once with a fifth harmonic component which had different amplitudes and phase delays with respect to the fundamental harmonic component. The obtained results will be presented in this chapter.

Since the goal of this PhD work is calculating the deformation of the transformer cores due to the magnetic sources, i.e. electromagnetic forces and magnetostriction, a computation technique is applied. Such technique, which is based on a 2D FE method, has been developed in the past. The contribution of the electromagnetic forces can be calculated based on analytical expressions. However, for the deformation due to the magnetostriction a model of the magnetostrictive behaviour of the material is required for the calculations. Such models are made by using Artificial Neural Network (ANN) based on the magnetostriction strain measurement results obtained by the laser setup. In chapter 5 an overview of the FE technique and the ANN modelling will be presented.

In chapter 6 a validation of the FE computation technique will be presented. In the past, an attempt was made to compute the deformation of a three-phase transformer core by using the aforementioned method. The vibrations of the same core were then measured and the obtained deformation was compared with the computed results. However, the validation was not successful and the results were not analogous. In this work, a new validation has been performed for a single-phase transformer core, for which the results showed rather good agreement. The design of this new test transformer and the validation, the computation versus the measurement, will be thoroughly presented in chapter 6.

In chapter 7, an application for the FE computation technique is presented. The influence of the higher harmonics of the grid on the magnetostrictive deformation of the transformer cores is of interest to us. To this end, the deformation of a three-phase transformer core is computed by using the FE technique under a magnetisation with a fifth harmonic component. Different amplitudes and phase delays of the fifth harmonic

are studied, with respect to the fundamental harmonic. The results are then compared with those under a purely sinusoidal magnetisation.

In the final chapter, chapter 8, a conclusion of the work is drawn. In addition, a few suggestions for the future research are made.

CHAPTER 2

Magnetostriction and magnetic forces

2.1. Introduction

In this chapter a theoretical background will be provided on the magnetisation of ferromagnetic materials with a focus on magnetostriction and electromagnetic forces. First a short overview of the micromagnetism of ferromagnetic materials will be presented in order to help the understanding of the magnetisation and magnetostriction process. After that, the macroscopic effect of magnetostriction will be presented. At the end, the continuum description of magnetoelastic materials based on the Chu model formulation will be presented. Such description is later applied in a technique for the computation of the deformation of magnetic cores as a result of electromagnetic forces and magnetostriction, which were discussed in chapter 1. The technique to compute the deformation will be presented in chapter 5.

2.2. Microscopic magnetisation

Atoms in a ferromagnetic material are arranged in a crystalline structure. A crystal lattice of iron is shown in Fig. 2.1. In the iron lattice, there are three preferred magnetisation directions which are the easy $\langle 100 \rangle$, medium $\langle 110 \rangle$ and hard $\langle 111 \rangle$ directions. They refer to the orientations along the edge of the lattice basis cell, the plane and space diagonal respectively. Once a uni-directional magnetic field H is applied, the magnetisation along one of the easy directions requires rather low magnetic filed. The magnetisation along the medium directions requires relatively larger magnetic field. The magnetisation along the hard directions requires even a larger magnetic field.

In fact, the ferromagnetic materials are formed once the material cools down below the Curie point. At temperatures higher than the Curie point, the magnetic moments

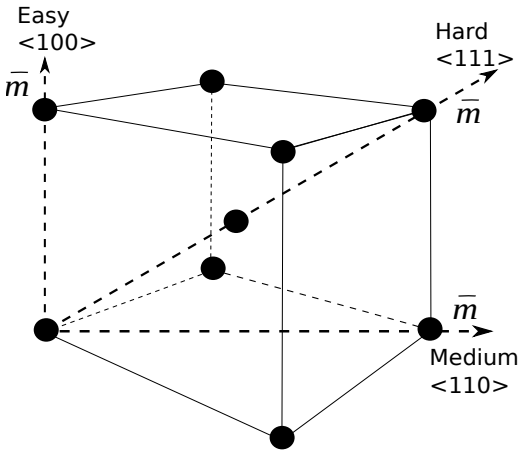

Figure 2.1: A cubic crystal lattice of iron with indication of easy, medium and hard magnetisation directions for which low, medium and large magnetic fields are required respectively.

inside the material are completely randomly aligned and the material is paramagnetic. However, when it is cooled down below the Curie temperature, the material spontaneously divides into many small regions called magnetic domains and becomes ferromagnetic. Each ferromagnetic material has a different Curie temperature (e.g. for pure iron 770°C). To explain the formation of the magnetic domains, we first need to discuss the competing energy terms at the microscopic level.

Minimisation of the free energy

In general, the total energy of a ferromagnetic material is called the Gibbs free energy E_{G}, which is a contribution of the following energy terms: exchange energy E_{exch}, anisotropy energy E_{ani}, magnetostatic energy E_{MS}, magenetoelastic energy E_{me} and externally applied magnetic field energy (Zeeman energy) E_{a}.

$$E_{\mathrm{G}} = E_{\mathrm{exch}} + E_{\mathrm{ani}} + E_{\mathrm{MS}} + E_{\mathrm{me}} + E_{\mathrm{a}} \tag{2.1}$$

This total energy depends on the magnetisation state of the material and always attempts to find an equilibrium state with a minimum energy value. The presence of a magnetic field, external stress or a temperature variation unbalances the equilibrium state. Therefore, the domain structure of the material is subjected to a change in order to reach a new equilibrium. A brief overview of the different energy terms will be given here but for a more detailed study we refer to [10], [11] and [12].

- **Exchange energy** E_{exch}
  The exchange energy is a result of the interaction between neighbouring magnetic

dipoles. For the ferromagnetic materials a parallel alignment of the neighbouring dipoles is energetically favoured.

- **Anisotropy energy** E_{ani}
  As shown in Fig. 2.1, the ferromagnetic materials have preferred crystallographic directions and any other directions are thus energetically unfavourable. The anisotropy at the magnetic moment scale means that the atomic magnetic moments preferably align with one of the easy crystallographic directions and the energy needed to do so is called the anisotropy energy. The anisotropy energy is caused by the magnetic moments which are not aligned along the crystallographic easy direction. Such energy per unit volume for iron alloys, which have a cubic lattice with three easy directions, can be described as follows

$$E_{\text{ani}}(\bar{r}) = K_1(\alpha_1^2(\bar{r})\alpha_2^2(\bar{r}) + \alpha_2^2(\bar{r})\alpha_3^2(\bar{r}) + \alpha_3^2(\bar{r})\alpha_1^2(\bar{r})) + K_2(\alpha_1^2(\bar{r})\alpha_2^2(\bar{r})\alpha_3^2(\bar{r})), \tag{2.2}$$

  where α_{i} $(i = 1,2,3)$ is the local magnetisation with respect to the crystallographic direction of the material ($\alpha_1 = \cos(\overline{M},\langle 100\rangle)$, $\alpha_2 = \cos(\overline{M},\langle 010\rangle)$ and $\alpha_3 = \cos(\overline{M},\langle 001\rangle)$). The K_1 and K_2 are the first and second order anisotropy constants. For 3% silicon iron K_1 is large and positive which as a result forces all domains to be parallel to the $\langle 100\rangle$ direction under low and medium magnetisation[1].

- **Externally applied magnetic field (Zeeman energy)** E_{a}
  In the presence of an applied (external) magnetic field $\overline{H}(\bar{r})$ the magnetisation of a magnetic moment changes. The energy consequently released can be calculated as follows

$$E_{\text{a}}(\bar{r}) = -\mu_0 \overline{H}(\bar{r}).\, \overline{M}(\bar{r}), \tag{2.3}$$

  where $\overline{M}(\bar{r})$ is the local magnetisation vector. In fact, if there was only the Zeeman energy, the magnetisation direction of the material would completely align with the applied magnetic field.

- **Magnetostatic energy** E_{MS}
  Magnetostatic energy refers to the energy of a magnetic moment as a result of the magnetic field produced by all the other magnetic moments. Regardless of the space variation of the energy, based on the Maxwell's equations, the following is valid

$$E_{\text{MS}}(\bar{r}) = -\frac{1}{2}\sum_{i=1}^{N} \mu_0 \overline{M}_{\text{i}}(\bar{r}).\overline{H}_{\text{MS,i}}(\bar{r}), \tag{2.4}$$

[1] It corresponds to the regions up to the knee of the B-H loop of the magnetisation shown in Fig. 3.15.

where $\overline{H}_{\mathrm{MS,i}}(\bar{r})$ is the magnetic field of the other magnetic moments on the i magnetic moment. This energy is analogous to the Zeeman energy except for the factor of $\frac{1}{2}$. Since the magnetostatic energy is a mutual term, the $\frac{1}{2}$ factor is required in order to calculate the energy between each two dipoles only once. The dipole field can be driven from

$$\overline{\nabla}.\overline{H}_{\mathrm{MS}} = -\overline{\nabla}.\overline{M} = \rho_{\mathrm{m}}, \tag{2.5}$$

$$\overline{\nabla} \times \overline{H}_{\mathrm{MS}} = 0, \tag{2.6}$$

where ρ_{m} is the fictitious magnetic charge density caused by the $\overline{M}$ varying in space. In fact, for the formation of the magnetic domains a pattern with the lowest magnetostatic energy level is formed. As shown in Fig. 2.2(a), there is a single domain material and large stray fields are introduced in the surrounding air. In Fig. 2.2(b) and 2.2(c), the formation of domain walls are shown (with dotted lines) which separates one domain in two and four parallel domains. Thus, instead of a uni-directional domain with a large stray field, parallel domains with lower energies are formed separated by 180° domain walls. These domain walls are in fact the boundaries where the magnetic moments change their direction and alignment. Fig. 2.2(d) and 2.2(e) show the formation of the closure domains, which eliminates the stray fields outside the domains. The emergence of the closure domains happens early in the domain formation process and disappears rather late in the saturation process. Such a pattern is energetically favoured and is in agreement with reaching the minimum energy. The closure domains have 90° domain walls and thus the field follows a closed path inside the domains. The 180° and 90° domain walls and how the direction of the magnetisation is at these walls are shown in Fig. 2.3. Because of the cubic lattice structure of the material, the 180° and 90° domain walls ensure the magnetisation along one of the easy directions [13].

- **Magnetoelastic energy** E_{me}
  Magnetoelastic refers to the interaction between the magnetic and the elastic properties of the ferromagnetic materials. The magnetostriction and magnetomechanic phenomena both belong to the magnetoelastic properties of the material. From macroscopic point of view, while the magnetostriction refers to the deformation of the material in presence of a magnetic field, the magnetomechanical effect is the reverse effect. In another word, in response to the application of external mechanical stress to a ferromagnetic material, not only the deformations happen but also a change of the magnetisation state occurs. In general, the magnetoelastic energy E_{me} is a contribution of both external stress and internal factors. We limit us here to the definition of the magnetomechanical effect. More about it will be given in relation to the macroscopic aspect and external stress effect. The magnetostriction phenomenon will be thoroughly studied in the following sections.

As all different contributing factors to the total energy have been discussed, we can now consider the total energy. The equilibrium state of the material is the result of this

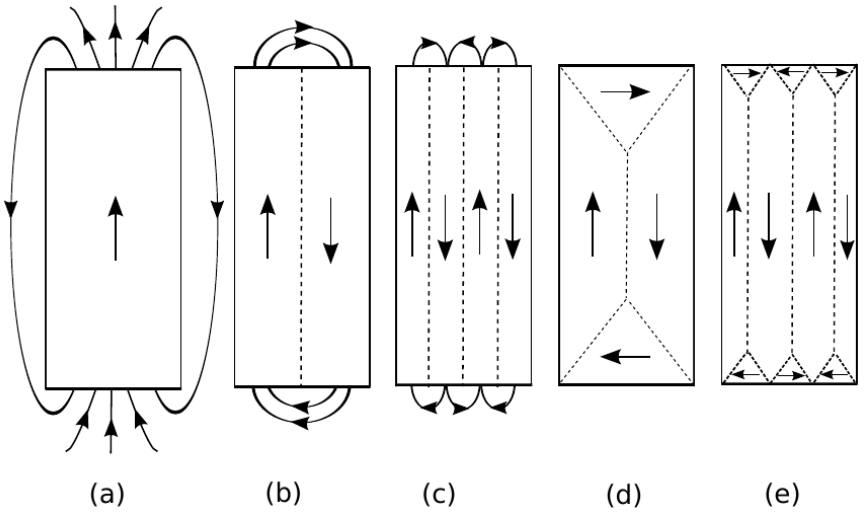

Figure 2.2: The formation of the magnetic domains with the aim of the minimum energy level (a) the formation of a uniformly magnetised domain with large stray fields (b) formation of a 180° domain wall which separates the single domain in two anti-parallel domains and decreases the stray field and the magnetostatic energy (c) appearance of more 180° and smaller domains (d) elimination of the stray fields out of the domain and formation of the closure domains with 90° domain walls (e) further formation of the closure domains which is energetically favourable.

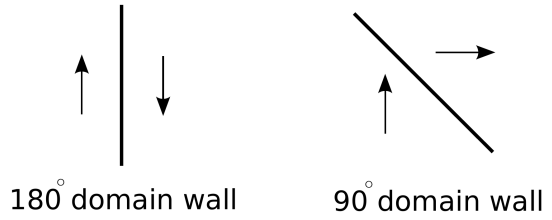

Figure 2.3: The 180° and 90° domain walls and the magnetisation direction.

total energy, as reported in (2.1). There is a trade off among all different contributing energy terms and they are balanced with each other in a way to make sure that the total free magnetic energy is minimum. Every change such as a variation in the external applied magnetic field, external applied stress or temperature disturbs the balance and results in a change of these factors. Thus, once again all the energy terms compete with each other to reach a new balance and keep the total energy minimum. In short, we assume that $\overline{H}_{\text{eff}}$ is the sum of the fields that stands for all the micromagnetic

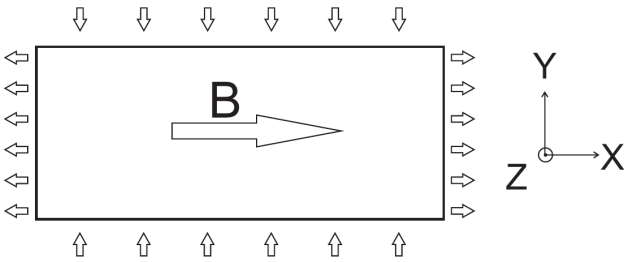

Figure 2.4: A two-dimensional magnetostriction strains of a sample of ferromagnetic material and the coordinate system, representing the elongation along the magnetisation direction and the shrinkage perpendicular to that.

interactions in the material

$$\overline{H}_{\text{eff}} = \overline{H}_{\text{exch}} + \overline{H}_{\text{ani}} + \overline{H}_{\text{MS}} + \overline{H}_{\text{me}} + \overline{H}_{\text{a}}. \tag{2.7}$$

The minimal Gibbs free energy states are the magnetic configurations where in each point of the material the micromagnetic torque $\overline{N}$ is zero, which is defined as

$$\overline{N} = \mu_0 \overline{M} \times \overline{H}_{\text{eff}}. \tag{2.8}$$

A positive value of torque $\overline{N}$ implies that there is a driving force to a new micromagnetic state equilibrium. For a detailed description we refer to [10].

2.3. Magnetostriction and microscopic behaviour

As mentioned in the §1.1, in general the magnetisation of ferromagnetic materials is accompanied by changes in their dimension, which is known as magnetostriction. The magnetostriction phenomenon was first discovered by Joule in 1842 when he was able to demonstrate the deformation of an iron bar when magnetised [14].

Under low and medium fields the magnetisation of the sample is only followed by a three-dimensional deformation without any volume changes. A two-dimensional deformation of a sample is shown in Fig. 2.4, where the sample elongates along the magnetisation direction and shrinks in the perpendicular direction. The magnetostriction strain λ in one direction is defined as follows, where l_0 is the original length of the sample in that direction and l is the length of the magnetised sample

$$\lambda = \frac{\triangle l}{l_0} = \frac{l - l_0}{l_0}. \tag{2.9}$$

A two-dimensional approach is taken throughout this work to measure the magnetostriction strains parallel and perpendicular to the applied magnetic field (for which hereafter the notations $\lambda_{\parallel}$ and $\lambda_{\perp}$ will be used).

As a result of magnetostriction not only the material is deformed, which is a macroscopic effect, but also the microscopic structure of the material undergoes changes. Here, first the microscopic effect on the domain structure of the material will be presented and thereafter the macroscopic effect will be discussed. Looking at the microscopic behaviour, there are two types of magnetostriction, the so-called spontaneous magnetostriction and the field-induced magnetostriction.

Spontaneous magnetostriction

The spontaneous magnetostriction λ_0 of the material refers to the instant when the temperature descends below the Curie point. This is in fact when the material becomes ferromagnetic and the magnetic domains are formed. Due to the spontaneous magnetisation, a sudden magnetostriction strain λ_0 occurs. The direction of the spontaneous magnetisation varies from domain to domain while the bulk magnetisation in total stays zero. Fig. 2.5(a) shows a spherical volume of unstrained anisotropic solid above the Curie temperature which is in fact paramagnetic. In Fig. 2.5(b), the spontaneous magnetostriction is presented which is when the material is ferromagnetic but not magnetised. For isotropic material, the spontaneous strain e with an angle of θ with respect to the magnetisation direction can be written as follows

$$e(\theta) = e\ \cos^2(\theta), \tag{2.10}$$

The average spontaneous magnetostriction λ_0 is the sum of the spontaneous magnetostriction of the domains throughout the material

$$\lambda_0 = \int_{-\pi/2}^{\pi/2} e\ \cos^2(\theta)\ \sin(\theta)\ d\theta = e/3. \tag{2.11}$$

Field-induced magnetostriction

The field-induced magnetostriction is directly linked with the magnetisation of the material. In a cubic material, in demagnetized state, the different domains are randomly aligned along the easy directions ($\langle 100\rangle$,$\langle 010\rangle$,$\langle 001\rangle$) (equally the same in every direction) and thus the resultant magnetization of the material as a whole is zero. When low and medium magnetic fields are applied, the domains which their magnetisation is energetically in favour with the field, grow in volume at the expense of the less favourably oriented neighbours.

In the case of polycrystalline iron the magnetostriction-field curve is divided into three regions, as shown in Fig. 2.6. In zone 1 the domains which their magnetising direction corresponds to the external field direction grow at the expense of domains of

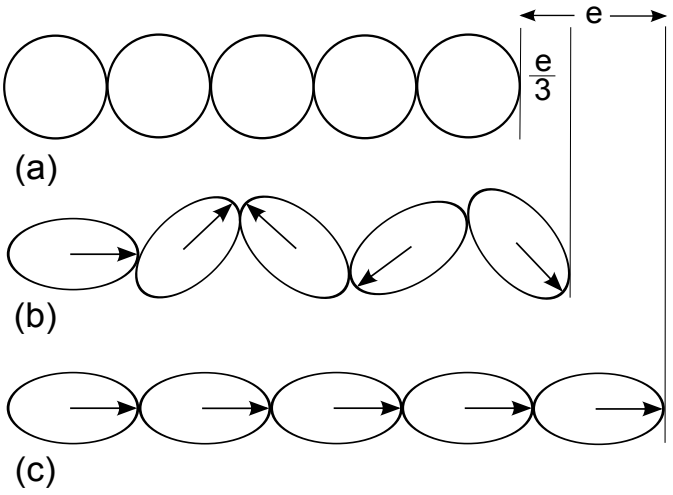

Figure 2.5: A schematic diagram of a ferromagnetic material in (a) above the Curie temperature with a disordered regime or paramagnetic properties (b) the ferromagnetic regime with ordered domains but unaligned with respect to the applied magnetic field (c) in the ferromagnetic regime magnetised to saturation with ordered and completely aligned domains with respect to the applied magnetic field [15].

which the magnetising direction is not completely aligned with the external field. This implies that the boundaries will move. Then also the magnetostriction of these domains will change. On the B-H curve of the material, which is shown in Fig. 3.15, this boundary movement represents the magnetization states corresponding to the instep and the knee of the curve.

With a further increase of the magnetic field strength, when the boundary displacements are almost complete, a gradual contraction begins, as shown in Fig. 2.6, zone 2. In fact, now a rotation mechanism of the domains becomes dominant and the atomic magnetic moments, aligned along an easy direction rotate from their original direction of magnetization into the field direction. The contraction of the material continues until the rotation mechanism is complete and the magnetisation saturation and consequently the magnetostriction saturation are reached.

In the zones 1 and 2, the volume of the material remains constant. However, further increase of the magnetic field causes a volume increase of the material accompanied by an expansion which is the same in all directions, as shown in Fig. 2.6, zone 3. The volume magnetostriction is observed in the presence of very large fields which are not within the focus of this work [16], [17]. Back to the saturation magnetisation state, the corresponding magnetostriction saturation λ_s might be compared with the case of the

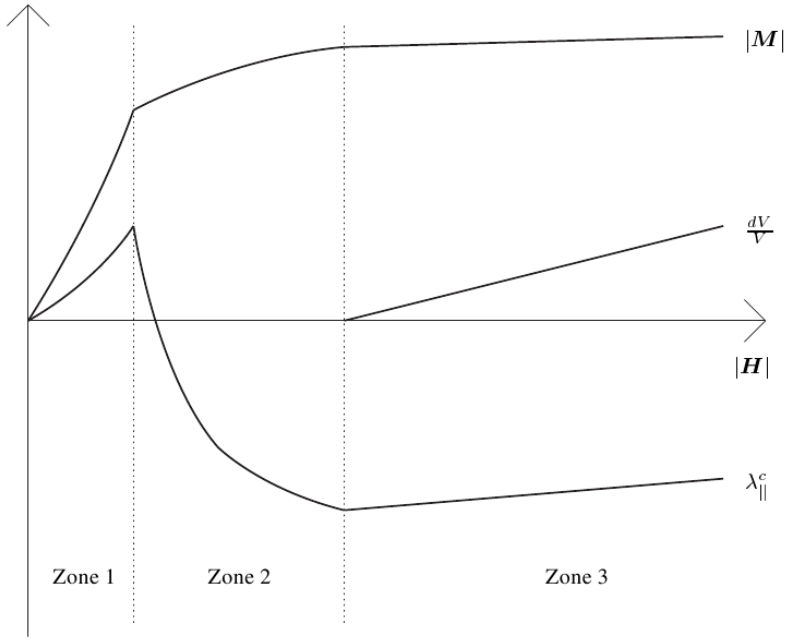

Figure 2.6: Diagram of magnetisation, linear magnetostriction (parallel to the magnetisation direction) and volume magnetostriction of iron as a function of applied magnetic field H where zone 1 represents the boundary movement of the domains (up to almost 800 A/m), zone 2 represents the domain rotation (800-8000 A/m) and zone 3 represents the volume magnetostriction (fields higher than 8000 A/m) [17], [18].

demagnetised ferromagnetic state as follows

$$\lambda_s = e - \lambda_0 = \frac{2}{3}e. \tag{2.12}$$

The saturation magnetostriction of an isotropic material is shown Fig. 2.5(c), where all the domains are completely aligned with the applied magnetic field (M is parallel with H). In general, the saturation magnetostriction for an isotropic material with an angle θ to the field direction is calculated as

$$\lambda_s(\theta) = \frac{3}{2}\lambda_s(\cos^2(\theta) - \frac{1}{3}), \tag{2.13}$$

where λ_s is the saturation magnetostriction along the direction of the magnetisation. (2.13) assumes a polycrystalline material with no preferred orientation of the crystal axes. However, for a single crystal structure the saturation magnetostriction should be defined in relation to the crystal axis along which the magnetisation lies. The satura-

tion magnetostriction in single domain, single crystal cubic materials is then given by a generalised version of (2.13)

$$\lambda = \frac{3}{2}\lambda_{100}(\alpha_1^2\beta_1^2 + \alpha_2^2\beta_2^2 + \alpha_3^2\beta_3^2 - \frac{1}{3}) \\ +3\lambda_{111}(\alpha_1\alpha_2\beta_1\beta_2 + \alpha_2\alpha_3\beta_2\beta_3 + \alpha_3\alpha_1\beta_3\beta_1), \tag{2.14}$$

where λ_{100} is the saturation magnetostriction measured along the $\langle 100 \rangle$ direction and λ_{111} is the saturation magnetostriction along the $\langle 111 \rangle$. The direction cosines relative to the field direction in which the saturation magnetostriction is measured are β_1, β_2 and β_3. α_1, α_2 and α_3 are the direction cosines of the axis, relative to the field direction, along which the magnetic moments are saturated.

2.3.1 Grain-oriented versus nonoriented electrical steel

Electrical steels are iron-silicon alloys with enhanced magnetic properties, such as small hysteresis loss and high permeability. The percentage of silicon is often up to 3.2%, since a higher silicon concentration provokes brittleness. Electrical steels can be divided in two groups according to their production process, i.e. nonoriented and grain-oriented steel. A representation of their domain structure in the demagnetised state for the domains inside material and not at the surface is shown in Fig. 2.7. Only the main magnetisation directions are shown without the closing domains for the sake of simplicity. Since the domain structure in the demagnetised state is shown, the average magnetisation is zero[2].

Fig. 2.7(a) gives a representation for nonoriented material which is isotropic and has the same magnetic characteristics in every direction. This type of material is preferred for applications where a rotational magnetic flux is required, such as in electrical machines. For grain-oriented material, the grains are favoured in the rolling direction which is therefore a preferred magnetisation direction, see Fig. 2.7(b). It turns out that the $\langle 100 \rangle$ direction of most grains are approximately parallel to the rolling direction of the material as shown in Fig. 2.8. These materials, which are thus anisotropic, are preferred for applications which require a uni-directional magnetisation, e.g. transformer cores.

2.3.2 Stress effect

External stress

For a single crystal of a cubic ferromagnetic material, the magnetostriction strain has been presented in (2.14). If a uniform tensile stress σ is applied to a cubic ferromagnetic material, the resulting magnetoelastic energy due to the external stress $E_{\mathrm{me}_{\mathrm{ext}}}$ is

[2] It is assumed that there is no remanence magnetic induction B. Once again, the magnetisation $\overline{M}$ of all the domains are always aligned with the easy magnetisation directions.

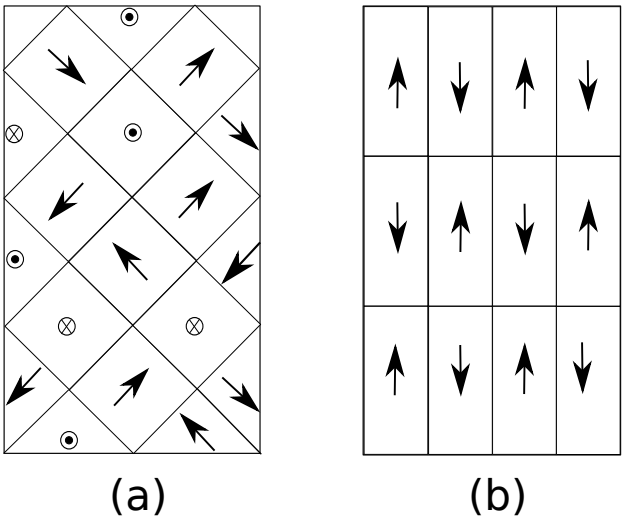

Figure 2.7: The domain structure of electrical steel illustrating the domain magnetisation in the demagnetised state (without showing the closing domains for simplicity) in (a) nonoriented type in which the magnetisation $\overline{M}$ has a different directions for different domains (b) grain-oriented type in which the domains are more developed along the rolling direction of the material.

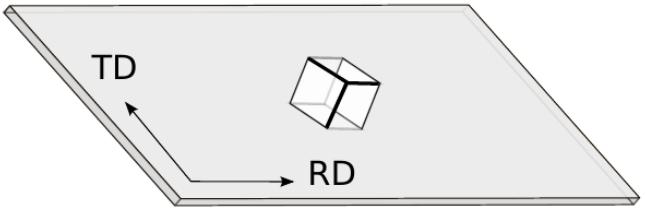

Figure 2.8: The orientation of the grains in a samples of grain-orientated electrical steel.

as follows

$$E_{\mathrm{me_{ext}}} = -\frac{3}{2}\lambda_{100}\sigma(\alpha_1^2\gamma_1^2 + \alpha_2^2\gamma_2^2 + \alpha_3^2\gamma_3^2) \qquad (2.15)$$
$$-3\lambda_{111}\sigma(\alpha_1\alpha_2\gamma_1\gamma_2 + \alpha_2\alpha_3\gamma_2\gamma_3 + \alpha_3\alpha_1\gamma_3\gamma_1),$$

where α_{i} $(i = 1,2,3)$ have been previously defined as the direction cosines of the magnetisation within a domain with respect to the cube axes. γ_{i} $(i = 1,2,3)$ are the direction cosines of the uniform tensile stress σ with respect to the cube axes. λ_{100}

and λ_{111} are the saturation magnetostriction constants in the $\langle 100 \rangle$, $\langle 111 \rangle$ directions, respectively.

In the case of 3% Si-Fe, in which the domains are locked to certain crystallographic directions by crystalline anisotropy and K_1 is positive, (2.15) can be simplified to

$$E_{\mathrm{me}_{\mathrm{ext}}} = -\frac{3}{2}\lambda_{100}\sigma\cos^2\theta_{\mathrm{c}}, \tag{2.16}$$

where, as mentioned in §2.2, K_1 is the first order anisotropy constant, which for the case of the grain-oriented electrical steel is in fact along the easy direction $\langle 100 \rangle$. θ_{c} is the angle between the uniform tensile stress σ and the domain which their magnetisation is assumed to be parallel to an easy direction. The minimum of (2.16) is then $-\frac{3}{2}\lambda_{100}\sigma$ for the domains which lie parallel to the tensile stress [19], [20].

In fact, for iron, if there is a tensile stress applied along the $\langle 100 \rangle$ direction, the energy along the $\langle 100 \rangle$ direction decreases. Thus, the energetically favourable domains grow at the expense of less favourable domains. As a result, the domains with 180° domain walls grow and the closure domains decrease. To this end, the 180° domains walls remain unaffected while the 90° domain walls move. This process shows that the 90° domain walls are stress-sensitive [15].

Coating stress

Electrical steels are usually coated, mainly in order to reduce eddy current losses, increase resistance between laminations and to protect the material against corrosion. There are different types of coating depending on the application where the electrical steel is to be used. For an excitation and the resulting magnetostriction in the rolling direction, as applied to grain-oriented material, it turns out to apply a pre-stress (tensile stress) in this direction. For nonoriented material, compared to grain-oriented material, the coating stress is much smaller. To observe the effect of the coating stress measurements are performed on coated and non-coated samples of some grain-oriented and nonoriented electrical steel types, the results of which will be shown in chapter 4.

In fact, the effect of the coating tensile stress can be explained based on the domain structure. As explained in §2.3.2, the coating stress makes the closure domains smaller. All magnetostriction strains are related to these closure domains. This has been also previously shown in a simple way in Fig. 2.5 (b) and (c), in which the magnetostriction strains are proportional to the strains of the domains which are not fully aligned with the applied magnetic field.

Looking at the domain structure of grain-oriented material, the crystals are oriented in the rolling direction of the material, which is the preferred magnetisation direction. In another word, the majority of the domains are aligned with the rolling direction of the material. The coating tensile stress removes much of the closure domains in the absence of an external magnetic field. However, these domains reappear in the presence of a magnetic field and as a result a small negative strain occurs. In the case of nonoriented materials, there is no preferred direction for the domains and thus,

the tensile coating effect, compared with the case of the grain-orientated material, is much smaller. To conclude, the application of the coating, especially on grain-oriented materials, is beneficial to lower the magnetostriction strains.

2.4. Theoretical approaches to calculate magnetostriction

The presented equations on magnetostriction calculation only apply to monocrystals which their magnetostriction is the average of all domains. However, electrical steels have a polycrystalline structure which means the crystalline structure are arranged in regions, so-called grains. The grains have the same crystal structure but the orientation of the lattice differs from grain to grain. The amount of grains and their size strongly depend on the material structure and vary from material to material.

In addition, a continuous change in the applied magnetic field results in a discontinuous change in the magnetic flux density B, which is known as the Barkhausen effect. Briefly speaking, this effect is a consequence of the domain boundary movement and domain rotation of the material. Further study of this effect is beyond the scope of this work and can be found elsewhere [15], [16].

To conclude, analytical approaches are incapable of calculating the magnetostrictive deformation under a random applied magnetic field in the microscopic scale. Thus, to identify the magnetostrictive behaviour experimental approaches are required, which will be discussed in chapter 3.

2.5. Macroscopic behaviour

The magnetostrictive strains are often plotted as a function of the magnetic induction B, the so-called butterfly loop (B-λ). The strains along the magnetisation direction $\lambda_{\parallel}$ for nonoriented and grain-oriented materials are shown in Fig. 2.9 and Fig. 2.10, respectively. For electrical steel the strains are in general in the order of micrometer per meter. Grain-oriented materials normally show less magnetostriction deformation than nonoriented materials, which is due to their domain structure. These grain-oriented materials have most of the domains along the rolling direction and thus the closure domains are relatively smaller. The smaller the closure domains, the less magnetostriction strains.

The macroscopic observations show that the magnetostrictive behaviour of every ferromagnetic material type is different from the others. In general, the defining factors can be categorised as follows

- **The crystal structure of the material and the grain pattern**
  Every ferromagnetic material has a different magnetostrictive behaviour due to a different crystalline structure. The material structure affects not only the amplitude of the strain but also the sign of the strains significantly. Fig. 2.11 shows the am-

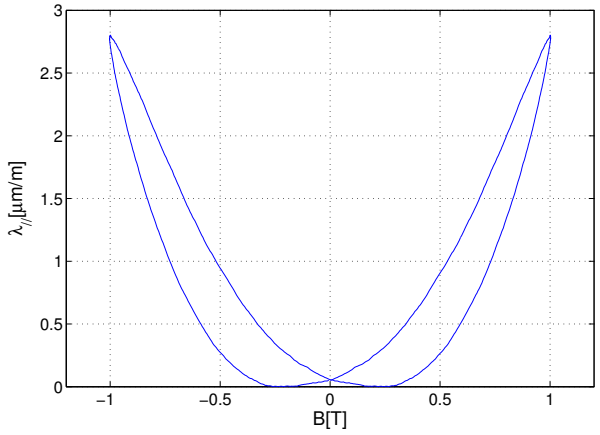

Figure 2.9: The magnetostriction strains along the magnetisation direction $\lambda_{\parallel}$ versus the magnetic induction B for a nonoriented electrical steel under a sinusoidal magnetisation with a 50Hz frequency.

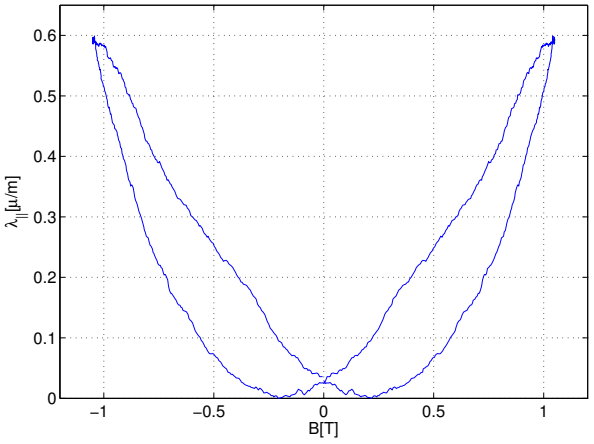

Figure 2.10: The magnetostriction strains along the magnetisation direction $\lambda_{\parallel}$ versus the magnetic induction B for a grain-oriented electrical steel under a sinusoidal magnetisation with a 50Hz frequency.

plitude of magnetostriction strains of several materials versus the magnetic field H[A/m] from zero strain up to the saturation state.

Even for the same material type, for instance electrical steel, the composition of the material and the production process result in different grain size with

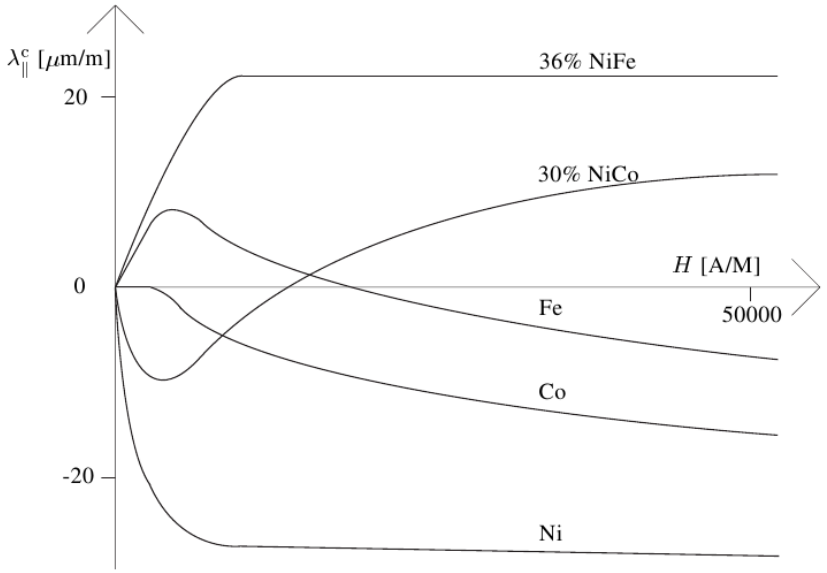

Figure 2.11: The amplitude of the magnetostriction strains $\lambda[\mu\text{m/m}]$ of several ferromagnetic materials versus the amplitude of the applied magnetic field H[A/m] [17].

different orientation which as a result affect the magnetostrictive behaviour. An increase of the silicon (Si) percentage decreases the magnetostrictive strains, at the expense of the increase of the brittleness [21].

- **The applied magnetic field**
  With different types of magnetisation signals and various amplitudes the magnetostrictive behaviour varies. In addition, the presence of higher harmonics affects the behaviour and creates minor loop inside the B-λ butterfly loop. The presence of a fifth harmonic on a sinusoidal magnetisation signal with the fundamental frequency of 50Hz is shown in Fig. 2.12. The fifth harmonic has an amplitude of 10% of that of the fundamental.
- **Application of external stress**
  There have been several studies on the influence of an external stress on the magnetostrictive behaviour, [20], [19], [22], [23]. A study on grain-oriented materials shows that application of a compressive or tensile stress less than 2MPa has a minor effect on the magnetostriction behaviour. However, compressive stresses larger than that (in the order of a few MPa) increase the magnetostriction strains. The effect of tensile stress on the magnetostrictive behaviour of the material is opposite to that of compressive stress, as shown in Fig. 2.13 [23]. The study of

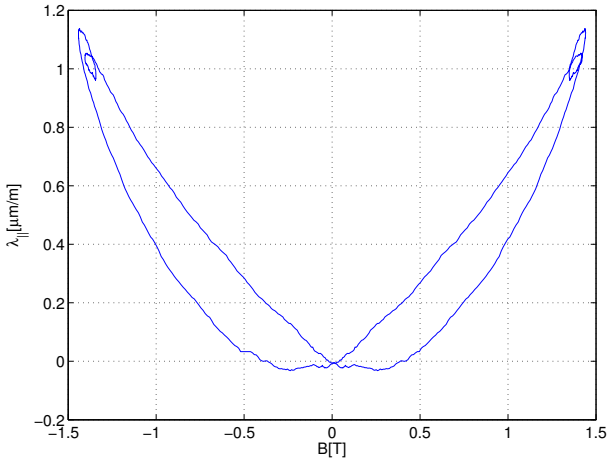

Figure 2.12: The magnetisation strains $\lambda_{||}$ versus the magnetic induction B for a grain-orientated electrical steel under a sinusoidal magnetisation with a fifth harmonic component which has an amplitude of 10% of that of fundamental.

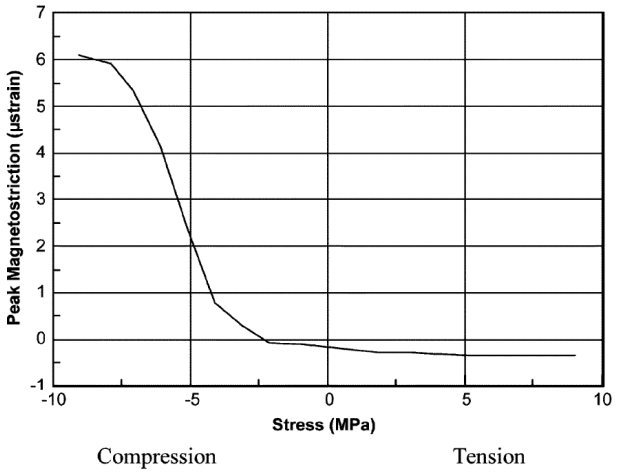

Figure 2.13: Magnetostriction characteristic versus externally applied stress of a grain-oriented silicon steel measured along the rolling direction at the magnetic indication B of 1.5T at 50Hz frequency [23].

the effect of external strain and stress is especially useful for the magnetostrictive behaviour of transformers, since in all laminated magnetic cores stress occurs. A non-uniform applied clamping force in the assembly of the core or a temperature variation can all contribute to the appearance of stress. To this end, information about the influence of the externally applied stress (both compressive and tensile) on the magnetostriction behaviour is useful. However, such study was beyond the scope of this PhD work and only the magnetostriction behaviour of different materials as a function of applied magnetic field under zero externally applied stress has been studied.

Magnetoelastic effect

As discussed, variations of the magnetic field result in a change of the shape of magnetic materials (the magnetostriction deformation) and its Young's modulus. The Young's elasticity modulus E is a measure of the stiffness of the material and is defined as the ratio of the mechanical stress σ over elastic strain ε

$$E = \frac{\sigma}{\varepsilon}. \tag{2.17}$$

In addition, according to the magnetomechanical effect, the magnetic properties of the material as a result of the application of stress (tensile or compressive) varies. The magnetomechanical coupling models are based on the following constitutive equations

$$dB = \left(\frac{\partial B}{\partial H}\right)_{\sigma} dH + \left(\frac{\partial B}{\partial \sigma}\right)_{H} d\sigma, \tag{2.18}$$

$$d\lambda = \left(\frac{\partial \lambda}{\partial H}\right)_{\sigma} dH + \left(\frac{\partial \lambda}{\partial \sigma}\right)_{H} d\sigma. \tag{2.19}$$

The indices mean that the derivations are at a constant mechanical stress σ or a constant magnetic field H respectively. If the changes in the stress and the magnetostriction are small and reversible, the magnetoelastic coupling can be represented as

$$\left(\frac{\partial \lambda}{\partial H}\right)_{\sigma} = \left(\frac{\partial B}{\partial \sigma}\right)_{H}. \tag{2.20}$$

In fact, if the magnetostriction λ is positive and increases continuously by the applied field H, the magnetisation B will also increase by tension. On the contrary, once the magnetostriction is negative the magnetisation B decreases. This effect is one of the indirect approaches for quantitatively calculating the magnetostriction strains without measuring them [16], [24].

2.6. Continuum description of magnetoelastic material

So far some basics of microscopic magnetisation and different energy terms have been presented. The magnetostriction phenomenon has been also explained from both the microscopic and macroscopic points of view. In order to calculate vibrations and deformation of ferromagnetic cores due the magnetic sources, which has been presented in §1.1, a computational method is required. However, as explained in §2.4, the computation of the magnetostrictive deformation is not possible on the microscopic scale. To this end, a method has been developed in the past based on a continuum model of the core material. For the contribution of the magnetostriction a model of the magnetostrictive behaviour of the core material is required, which the latter needs to be experimentally obtained. Further on, the theory behind this method will be described. It starts with magnetic computations which are based on the Maxwell's laws and the theory explained so far. Then the elasticity equations for the calculations of the mechanical deformation are applied.

The electromagnetic forces applied on a material from other sources e.g. currents may act on a long-range, while the magnetostriction is a local effect as a result of the magnetisation process. Since both phenomena always occur together, they have to be considered simultaneously for solving magnetoelastic problems. To this end, various formulations are common such as the Chu model and the Ampère model. A thorough elaboration of different models to describe magnetic forces and magnetostriction can be found elsewhere [25]. For the description of the Chu model and the Ampère model we refer to [26], [27], [28], [29]. In this work only the Chu model formulation is considered and is later applied for a deformation computation technique, which will be presented in chapter 5.

2.6.1 Long-range magnetic forces based on Chu model formulation

In the magnetisation model of Chu, elementary magnetic dipoles are modelled as two opposite magnetic charges q_m and $-q_m$ separated from each other by a distance $\overline{d}$, which have a magnetic moment of $\overline{m} = q_m \overline{d}$.

We consider that such magnetic dipole is in free space, i.e. while the other magnetic sources which generate the external field of $\overline{H}_\mathrm{e}$ are far on a molecular scale. The force acting on this dipole is then

$$\overline{F} = (\overline{m}.\overline{\nabla})\overline{H}_\mathrm{e}. \tag{2.21}$$

We now consider a part V_1 inside the surface S_1 of a magnetised body, as presented in Fig. 2.14. For calculating the magnetic long-range force acting on V_1, it is assumed that it is separated from the rest of the magnetic material (V_0) by means of an infinitesimal gap. Thus, the short-range forces, i.e. interactions on a microscopic scale between the material V_1 and V_0 vanish. We can then replace the magnetic moment $\overline{m}$ of a single dipole with the magnetic moment per unit volume $\mu_0 \overline{M}$ and the external

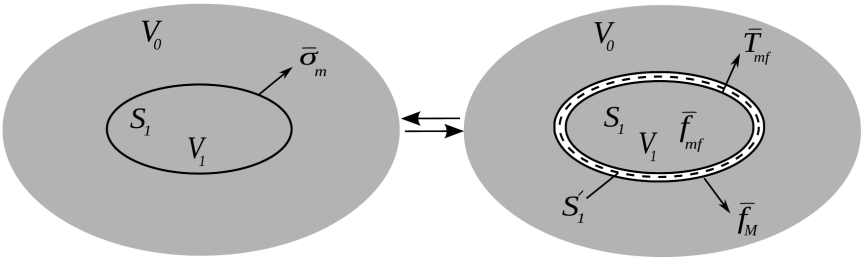

Figure 2.14: Definition of long-range magnetic forces [28].

field $\overline{H}_\mathrm{e}$ with the macroscopic field $\overline{H}$ because

$$\int (\mu_0 \overline{M} \cdot \overline{\nabla}) \overline{H} dv = \int (\mu_0 \overline{m} \cdot \overline{\nabla}) \overline{H}_\mathrm{e} dv \tag{2.22}$$

The force density $\overline{f}_\mathrm{mf}$ is as follows, for which the force density acting on the current density $\overline{J}$ is also considered:

$$\overline{f}_\mathrm{mf} = \overline{J} \times \mu_0 \overline{H} + (\mu_0 \overline{M} \cdot \overline{\nabla}) \overline{H} \tag{2.23}$$

$$= \overline{\nabla} \cdot \overline{\overline{T}}_\mathrm{mf}, \tag{2.24}$$

where the tensor $\overline{\overline{T}}_\mathrm{mf}$ is given by

$$\overline{\overline{T}}_\mathrm{mf} = \overline{B}\,\overline{H} - \frac{\mu_0}{2} H^2 \overline{\overline{I}}. \tag{2.25}$$

On the material boundary S_1 the force density displays a singularity i.e. a surface traction:

$$\overline{T}_\mathrm{mf}(\overline{n}) = \overline{n} \cdot (\overline{\overline{T}}_\mathrm{mf,ext} - \overline{\overline{T}}_\mathrm{mf,int}), \tag{2.26}$$

where $\overline{\overline{T}}_\mathrm{mf,ext}$ and $\overline{\overline{T}}_\mathrm{mf,int}$ are the magnetic stress tensor just outside and inside the material respectively and $\overline{n}$ is the outward normal unit vector on the surface. For the boundaries between the material and air (2.26) results in

$$\overline{T}_\mathrm{mf}(\overline{n}) = \frac{\mu_0}{2} M_\mathrm{n}^2 \overline{n}, \tag{2.27}$$

where M_n is the normal component of the magnetisation $\overline{M}$ inside V_1. Based on the force density (2.23) and the corresponding surface force density (2.27) on the material boundaries, the long-range force acting on the material inside V_1 can be calculated as

$$\overline{F}_\mathrm{mf} = \int_{V_1} \overline{f}_\mathrm{mf} dv + \int_{S_1} \overline{T}_\mathrm{mf}(\overline{n}) ds, \tag{2.28}$$

$$= \int_{S_1} [\overline{n} \cdot \overline{\overline{T}}_{\mathrm{mf}} + \overline{T}_{\mathrm{mf}}(\overline{n})] ds. \tag{2.29}$$

According to (2.28), the long-range magnetic force does not only depend on the volume foce density, since the surface tractions $\overline{T}_{\mathrm{mf}}$ cannot be expressed in a tensor formulation of form $\overline{n} \cdot \overline{\overline{T}}_{\mathrm{mf}}$.

Back to (2.29), the long-range magnetic force acting on a part of a magnetised body can be calculated by integrating the "magnetic stress vector" $\overline{\sigma}_{\mathrm{m}}$ over its surface, defined as follows [30], [28]

$$\overline{\sigma}_{\mathrm{m}}(\overline{n}) = \overline{n} \cdot \overline{\overline{T}}_{\mathrm{mf}} + \overline{T}_{\mathrm{mf}}(\overline{n}). \tag{2.30}$$

2.6.2 Stresses in magnetised material

Except for the long-range magnetic forces, all other phenomena e.g. magnetostriction and mechanical stresses can be defined by means of stress vector $\overline{\tau}(\overline{n})$, i.e. the force per unit surface area acting on an imaginary surface with normal vector $\overline{n}$. It is found that the stress vector $\overline{\tau}(\overline{n})$ can be presented in terms of a stress tensor $\overline{\overline{\tau}}$ and the surface traction $\overline{T}_{\mathrm{mf}}$ as follows

$$\overline{\tau}(\overline{n}) = \overline{n} \cdot \overline{\overline{\tau}} - \overline{T}_{\mathrm{mf}}(\overline{n}). \tag{2.31}$$

In fact, in the classical elasticity equation only the first term is present $\overline{n} \cdot \overline{\overline{\tau}}$. However, the surface traction $\overline{T}_{\mathrm{mf}}$, which corresponds to the case with a fictitious boundary with air is added to the (2.31), assuming an equilibrium condition is reached for an infinitesimal part of the magnetised body.

The stress vector $\overline{\tau}(\overline{n})$ includes local interactions which consists of elastic stress and magnetostriction. Based on (2.27), (2.31) it can be expressed as follows

$$\overline{\tau}(\overline{n}) = \overline{n} \cdot \overline{\overline{\tau}} - \frac{\mu_0}{2} M_{\mathrm{n}}^2 \overline{n}. \tag{2.32}$$

The stress can be analysed by considering the equation of motion of arbitrary infinitesimal parts of the magnetised body. The forces on such parts consists of the stress on its surface $\overline{\tau}$, the long-range magnetic forces presented in (2.28), and any external volume forces $\overline{f}_{\mathrm{ext}}$ e.g. gravity force and finally external surface force $\overline{T}_{\mathrm{ext}}$ at material boundaries. Assuming an arbitrary volume, the equation of linear motion for this volume can be expressed as

$$\rho \overline{a} = \overline{f}_{\mathrm{mf}} + \overline{f}_{\mathrm{ext}} + \overline{\nabla} \cdot \overline{\overline{\tau}}, \tag{2.33}$$

where ρ and $\overline{a}$ are the mass density and the acceleration, respectively. At material boundaries the equilibrium condition is valid for the equation of linear motion, thus:

$$\overline{n} \cdot \overline{\overline{\tau}} = \overline{T}_{\mathrm{ext}} + \overline{T}_{\mathrm{mf}}. \tag{2.34}$$

2.6.3 Work, energy and constitutive laws

For a deformable magnetised media, the work and energy terms will be discussed in this section. First we consider an infinite space V_∞ containing moving and deformable magnetic media, for which we have displacement $\overline{u}$, magnetisation $\overline{M}$ and current density $\overline{J}$. Considering sufficiently small deformations, they can be described by means of the strain tensor $\overline{\overline{\varepsilon}}$ given by the symmetric part of the Jacobian of the displacement

$$\overline{\overline{\varepsilon}} = \frac{1}{2}(\overline{\nabla}\overline{u} + (\overline{\nabla}\overline{u})^{\mathsf{T}}). \tag{2.35}$$

Then we consider an infinitesimal displacement variation $d\overline{u}$, which corresponds to the deformation $d\overline{\overline{\varepsilon}}$. Moreover, it corresponds to a change of the magnetisation $d'\overline{M}'$, where d' denoted the variation from the point of view of an observer that follows the material displacement and $\mu_0\overline{M}'$ is the magnetic moment per unit mass defined as

$$\mu_0\overline{M}' = \frac{\mu_0\overline{M}}{\rho}. \tag{2.36}$$

Based on the Maxwell's equations and the equations of motion (2.33), (2.34), the total work in the volume V_∞ done by the external voltage sources $đW_\mathrm{e}$ and by the external forces $đW_\mathrm{ext}$ can be expressed as

$$\begin{aligned} đW_\mathrm{e} + đW_\mathrm{ext} = & đW_\mathrm{J} + dE_\mathrm{kin} + dW_\mathrm{s} \\ & + \int_{V_\infty} (\mu_0\overline{H}\cdot d'\overline{M}' + \frac{1}{\rho}\overline{\overline{\tau}} : d\overline{\overline{\varepsilon}})dm, \end{aligned} \tag{2.37}$$

where $đW_\mathrm{J}$ is Joule losses, E_kin is the kinetic energy and : denotes a contracted product. W_s is the magnetic self-energy defined as

$$W_\mathrm{s} = \int_{V_\infty} \frac{\mu_0}{2} H^2 dv. \tag{2.38}$$

The last term in (2.37) represents the energy which is absorbed by the magnetic deformable material. Assuming a reversible process, for the case of non-hysteretic materials, the energy of such work is a form of free energy U_f defined as

$$dU_\mathrm{f} = \int_{V_\infty} (\mu_0\overline{H}\cdot d'\overline{M}' + \frac{1}{\rho}\overline{\overline{\tau}} : d\overline{\overline{\varepsilon}})dm, \tag{2.39}$$

where the free energy density u_f (free energy per unit mass) is defined as

$$du_\mathrm{f} = \mu_0\overline{H}\cdot d'\overline{M}' + \frac{1}{\rho}\overline{\overline{\tau}} : d\overline{\overline{\varepsilon}}. \tag{2.40}$$

We can then present the free energy density in terms of the magnetisation $\overline{M}'$ and the strain $\overline{\overline{\varepsilon}}$ as

$$u_{\mathrm{f}} = u_{\mathrm{f}}(\overline{M}', \overline{\overline{\varepsilon}}). \tag{2.41}$$

The constitutive law for the magnetic field $\overline{H}$ and the symmetric part of the stress tensor $\overline{\overline{\tau}}^{s}$ can be presented as[3]

$$\overline{H} = \frac{1}{\mu_0} \frac{\partial u_{\mathrm{f}}(\overline{M}', \overline{\overline{\varepsilon}})}{\partial \overline{M}'}, \tag{2.42}$$

$$\overline{\overline{\tau}}^{s} = \rho \frac{\partial u_{\mathrm{f}}(\overline{M}', \overline{\overline{\varepsilon}})}{\partial \overline{\overline{\varepsilon}}}. \tag{2.43}$$

Based on (2.42) and (2.43), the relation between the magnetic field $\overline{H}$ and the symmetric part of the stress tensor $\overline{\overline{\tau}}^{s}$ is coupled, which can be expressed as

$$\frac{\partial \mu_0 \overline{H}}{\partial \overline{\overline{\varepsilon}}} = \frac{\partial \overline{\overline{\tau}}^{s}}{\rho \partial \overline{M}'}. \tag{2.44}$$

We can see that (2.42), (2.43) and (2.44) are equivalent to (2.18), (2.19) and (2.20) which were presented in §2.5. The variations of stress tensor $\overline{\overline{\tau}}^{s}$ as a function of the magnetisation $\overline{M}'$ are equivalent to the variations of magnetostriction strains λ as a function of applied magnetic field H. Moreover, the variations of the magnetic field $\overline{H}$ as a function of strain $\overline{\overline{\varepsilon}}$ are equivalent to the variations of the magnetic induction B as a function of the stress σ [30], [28].

2.6.4 Magnetic equivalent forces

Next we make the assumption that the free energy density function u_{f} consists of three terms as follows

$$u_{\mathrm{f}}(\overline{M}', \overline{\overline{\varepsilon}}) = u_{\mathrm{mag}}(\overline{M}') + \frac{1}{\rho} \overline{\overline{T}}_{\mathrm{ms}}(\overline{M}') : \overline{\overline{\varepsilon}} + \frac{1}{2\rho} \overline{\overline{\varepsilon}} : \overline{\overline{E}} : \overline{\overline{\varepsilon}}, \tag{2.45}$$

where $\overline{\overline{T}}_{\mathrm{ms}}$ is a symmetric tensor and $\overline{\overline{E}}$ is the elasticity tensor. The first term is independent of the strain. The second term is a link between magnetisation and the strain. The third term is a quadratic function of the strain. The free energy density u_{f} can be further expressed as follows

$$u_{\mathrm{f}}(\overline{M}', \overline{\overline{\varepsilon}}) = u_{\mathrm{mag}}(\overline{M}') + u_{\mathrm{mstr}}(\overline{M}', \overline{\overline{\varepsilon}}) + u_{\mathrm{el}}(\overline{\overline{\varepsilon}}), \tag{2.46}$$

[3] The stress tensor $\overline{\overline{\tau}}$ has a symmetric and antisymmetric part. However, since the the strain $\overline{\overline{\varepsilon}}$ is symmetric the contracted product $\overline{\overline{\tau}} : d\overline{\overline{\varepsilon}}$ does not depend on the antisymmetric part of $\overline{\overline{\tau}}$ [30], [28].

which consists of the "magnetostatic energy $u_{\text{mag}}(\overline{M}')$", the "magnetostriction energy $u_{\text{mstr}}(\overline{M}', \bar{\bar{\varepsilon}})$" and the "magnetoelastic energy $u_{\text{el}}(\bar{\bar{\varepsilon}})$".

For isotropic materials the elasticity tensor $\bar{\bar{\bar{E}}}$ only depends on the Young's elasticity modulus, Poisson's ratio[4] and shear modulus G. The shear modulus itself is a function of the Young's elasticity modulus and the Poisson's ratio defined as

$$2G = \frac{E}{1+\nu}. \tag{2.47}$$

The mass density ρ is considered as a constant (if $\varepsilon_{xx} + \varepsilon_{yy} + \varepsilon_{zz} \ll 1$).

The constitutive law for the magnetic field $\overline{H}$ (2.42) is then presented as

$$\bar{H} = \frac{1}{\mu_0}\left(\frac{du_{\text{mag}}(\overline{M}')}{d\overline{M}'} + \frac{\partial u_{\text{mstr}}(\overline{M}', \bar{\bar{\varepsilon}})}{\partial \overline{M}'}\right) \tag{2.48}$$

$$= \tilde{\bar{H}} + \frac{1}{\mu_0 \rho}\frac{d\bar{\bar{T}}_{\text{ms}}}{d\overline{M}'} : \bar{\bar{\varepsilon}}, \tag{2.49}$$

where $\tilde{}$ indicates the constitutive law in the undeformed state. The stress tensor $\bar{\bar{\tau}}$ can be defined as follows

$$\bar{\bar{\tau}} = \bar{\bar{T}}_{\text{ms}}(\overline{M}') + \bar{\bar{\varepsilon}} : \bar{\bar{\bar{E}}}. \tag{2.50}$$

According to the equation of linear motion (2.33) and (2.24), the following results:

$$\rho \bar{a} = \overline{\nabla} \cdot \bar{\bar{T}}_{\text{mf}} + \overline{f}_{\text{ext}} + \overline{\nabla} \cdot \bar{\bar{\tau}}. \tag{2.51}$$

Based on (2.50), we can define the equivalent stress tensor $\bar{\bar{\tau}}^*$ as follows

$$\bar{\bar{\tau}}^* = \bar{\bar{\tau}} - \bar{\bar{T}}_{\text{ms}}(\overline{M}') \tag{2.52}$$

for which according to the Hooke's law we have

$$\bar{\bar{\tau}}^* = \bar{\bar{\varepsilon}} : \bar{\bar{\bar{E}}}. \tag{2.53}$$

Back to (2.51), we have the following

$$\rho \bar{a} = \overline{\nabla} \cdot \bar{\bar{T}}_{\text{mf}} + \overline{f}_{\text{ext}} + \overline{\nabla} \cdot \bar{\bar{T}}_{\text{ms}} + \overline{\nabla} \cdot \bar{\bar{\tau}}^*. \tag{2.54}$$

Further on, we define the "magnetic equivalent stress tensor" $\bar{\bar{T}}^*$ as the following

$$\bar{\bar{T}}^* = \bar{\bar{T}}_{\text{mf}} + \bar{\bar{T}}_{\text{ms}}, \tag{2.55}$$

[4] Poisson's ratio ν is defined as the negative of transverse to lateral strain $(-\frac{\delta\varepsilon_{transverse}}{\delta\varepsilon_{lateral}})$. In another word, if a sample is extended or contracted in the direction of the applied stress (the axial direction), it contracts or extends in the transverse direction to the applied stress respectively, where the ratio of the deformations in the two directions is the Poisson's ratio.

Then the "magnetic equivalent force density" $\overline{f}^*$ is defined as

$$\overline{f}^* = \overline{\nabla} \cdot \overline{\overline{T}}^* = \overline{\nabla} \cdot \overline{\overline{T}}_{\text{mf}} + \overline{\nabla} \cdot \overline{\overline{T}}_{\text{ms}} \tag{2.56}$$

$$= \overline{f}_{\text{mf}} + \overline{\nabla} \cdot \overline{\overline{T}}_{\text{ms}}. \tag{2.57}$$

Thus, (2.54) can be expressed as

$$\rho \overline{a} = \overline{f}^* + \overline{f}_{\text{ext}} + \overline{\nabla} \cdot \overline{\overline{\tau}}^*. \tag{2.58}$$

In (2.51) the stress tensor $\overline{\overline{\tau}}$ represented all local interactions. In fact, magnetostriction was then represented by a local stress tensor.

We could also define the equation of linear motion slightly different with considering only the elastic stress, although it would result in the same. To this end, (2.51) can be presented as follows

$$\rho \overline{a} = \overline{\nabla} \cdot \overline{\overline{T}}_{\text{mf}} + \overline{f}_{\text{ext}} + \overline{\nabla} \cdot \overline{\overline{\tau}}_{\text{el}}, \tag{2.59}$$

where $\overline{\overline{\tau}}_{\text{el}}$ is the elastic stress tensor, which according to Hooke's law is related to the elastic strain tensor $\overline{\overline{\varepsilon}}_{\text{el}}$ as

$$\overline{\overline{\tau}}_{\text{el}} = \overline{\overline{\varepsilon}}_{\text{el}} : \overline{\overline{E}}. \tag{2.60}$$

If we then define that in addition to the elastic strain tensor $\overline{\overline{\varepsilon}}_{\text{el}}$, there is also strain due to the magnetostriction which depends on the magnetic induction B, the total strain tensor $\overline{\overline{\varepsilon}}$ is then the sum of the both elastic and magnetostriction strain tensors, as follows

$$\overline{\overline{\varepsilon}} = \overline{\overline{\varepsilon}}_{\text{el}} + \overline{\overline{\varepsilon}}_{\text{ms}}. \tag{2.61}$$

Replacing $\overline{\overline{\varepsilon}}_{\text{el}}$ in (2.60), with (2.61) we have

$$\overline{\overline{\tau}}_{\text{el}} = (\overline{\overline{\varepsilon}} - \overline{\overline{\varepsilon}}_{\text{ms}}) : \overline{\overline{E}} \tag{2.62}$$

If we replace $\overline{\overline{\varepsilon}} : \overline{\overline{E}}$ with $\overline{\overline{\tau}}^*$, (2.62) can be re-written as

$$\overline{\overline{\tau}}_{\text{el}} = \overline{\overline{\tau}}^* - \overline{\overline{\varepsilon}}_{\text{ms}} : \overline{\overline{E}}. \tag{2.63}$$

If we replace the magnetostriction contribution as follows

$$\overline{\overline{T}}_{\text{ms}} = -\overline{\overline{\varepsilon}}_{\text{ms}} : \overline{\overline{E}}, \tag{2.64}$$

in (2.63) will be

$$\overline{\overline{\tau}}_{\text{el}} = \overline{\overline{\tau}}^* + \overline{\overline{T}}_{\text{ms}}, \tag{2.65}$$

which would result in the same as (2.54) [30], [28].

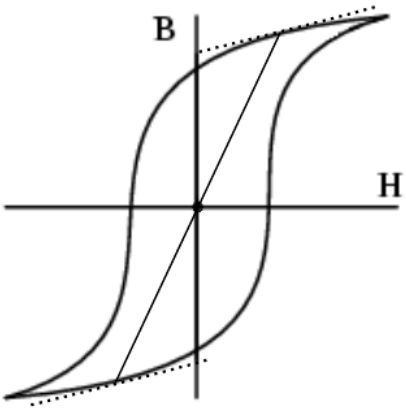

Figure 2.15: B-H hysteresis loop which is symmetrical around the origin point.

Discussion

The presented method for the computation of the deformation due to the magnetic forces and magnetostriction is mainly derived from basic elasticity equations. The only term defined differently is the magnetic equivalent force density $\overline{f}^*$, which includes the magnetostriction tensor term. This has been defined based on the work, energy and constitutive laws.

To the definition of the magnetostriction tensor two different approaches were proposed, which both result in the same equation of motion. This equation is independent of the symmetric tensor $\overline{\overline{T}}_{\mathrm{ms}}$.

2.6.5 Relevance of even harmonics to the magnetostriction strains

Here we consider the case of a unidirectional magnetisation, which means that the magnetic induction B, the magnetic field H and the magnetostriction λ are all one-dimensional quantities. Ferromagnetic materials show a permeability which depends on the field strength (or magnetic induction). Assuming steady state case, the B-H loop is symmetrical around the origin point as shown in Fig. 2.15. Therefore, for a non-linear material with hysteresis loops the differential reluctivity will be an even function. A first order approximation (series expansion) for the reluctivity will show a term proportional to the square of the induction.

In addition to the reluctivity, the strain ε, the magnetostriction strain λ and the magnetic force density $\overline{f}_{\mathrm{mf}}$ contain only even harmonics. Regarding the magnetostriction strains, the relevance of the even harmonics can also be explained based on the microscopic behaviour and the domain structure of the material, discussed in chapter

2.3. A magnetic domain with a 0° angle with respect to the magnetic field shows the same strain as that of a domain with 180° angle with respect to the magnetic field, although they have opposite magnetisation signs, see Fig. 2.5. This means that the magnetostriction is independent of the sign of the external field, as long as the direction remains the same. Such relation is always valid, regardless of hysteresis and saturation of the magnetic material. The behaviour of the magnetic induction B and the magnetic field H are the same as those of the voltage V and the current I, respectively. The voltage V and the current I will only contain odd harmonics.

We then assume the case when the relation between the magnetic induction B and the magnetic field H is linear (a constant reluctivity). We assume the following relation between the magnetostriction strain λ and the magnetic induction B

$$\lambda = \lambda_0 + \lambda_2 B^2, \tag{2.66}$$

where λ_0 and λ_2 are constants, which depend on the material properties. If we assume an applied voltage V, which contains only a single fundamental harmonic, the current I, the magnetic field H and the magnetic induction B contain only the same fundamental harmonics. Assuming the following magnetic induction B

$$B(t) = \hat{B}\cos(\omega t),\ \omega = 2\pi f, \tag{2.67}$$

according to (2.66), where $\lambda \propto B^2$ it results in

$$\begin{aligned} \lambda &\propto \cos^2(\omega t) \\ &= \frac{1+\cos(2\omega t)}{2}. \end{aligned} \tag{2.68}$$

Thus, the magnetostriction strain λ only contains even harmonics of the magnetisation frequency. For the case of a magnetisation frequency of 50Hz the magnetostriction strains contain harmonics of 0, 100Hz.

Assuming once again the case of the linear relation between the magnetic induction B and the magnetic field H, we can now consider an applied voltage V which contains a fundamental harmonic and odd higher harmonics. In this case, the magnetic induction B, the magnetic field H and the magnetisation current I would contain also only odd harmonics. The magnetostriction strain λ would then contain even higher harmonics.

If the relation between the magnetic induction B and the magnetic field H is nonlinear, even if the applied voltage contains only a fundamental harmonic without any higher harmonics, the magnetostriction strain λ would contain even higher harmonics. The presence of the even higher harmonics on the magnetostriction strain is then due to the nonlinearity.

Assuming again the nonlinear case, if there are odd higher harmonics present in the applied voltage, the magnetostriction strain λ would contain higher even harmonics.

The presence of these higher even harmonics can be both due to the higher harmonics on the applied voltage and due to the nonlinearity of the material.

To conclude, we can say that once a sample is magnetised, the magnetostriction deformations depend only on the absolute value of the magnetisation and not its sign. In another word, if we look at the frequency spectrum of the strains, only the even harmonics are relevant.

2.7. Conclusion

A theoretical background of the work was presented in this chapter. The magnetisation process and the formation of the magnetic domains based on the minimisation of the different energy terms were discussed. Thereafter, magnetostriction phenomena was presented both from microscopic and macroscopic points of view.

For the FE method for the computation of the effects of the magnetic forces and magnetostriction on the deformation of magnetic cores a continuum model of the material was considered. The method is mainly drived based on elasticity equations, for which a Chu model formulation is considered. The effect of the magnetic forces can be analytically calculated. For the contribution of the magnetostriction a set of forces were introduced in order to generate the magnetostriction strains in the material. To this end, a model of the magnetostrictive behaviour of the core material is required. The magnetostrictive behaviour of each material needs to be obtained experimentally. In the next chapter, the magnetostriction strain measurement technique will presented.

CHAPTER 3

Magnetostriction measurement

3.1. Introduction

As explained in chapter 2, analytical approaches are incapable of determining the magnetostrictive behaviour of ferromagnetic materials under a random magnetisation. Thus, several strain measurement techniques have been applied to measure the magnetostriction strains of ferromagnetic materials. The focus of this work is on the magnetostrictive behaviour of electrical steels with their application in transformers. In general the electrical steel samples show deformations in the order of a few micro meter per meter which for instance compared with the magnetostriction strains of iron-nickel alloys are significantly smaller[1]. In addition to the small deformation scale, the sensitivity of such measurements to any external stress requires an accurate measurement setup.

In this chapter, first a short overview of the commonly applied techniques for the magnetostriction strain measurement of electrical steel will be given. Thereafter, the magnetostriction strain measurement setups which have been developed in EELAB will be presented. In the past a magnetostriction strain measurement setup was based on the strain gauge technique. The design of this setup and its advantages and limitations will be overviewed. Although the measurement results obtained by strain gauge setup proved to be accurate and repeatable, due to some limitations which will be discussed in this chapter, a new measurement approach was required. To this end, a new magnetostriction measurement setup was designed and developed during this PhD work.

After that, the new setup which is based on the laser technique will be concisely presented. The optical components and their arrangement as well as the magnetic design of the setup will be discussed. The steering software to control the setup will be

[1] Even among electrical steels, the magnetostrictive behaviour strongly depends on the composition of the material.

explained too. The measurement results obtained by the laser setup and comparison with those of the strain gauge setup will be presented in the next chapter.

3.2. Magnetostriction measurement techniques: a literature overview

3.2.1 Measurements condition

Several techniques have been applied so far to measure the magnetostriction strains of electrical steel sheets. Before going into a literature review of the applied measurement techniques, first the conditions under which the measurements are performed will be explained. As reported in §2.5, and in (2.19), the strains highly depend on the applied magnetic field H, the material composition and also on the application of an external stress. This means that for the magnetostriction strain measurement of a sample, several factors significantly affect e.g. the magnetisation waveform type, the presence of any compressive or tensile stress.

Regarding the magnetisation waveform, to resemble the magnetostrictive behaviour of the transformers in their real working conditions, the measurements reported are carried out under a purely sinusoidal magnetisation signal with 50Hz or 60Hz frequency, dependent on the grid frequency of the country. Also some measurements are performed under sinusoidal magnetisation with higher harmonic components, as will be discussed in later chapters.

With respect to the applied external stress, setups have been developed to measure the magnetostrictive behaviour without external stress [18] and setups in which the sample is under a compressive or tensile stress [31]. The application of the stress is useful to investigate the magnetostrictive behaviour of the materials for those applications in which the material is under stress, e.g. transformer cores. Due to the windings and the assembly of the cores, there is always some stress present. The main purpose of the clamping is to have a rigid and strong core assembly. However, the cores contain areas of increased stress due to non-uniform clamping forces and temperature variations across the core, which are inevitable [32].

The focus of this PhD research is on identifying the magnetostrictive behaviour of nonoriented and grain-oriented electrical steel samples as a function of the applied magnetic field without external stress. Thus, the setups which have been developed in the past and during this PhD work are designed so that the sample can deform without being subjected to friction. After a short overview of the most common magnetostriction strain measurement techniques, the setups developed in EELAB will be presented.

3.2.2 Measurement techniques

In general, one of the challenges with the magnetostriction measurement setups is the repeatability of the measurement results. In the productions lines of electrical steels, the steel plates are often rolled in thin sheets. Given the small thickness of the samples, which makes them rather light in weight, the magnetisation is followed by vibrations and movements of the sample. These movements, especially the out-of-plane movements of the sample, reduce the repeatability of the measurements [33].

The most common techniques for the measurement of the magnetostriction strains of the electrical steel are the following:

- **Strain gauge**
  The strain gauge technique is the most common approach for the magnetostriction strain measurements. In this method, the strain gauge is attached to the specimen by a suitable adhesive to make a good contact with the specimen. Once the specimen is magnetised, the magnetostriction strains deform the conductor inside the gauge, which is a metallic foil pattern. As a result, the electrical resistance of the metallic conductor changes. Based on the resistance change, the magnetostriction strains of the samples are obtained by a quantity known as the gauge factor K_{GF}

$$K_{\mathrm{GF}} = \frac{\Delta R/R}{\Delta l/l} \tag{3.1}$$

  where R and ΔR refer to the resistance and the resistance change of the conductor and l and Δl refer to the length and the length change of the strain gauge in the x-direction shown in Fig. 3.1.

Figure 3.1: A strain gauge with one measuring grid for one-dimensional strain measurements [18].

Strain gauges with more than one measuring grid (multiple channels) are available on the market, which thus allows measurements along more than one direction, as reported by Hilgert et al. [18] and Wakabayashi et al. [34]. To this end, the strain gauges are suitable especially for measuring the magnetostriction strains under rotational magnetisation, since they can measure strain along different angles. Such measurements are particularly useful for measurements of the magnetostrictive behaviour of the materials of electrical machine cores

with a rotational magnetic flux pattern. To this end, the strains in different angles with respect to the magnetisation direction can be easily measured as reported by Somkun et al. [35], [36].

- **Piezo-electric**
  Another strain measurement technique applied for the magnetostriction measurement is based on piezo-electric materials. This technique also requires some contact with the specimen. Piezo-electric materials are crystals or ceramic materials which, when exposed to a mechanical stress build up an electric charge. The value of this electric charge is proportional to the applied stress. In piezo-electric accelerometers, the generated electric charge is proportional to the acceleration. The displacement of the sample is then obtained by a double integration of the acceleration. The magnetostriction strains are then the fractional ratio of the displacement and the original length of the sample.

  In the literature, Anderson et al. and Fonteyn have reported setups to measure the magnetostriction strains based on the piezo-electric accelerometer technique [31], [37]. In the setup reported by Anderson et al., the Epstein samples are placed under a uni-axial stress which their pressure is controlled by electro-pneumatic values. An external stress in the range of $\pm$10MPa can be applied to the sample. The acceleration of the magnetised specimen is then measured by using two piezo-electric accelerometers and these signals are further post-processed in a PC based program to calculate the magnetostriction strains.

- **Laser**
  The optical approaches have the benefit of non-contact measurements which, considering the sensitivity of magnetostriction, can improve the accuracy of the measurements significantly. Laser setups belong to this class of optical approaches. They are increasingly applied for the magnetostriction strain measurements.

  Nakata et al. have reported one of the first setups based on a laser doppler vibrometer [38] in 1994. The sample size is reported as 50cm$\times$10cm with a measurement length of 17cm. The sample is placed on a single-yoke and a thin layer of glass-epoxy is placed on top of it. The setup is then placed on a car tube in order to reduce the effect of any external vibrations. Later, this setup was further studied by Nakase et al. and the accuracy of the measurements was re-investigated by a closed magnetic path (a closed type of SST) [39]. To improve the accuracy of the measurements even more an open magnetic path was suggested [40]. A comparison between the magnetostriction strain measurements by using a laser doppler vibrometer and a laser displacement meter was reported later [41]. The results showed a good agreement between the two, except for low magnetic flux densities.

  There are also some commercial magnetostriction strain measurement setups based on laser technique available in the market e.g. the setup of INTERMAGNET

Dr. Janosi [42] and Brockhaus measurements. The setup of INTERMAGNET Dr. Janosi is based on a laser displacement meter technique, while the Brockhaus setup has a laser vibrometer technique. In both setups the measurements are performed on a small reflecting surface which is mounted on the edge of the sample. A picture of the Brockhaus setup is shown in Fig. 3.2. Due to the out-of-plane vibrations of the sample the repeatability and the accuracy of the measurement results can be affected. Further on, in §3.5.2 the measurement principle of these setups will be compared with the laser setup developed in EELAB.

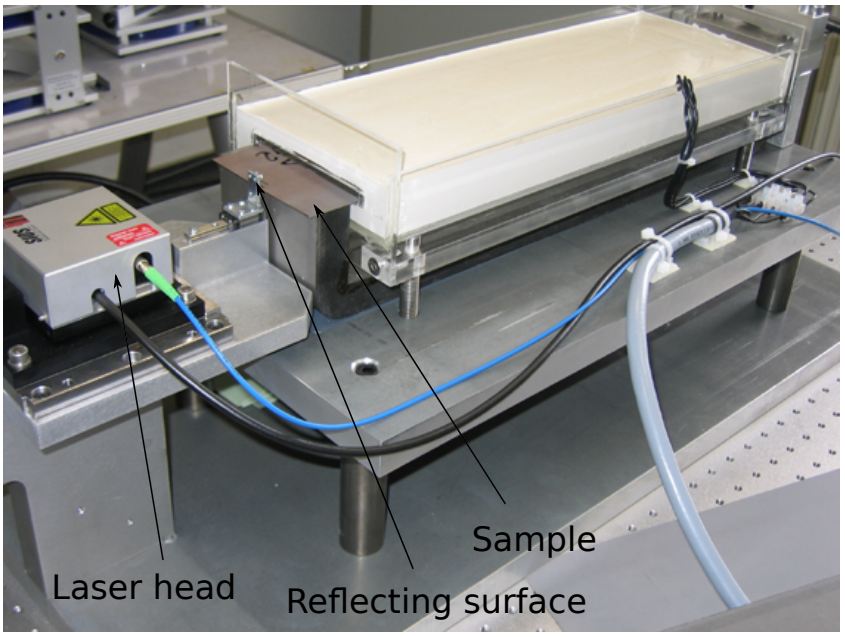

Figure 3.2: Magnetostriction measurement setup of Brockhaus measurements.

The International Electrotechnical Commission (IEC) released a report in 2010 regarding the general principles and technical details of the magnetostriction measurement of single sheet specimens and Epstein strip specimens [43]. The standard focuses on measurements by means of optical sensors and accelerometers. For single sheet specimens the intended sample size is preferred to be 50cm long and 10cm wide. The measurement results obtained by the setups developed in EELAB have not been compared with the IEC standards report. The difference among the setups and condition under which the measurements were performed do not allow a valid comparison.

3.3. General principles of the setups developed in EELAB

In this section, the general principles of the magnetostriction strain measurement setups developed in EELAB in the past and during this PhD study will be presented. The magnetisation condition, the magnetic flux path as well as the measurement approach will be explained. The designed setups are aimed at measuring the behaviour of electrical steel samples (Si-Fe) with deformations in the range of micro meter per meter length [μm/m]. Such measurement scale once again highlights the importance of an accurate setup. The setup developed in the past was based on the strain gauge technique and the setup developed during this PhD work is based on the laser technique. After introducing the general measurement principles, the two measurement setups will be presented in the next sections.

3.3.1 Magnetisation and measurement

- **Unidirectional magnetisation**
  In the framework of this research the measurements are performed under unidirectional excitation. With unidirectional excitation we mean that the time varying magnetic field is applied to the sample in one direction. For grain-oriented materials with application in transformers which is the focus of this research, the magnetic flux is almost always unidirectional along the transformer legs[2]. Also for the nonoriented materials, considering the isotropic properties[3], the response of the material to the magnetisation in one direction is similar to that under magnetisations at different directions. Thus, an unidirectional magnetisation can be sufficient to determine the magnetostrictive behaviour of electrical steel samples whether oriented or non-oriented.

- **Closed magnetic circuit**
  The area closed by the magnetic flux lines ϕ forms a magnetic circuit. A closed magnetic circuit refers to the case when the magnetic flux forms the closed loop entirely within a magnetic material. In this case, the magnetic material should have a high magnetic permeability. On the other hand, an open magnetic circuit refers to the case when the magnetic flux forms part of the closed loop thorough a magnetic material and the rest goes through a non-magnetic material, e.g. air. In an open magnetic circuit, compared to a closed one, a higher magnetisation field H is required to obtain the same magnetic induction B level. The reason is that the reluctance of the path will be higher and more stray fields will be present. In addition, the magnetic induction B may not be uniform everywhere along the magnetic circuit in the case of an open magnetic circuit. As a result,

[2] Except in the joint corners where the flux travels from one leg to another.

[3] There exists always some degree of anisotropy. However, nonoriented materials compared to the grain-oriented materials are regarded as isotropic.

the measurement of the magnetic induction B would have some uncertainty. Both the measurement setups developed in EELAB have a closed magnetic flux path (obtained by means of the SST method), which will be shortly explained.

- **Single Sheet Tester (SST)**
  In the SST approach, a closed magnetic flux path is ensured by means of two yokes, which have a low reluctance and high magnetic permeability. The sample is then placed between the two yokes, so that once the sample is magnetised, the magnetic flux forms a closed path through the two yokes. According to the IEC standards, the sample size in the SST should be 50cm$\times$50cm or larger [44]. However, smaller SSTs are comparable in accuracy and are often used especially because of a practical point of view as the components for the magnetic measurements are smaller. Indeed, a magnetisation coil must be wound around the sample, which is placed between the two yokes, to magnetise it, as shown in Fig. 3.3.

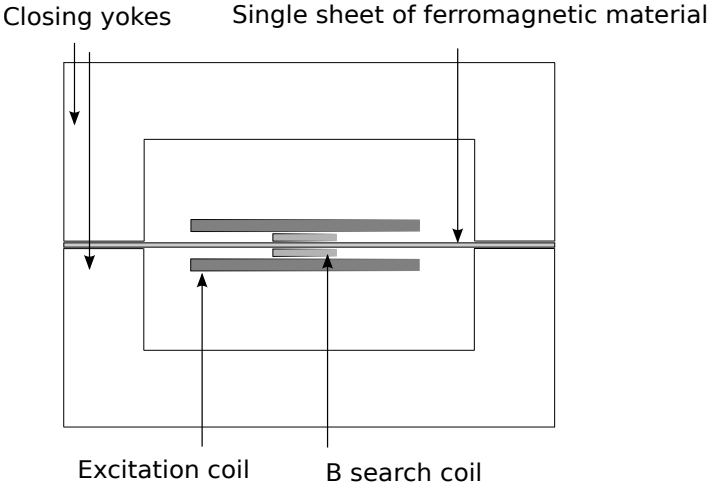

Figure 3.3: Schematic depiction of the magnetic measurement circuit with the SST method, in which the sample is embraced between two yokes with high magnetic permeability to provide a closed magnetic flux path. The magnetisation winding is wound around the sample and for the magnetic induction B measurement a search coil is also wound around the sample.

The SST measurement enables establishing a uniform magnetic flux along the sample, as shown in Fig. 3.4(a). The closing yokes avoid generation of the magnetic forces along the magnetic path length of the sample, which is the length closed by the inner sides of the yokes, as shown in Fig. 3.4(b). The magnetic forces exist on the sample sides where the yokes are placed on. However, since

these corners are out of the measuring length of the sample the presence of such forces are negligible. To this end, along the measurement length of the sample the only force present is due to the magnetostriction of the sample. This is necessary for the computation method which has been explained in chapter 2, considering the Chu model formulation.

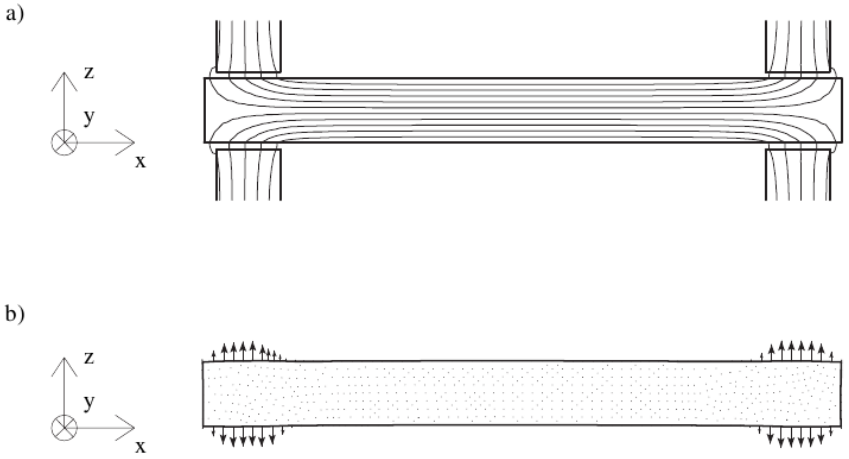

Figure 3.4: The sample in SST a) distribution of the uniform magnetic flux along the sample b) the presence of the magnetic forces only on the corners of the samples which are in contact with the yokes [18].

3.3.2 Setup scheme

The general principle of the magnetostriction measurement setups is shown in Fig. 3.5. The setup is fully steered from software programs written in *LabVIEW* version 8.5. By using a data-acquisition card (DAQ), which is plugged in the PC, analog-to-digital and digital-to-analog signal conversions are performed through a PXI platform. The *LabVIEW* user interface provides the possibility for the user to choose the signal type (e.g. sinusoidal), its frequency, amplitude and all the other parameters. Once a digital magnetisation waveform is generated in the *LabVIEW* user interface, it is first converted to analog and then amplified by using a power amplifier. The amplified signal is sent to the magnetisation coil in the SST. The magnetic induction B, the magnetic field H and the magnetostriction velocity signals are then measured. After analog signal processing, all the measured signals are converted to digital and sent back to the PC. All the signal calculations, post-processing and the visualisation of the signals are further processed in the *LabVIEW* software.

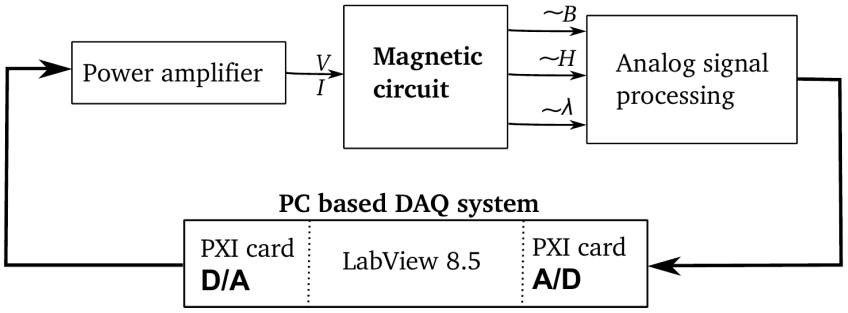

Figure 3.5: Schematic depiction of the magnetostriction measurement setups developed in EELAB.

3.3.3 Magnetic induction B measurement

The search coil method and the needle-probe method are common approaches to measure the magnetic induction B induced in a magnetic sample. The former method is used throughout this work. The search coil should feel the same flux ϕ as the sample and should therefore be placed as close as possible to the sample. If possible it is wound directly around it to avoid measurement errors.

Based on Faraday law, the induced voltage in the search coil V_{sc} is proportional to the time varying magnetic flux variation ($\frac{d\phi_{\mathrm{sc}}(t)}{dt}$) passing through the coil and the number of the turns of the search coil n_{sc}, as

$$V_{\mathrm{sc}}(t) = -n_{\mathrm{sc}} \frac{d\phi_{\mathrm{sc}}(t)}{dt}. \tag{3.2}$$

The induced flux density B_{sc} in the coil is the ratio of the flux ϕ_{sc} over the magnetic cross section A_{sc} of the sample. This means that we can calculate the flux density B_{sc} from the measured voltage over the search coil, as follows

$$B_{\mathrm{sc}}(t) = -\frac{1}{A_{\mathrm{sc}} n_{\mathrm{sc}}} \int V_{\mathrm{sc}}\, dt \tag{3.3}$$

To this end, the voltage measured over the search coil V_{sc} is integrated by an analog electronic integrator board. The output of the integrator V_{int} gives the following voltage

$$V_{int}(t) = -\frac{1}{RC} \int V_{\mathrm{sc}}\, dt \tag{3.4}$$

where R and C are a resistance and capacitance of the integrator board, the values of which are selected based on the measurement range. The RC combination are adjusted to give a gain of at least 10^2, in order to improve the accuracy of the analog signal before sending to the PC.

In the last step, once the integrated voltage V_{int} is sent to the PC it is divided by the magnetic cross section A_{sc} and the number of turns of the search coil n_{sc}, according to the 3.3, and the magnetic induction B_{sc} is obtained.

3.3.4 Effective magnetic field H measurement

The effective magnetic field H is measured either directly or indirectly. With the direct method, by using an H-sensor a local measurement of the magnetic field at the air gap close to the sample is performed. The effective magnetic field at the sample is determined then, knowing that the tangential component of the magnetic field is continuous across the sample and the air gap.

The approach used throughout this work is the indirect effective magnetic field measurement, as is common with the SST method. In fact, the effective magnetic field is calculated by knowing the magnetisation current. According to Ampère's law, if we have a current I going through the magnetisation winding with n_{mw} turns in a closed magnetic circuit with a magnetic path length of l_{mpl}, the effective magnetic field is

$$H(t) = \frac{n_{\text{mw}}}{l_{\text{mpl}}} I(t) \tag{3.5}$$

3.4. The magnetostriction measurement setup using strain gauges

The magnetostriction strain measurement setup developed in the past will be described in this section. As explained in §3.3.2, the setup is PC based and fully controlled through the *LabVIEW* software. The PC generated magnetisation waveform is first amplified and then sent to the excitation coil. The magnetostriction strains of the sample are measured by means of the strain gauges which are attached to the sample on the top and on the bottom. The strain gauges have two channels and are attached so that they measure the strains in the direction parallel ($\lambda_{\parallel}$) and perpendicular ($\lambda_{\perp}$) to the magnetisation direction simultaneously. The measurements are performed under no external stress and only as a function of the magnetic induction B[T]. To this end, a tiny air gap is provided on the sample sides to avoid the weight pressure of the top yoke on the sample. Any friction between the sample and the bottom yoke is eliminated by using Teflon tapes. The measured magnetostriction strains along with the magnetic induction B and the magnetic field H signals are sent to the PC. Since the strain gauges measure locally, where the gauges are attached, in fact even small samples are sufficient. The sample size for the SST designed for this setup is 6cm$\times$8cm large. A schematic of this setup is shown in Fig. 3.6.

An overview on the performance of this strain gauge setup, the advantages and the limitations of this setup are discussed further on.

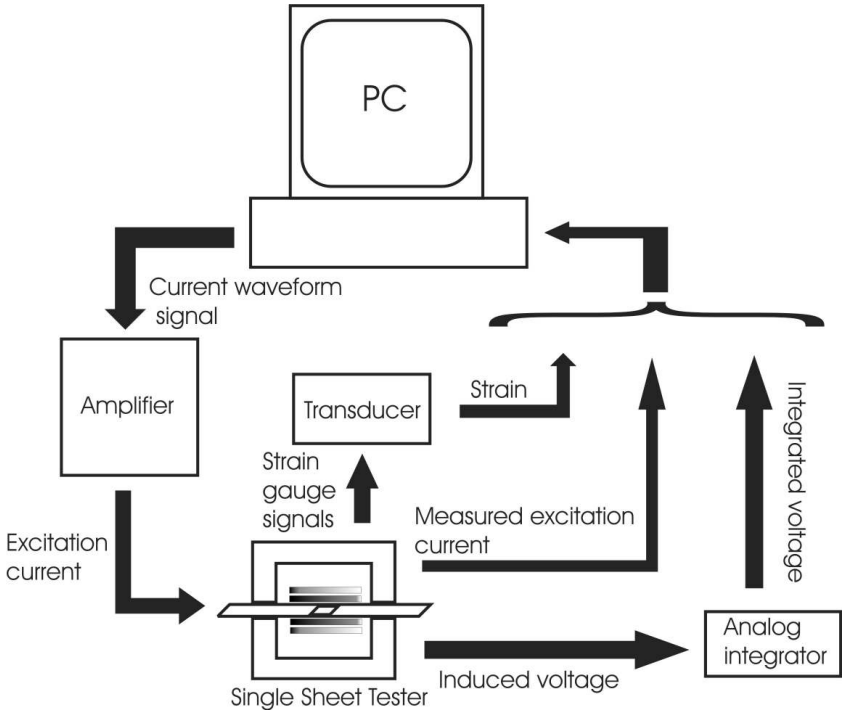

Figure 3.6: A schematic of the magnetostriction strain measurement setup based on the strain gauge technique.

3.4.1 The strain gauge setup advantages and limitations

The measurement results obtained by the strain gauge setup proved to be accurate and repeatable. Measurement results under a wide range of frequencies and amplitudes are reported in [18]. Another advantage of this setup is the possibility of two-dimensional magnetostriction measurements under a uni-directional magnetisation. Once a sample is placed in the SST, the strains in two directions, in parallel with and perpendicular to the magnetisation direction ($\lambda_{\parallel}$, $\lambda_{\perp}$), are simultaneously measured, which makes it rather easy and fast for the user.

On the one hand, the full contact of the strain gauges with the sample is advantageous because it results in repeatable measurements. On the other hand, if the gauges are not well attached to the sample, they may not follow the magnetostrictive strains of the sample well, which in turn causes measurement errors. To this end, for the measurements with this setup in EELAB, for a proper attachment of the strain gauges, the coating of the samples has been partially removed. However, the magnetostrictive behaviour of a coated sample of electrical steel is different from that of the non-coated one, especially in the case of grain-oriented materials. In fact, the magnetostrictive

behaviour of coated samples, as they are used as such for transformers and electrical machines cores, are of interest to us. Thus, the major limitation of the strain gauge setup is the inability to measure the behaviour of coated samples.

In addition, the sample preparation itself demands a lot of expertise, i.e. for removing the coating and attaching the strain gauges. Moreover, the measured strain signals must be filtered to eliminate the noise. To this end, several noise filters were programmed in the *LabVIEW* software. The measurements under low magnetic excitations ($B \leq 0.8$[T]) showed a lot of noise even after filtering. However, since for the application of the transformers, the magnetisation amplitude is higher that that (normally within the range of 1.2-1.4[T]), this problem at low excitations is not crucial.

3.4.2 Motivations for a new magnetostriction strain measurement setup

Considering the limitations of the strain gauge setup, there was a need to develop a new measurement method. Since the main cause of the limitations of the strain gauge setup was due to the contact of the strain gauges with the sample, a non-contact approach was preferred for the new setup. Lasers are commonly used for strain measurement, and since they do not require any contacts with the sample they could help to overcome the limitations of the strain gauge setup. Regarding the increasingly growing technologies of the laser vibration sensors which are designed for a vast amount of different applications and various measurement ranges e.g. [45], [46], such sensors are suitable candidates for the new setup. Moreover, they are compact, offer a user-friendly interface and provide high resolutions.

There are different types of vibrometers, such as: single-point, scanning and special vibrometers (e.g. for torsional vibration measurements). The measurement principles of a single-point vibrometer and scanning vibrometer are shown in Fig. 3.7. For the magnetostriction strain measurement, a single-point vibrometer is sufficient to measure the vibration at a single-point on an sample's surface. Polytec Industrial Vibrometer Sensor (IVS200) was chosen for our new magnetostriction strain measurement setup, which will be explained further on. Later on, in chapter 6 a Polytec laser scanning vibrometer is applied for the vibration measurement of a real transformer core.

3.5. The magnetostriction measurement setup using laser vibrometers

3.5.1 Principle of the Polytec Industrial Vibrometer Sensor (IVS200)

The IVS200 vibrometers are sensitive compact devices for non-contact vibration measurements. The optics and signal processing units are integrated inside the housing. Due to a non-contact approach, they do not mass load the vibrating object, which is an advantage for strain measurements. Moreover, the natural stiffness and damping of the

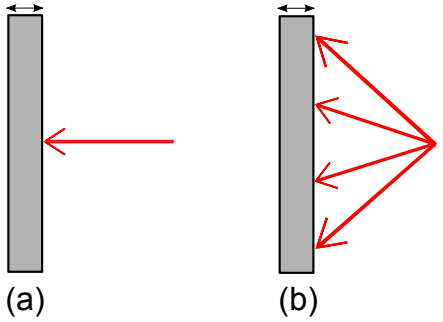

Figure 3.7: The measurement principle of (a) single-point vibrometer, (b) scanning vibrometer, where the red arrows show the laser signal and the black arrow show the direction of the movement of the object.

object do not change because of the measurement. The IVS belong to a type of Laser Doppler Vibrometers (LDV) which measures the instantaneous vibrational velocity of the object according to the heterodyne interferometer principle. The advantage of the heterodyne detection is that velocity is measured, not displacement: this makes the setup insensitive to slow motions caused by for instance thermal expansion of the sample. The beam of a helium neon laser is pointed at the vibrating object and then scattered back from it. A Doppler frequency shift of the back scattered light is demodulated to measure the velocity component. The Doppler frequency shift is described as

$$f_D = 2 \cdot |v_{\text{object}}| / \lambda_{\text{laser}} \tag{3.6}$$

where v_{object} is the moving object's relative velocity (with respect to the laser) and λ_{laser} is the laser wavelength. To calculate the velocity of the vibration, the (Doppler-) frequency shift should be performed at a known wavelength. In the sequel, the techniques behind the IVS200 vibrometer will be explained into some more detail.

Doppler effect

The Doppler effect is basically the frequency change of a wave for an observer relative to its source. A good example is the sound heard from a siren of a police car or an ambulance. The generated sound to an observer has a higher frequency when the vehicle comes closer, and a lower frequency when it drives away. Fig. 3.8, shows the effect when the source is moving to the left side. Once a wave is generated, the source moves to the left before it generates the second wave and as a result, the generated waves in front of the source are pressed together. The opposite happens to the waves behind the source which means that they are more apart or in another word, they have a lower frequency. This effect can be expressed in the following equation in a more general way

for a moving observer or a moving source or both. The relationship between observed frequency f_{observer} and the emitted frequency f_{emitted} is given by

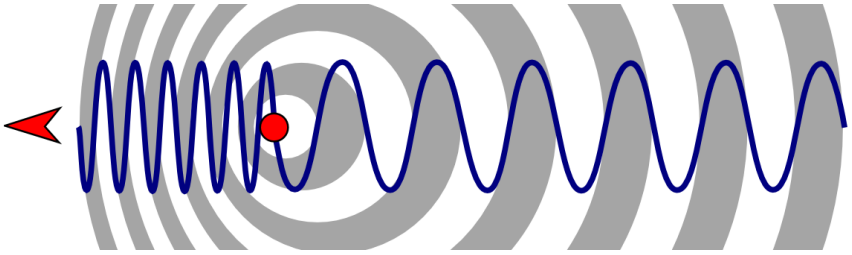

Figure 3.8: Doppler effect for a source moving to the left direction which as a result the waves in front of it are pressed together and the waves behind are far a part.

$$f_{\text{observer}} = \frac{c \pm v_{\text{observer}}}{c \pm v_{\text{source}}} f_{\text{emitted}} \tag{3.7}$$

where v_{observer} and v_{source} are the velocity of the observer and the source respectively. The variable c is the propagation velocity of the wave. The direction of movement of the observer and the source are indicated by the plus and minus sign. The source velocity v_{source} is subtracted if it moves toward the observer and added if it moves away. The observer velocity v_{observer} is subtracted if the observer moves away from the source and added if it gets closer.

For waves which need a medium (such as sound waves), the relative motion of observer and source with respect to the medium also needs to be taken into account. Since electromagnetic waves do not need a medium, this effect does not need to be taken into account, and a simple equation is obtained which only depends on the relative motion between source and observer.

Heterodyne interferometry

In general, interferometry refers to techniques to extract information of superimposed waves. In a heterodyne interferometer design, as shown in Fig. 3.9, the laser beam is first split in two beams, called reference beam and test beam. The test beam then passes through a second beam splitter and points at the vibrating object. Due to the Doppler effect the vibration of the object adds a Doppler shift to the frequency of the beam. After that the beam travels back to the second beam splitter and then goes through a third splitter, where it combines with the reference frequency. The combined beam reaches then a photo detector where they interfere. Due to the frequency difference between the two beams, a Frequency Modulated (FM) signal is generated. A demodulation of the FM signal delivers a signal which is proportional to the velocity of the vibrating object.

Since the Doppler frequency shift depends on the absolute value of the object velocity, as shown in 3.6, it is not possible to detect the direction of the object movement. The object moving away from the interferometer generates the same interference pattern (and frequency shift) as an object moving towards the interferometer. In order to detect the direction without any ambiguity, one of the interferometer beams needs to be shifted by a certain frequency that is higher than the maximum possible Doppler shift. To this end, an acousto-optic modulator (Bragg cell) is placed in one of the beams. The Bragg cell shifts the light frequency by a frequency f_B which is 70MHz for IVS200. As a result, it generates a modulation frequency of 70MHz when the object is at rest. In this way, when the object moves toward the interferometer, this modulation frequency is reduced and if it moves away from the vibrometer, the modulation frequency is increased (more than 70MHz). As a result, not only the amplitude but also the direction of the movement can be easily defined [47], [48].

Because the Bragg cell causes a fixed frequency shift of one of the beams (about 70MHz, as compared to the terahertz frequency of the optical carrier signal), a beat signal of that frequency is obtained on the detector when both beams interfere. If now the object moves, the probe beam gets an additional frequency shift due to the Doppler effect, which leads to a frequency modulation of the beat signal. If the object moves towards the vibrometer, the frequency of the beat signal increases, when the object moves away the beat signal decreases in frequency. The magnitude of the frequency change is linearly proportional to the object velocity in the direction of the probe beam. To obtain the velocity signal, the electrical signal of the photo detector is FM-demodulated. This delivers an electrical output signal which is linearly proportional to object velocity. When the amount of reflected light changes over time, the signal to noise ratio of the velocity signal may change, but the velocity calibration remains unaffected, which is a major advantage over homodyne interferometry techniques.

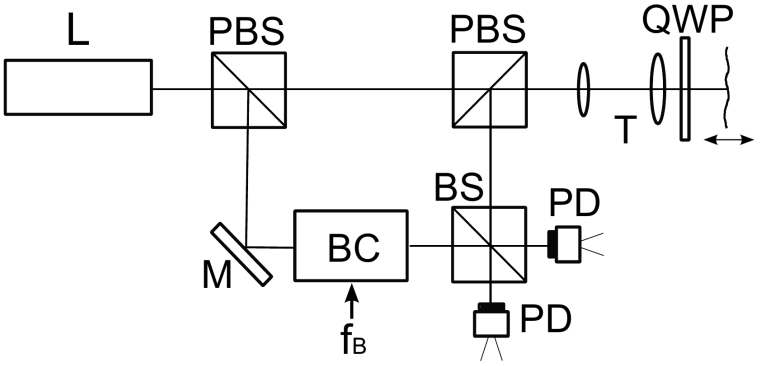

Figure 3.9: schematic of the optical arrangement of a heterodyne vibrometer. M is a mirror, BS is a beam-splitter, PBS is a polarising beam-splitter, L is a laser, QWP is a quarter-wave plate, PD is a photo detector, T is a telescopic lens array, and BC is a Bragg cell.

Laser resolution

Resolution, i.e. the smallest detectable magnitude of the desired measurement quantity, is a crucial parameter in laser vibrometry. In this work, the IVS200 vibrometers are adjusted for a measurement range (scaling factor) of 5mm/s/V with a full scale (peak) velocity of 20mm/s and the resolution of 1 μm/s for a bandwidth of 10Hz[4]. The time length of the measurements for the setup is 20ms.

3.5.2 The setup design

Laser beams path

Dual heterodyne laser vibrometers sensors are applied in the setup to measure the magnetostriction strains of the sample. To this end, two tiny pieces of aluminum (5mm$\times$5mm) are attached on the sample as mirrors to point the laser beam on. Aluminum has the advantage of low weight and non-magnetic properties, which as a result does not interfere the measurement accuracy. In the early design of the setups, the two aluminum pieces were placed in front of each other, each on one side of the sample, as shown in Fig. 3.10(a) [49], [50]. The distance l between the two mirrors M was then the measurement length of the sample. The difference between the velocity signals of the two vibrometers delivered the relative length change of the sample, e.g. the magnetostriction strains. However, due to the out-of-plane vibrations of the magnetised sample, the measurement results were unstable. Such approach is similar to that of the setup of INTERMAGNET Dr. Janosi and the setup of Brockhaus measurements. With a non-contact magnetostriction measurement technique the challenge is to achieve high accuracy and repeatability despite the sample vibrations. In fact, in this way the accuracy of the measurements can be affected by the vibrations of the sample.

Therefore the setup was adapted so that these mirrors were attached on the top and bottom sides of the sample at the end of the measurement length, while the sample was clamped on the other side of the measurement length. In this case, in fact the measurement length of the sample is the distance from the clamp side to the mirror side of the sample, as shown in Fig. 3.10(b). Knowing that the sample does not move on the clamped side, the average velocity of the two measured signals is used to calculate the deformation [51]. Moreover, with this arrangement of the mirrors if the magnetised sample slightly bends then one mirror moves toward and the other one moves far from the laser head. However, since the average of both velocities is calculated, the effect of the bending is canceled out. So only the true magnetostriction effect is measured.

[4] The resolution is defined as the signal amplitude (rms) at which the signal-to-noise ratio is 0dB in a 10Hz spectral bandwidth (RBW), measured on 3M Scotchlite Tape [48].

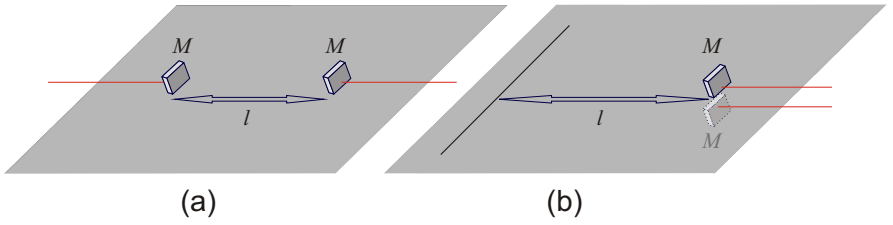

Figure 3.10: A sample with two mirrors attached on it where the laser beams are pointed. M stands for mirror and l stands for the measurement length of the sample, (a) the early design which turned out to be unrepeatable due to the out-of-plane vibrations (b) the adapted approach to cancel out the out-of-plane vibrations of the sample.

The SST and the sample placement

The size of the sample and the SST of the strain gauge setup was rather small (8cm$\times$6cm). Since the strain gauges measure locally, the sample size does not interfere with the measurement accuracy. However, for the laser setup the sensitivity of the measurements is proportional to the size of the sample and the measurement length [17]. In fact, on the one hand a longer measurement length results in a higher measurement accuracy. On the other hand, once the measurement length is too long, the out-of-plane movements of the sample grow and decrease the measurement accuracy. To this end, different SST sizes have been tried out and an optimal size was selected for the setup. The new SST is larger than that of the strain gauge setup (17cm$\times$17cm). The yokes are built from laminations with a high magnetic permeability to ensure a uniform magnetic flux in the sample.

With this setup the measurement of the magnetostriction strain of the sample is possible for one direction (at a time). In order to measure two-dimensional magnetostriction strains of the sample ($\lambda_{\parallel}$, $\lambda_{\perp}$), the SST needs to be turned 90° with respect to the laser beams. To this end, the yokes need to be placed in the setup so that for instance for the measurements of the parallel strains $\lambda_{\parallel}$ the beams reach the mirrors attached in that direction. Fig. 3.11 shows a top view of a sample and how it is placed on the bottom yoke in the SST. If the SST is placed so that the lasers measure the perpendicular magnetostriction strains $\lambda_{\perp}$, there is no problem for the beams to reach the mirrors, which are attached on the sample. However, for the parallel magnetostriction strains $\lambda_{\parallel}$ the laser beams need to pass through the yokes to reach the mirrors. To this end, two small holes are drilled on the yokes for the laser beam paths.

Since the drilled holes are very small compared to the size of the SST, the fringing flux because of the holes is small and negligible. For any measurement direction, the top yoke on the side of the mirrors is slightly lifted up to provide sufficient space for

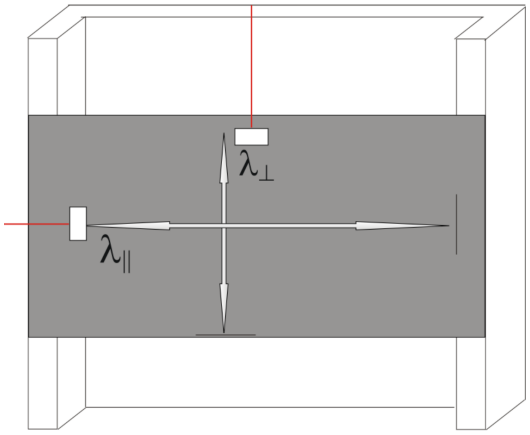

Figure 3.11: The measurement length and the laser beam path for a two dimensional magnetostriction strain measurement ($\lambda_\parallel$, $\lambda_\perp$) of a sample.

the sample to vibrate. Otherwise, the weight of the yoke works as an external stress and affects the measurement results.

The optical arrangement of the setup

The complete optical arrangement of the setup is shown in Fig. 3.12, showing the SST (without the top yoke) and the two laser vibrometers. The red lines show the laser beam paths to reach the two tiny aluminum pieces which are attached on the sample. The polarising beam splitter reflects one polarisation and transmits the other. As both lasers have the same polarisation direction, a half-wave plate is used to rotate the polarisation direction over 90° in one beam, so that it will be reflected by the beamsplitter. In this way the two laser beams can be combined very close and parallel to each other. Moreover, when the light is reflected by the object, each polarisation will again travel to its matching vibrometer, this preventing crosstalk between the two measurement channels. In a top view, as shown in Fig. 3.12, one might think that the beams leaving the cube in fact fall on each other. However, a side view would show that they are pointed at the two aluminum mirrors at different heights.

The idea is to have the beams from the lasers start at the same distance above or below the specimen, so that they are under the same angle. Once the beams reach the sample, if they are exactly retro-reflected, they follow the same path back to the vibrometer. However, considering that the two aluminum pieces may be tilted a bit, the reflections may not completely reach the vibrometers. In order to make sure that the reflections are received by the vibrometers, retro-reflective tapes are attached on the aluminum pieces. Such tape reflects the light in a broader angle which thus covers the mis-alignment of the aluminum pieces.

All these components are placed on an optical table, with a flat surface and interior honeycomb design. Such a table is designed for maximum stiffness and has an internal damping mechanism to minimise the effects of vibrations on the table surface. As the coherence length of the lasers is limited, the interference signal will be optimal with certain stand-off distances of the object from the laser source. The intensity can give a maximum visibility if the optical path is an even-numbered multiple of the laser cavity length (138mm). The optimal stand-off distances of the IVS200 are as follows

$$96\text{mm} + n.138\text{mm}, \quad n = 0,1,2,.. \tag{3.8}$$

For the installation of the mirrors and lasers and the SST position, the stand-off distance is taken into account to reach an optimal accuracy of the lasers [48].

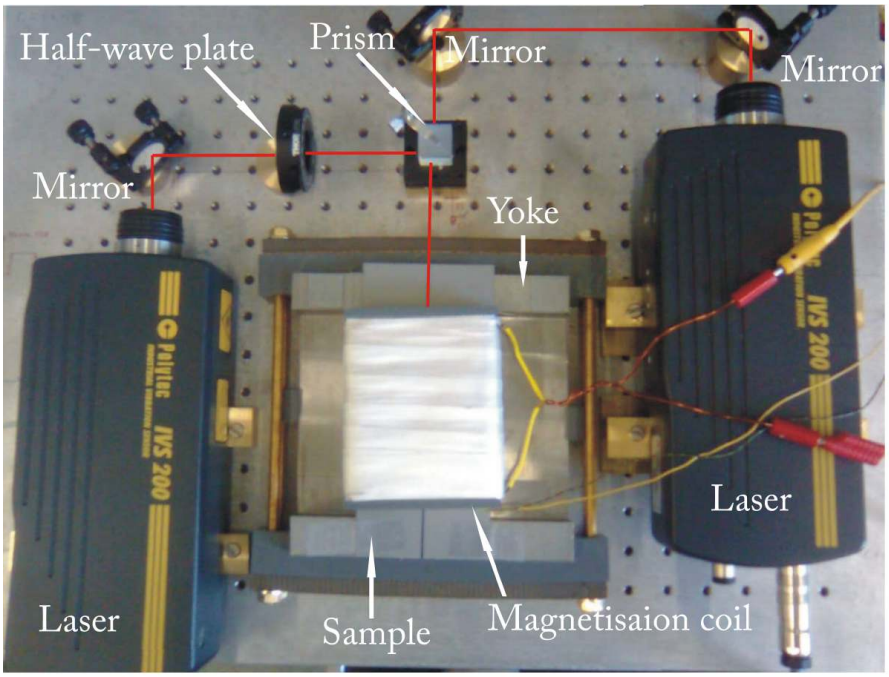

Figure 3.12: A honeycomb table, the SST and the lasers which their beams first reflect on the mirrors and then one passes through a half-wave-plate to rotate the polarisation. After that, both beams reach a cube in order to point on the two aluminum pieces which are attached on the sample.

The overall design of the setup

A general schematic of the magnetostriction strain measurement setup using dual heterodyne laser vibrometers is shown in Fig. 3.13. Similar to the strain gauge setup, a

PC-generated magnetisation waveform is first amplified and then sent to the magnetisation coil in the SST. The vibrational velocity signals of the magnetostriction strains of the sample are measured by using the laser vibrometers and sent back to the PC. In addition to the velocities, the magnetic induction B and the magnetic field H signals are measured.

The amplifier is a linear BOP (bipolar) DC power supply which has two control channels: voltage mode and current mode (36V and 12A). Depending on the amplifier mode, the magnetisation waveform is a current or a voltage signal. Further on, the *LabVIEW* programs for each magnetisation mode and the control algorithms will be explained.

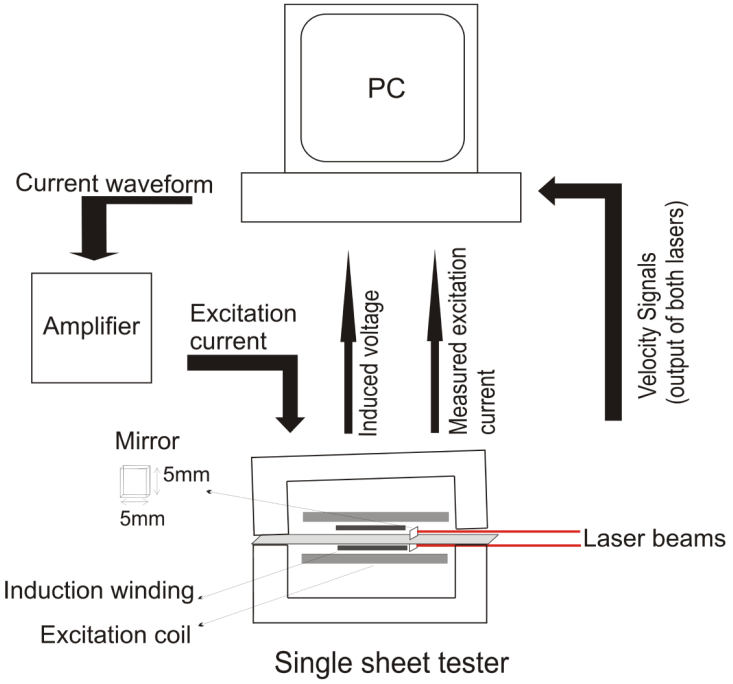

Figure 3.13: A schematic of the magnetostriction strain measurement setup based on the heterodyne laser vibrometer technique.

3.5.3 The *LabVIEW* programming

The setup controlling programs are performed in *LabVIEW* software version 8.5 . Two sets of programs are developed depending on the voltage or current magnetisation waveform, hereafter named as voltage-mode and current-mode, respectively. Since

the magnetostriction strains are directly related to the magnetisation waveform[5], the essence of the signal generation programs is to generate the desired magnetic induction B in the samples (e.g. if a sinusoidal magnetisation is desired, make sure that the induced induction in the sample is sinusoidal).

In addition, for the post-processing of the signals the *LabVIEW* programs are very useful. Since the magnetostriction strains are very small in amplitude, electromagnetic interferences can distort the actual electrical signal of the strain measurements. For the elimination of these electromagnetic interferences, a digital filtering is applied in the *LabVIEW* programs. In fact once a sample is magnetised, in the steady state only the even harmonics are relevant to the magnetostriction strains, see §2.6.5. Thus, all odd harmonics of the frequency of the applied magnetic field are removed from the spectrum of the measured strain signals by performing a Fast Fourier Transform (FFT) and reconstructing a time pattern by means of an Inverse Fast Fourier Transform (IFFT) of the even harmonics only [18], [52].

The algorithms of the programs to magnetise the samples will be overviewed here. For simplicity, only the case of a purely sinusoidal magnetisation will be explained. However, the programs are able to generate other magnetisation waveforms and even with higher harmonic components.

The voltage-mode magnetisation

In principle, the induced e.m.f. E is proportional to the magnetic induction B i.e. ($V \sim \frac{dB(t)}{dt}$), and thus the signal generation should be quite easy with the voltage mode. However, the voltage at the terminals not only contains the inductance ($E_L \sim L\frac{di(t)}{dt}$) but also the resistance drops. To this end, a *LabVIEW* program will compensate the voltage drop over the resistances. The amplitude of the desired voltage, which will be used to calculate the magnetic induction over the inductance, is as follows

$$|\frac{E}{E_L}| = \sqrt{\frac{(R_{\text{sum}}^2 + (L_{\text{coil}}\omega)^2)}{L_{\text{coil}}\omega}} \tag{3.9}$$

$$\phi = \tan^{-1}\frac{R_{\text{sum}}}{L_{\text{coil}}\omega} \tag{3.10}$$

where pulsation ω is $2\pi f$, and R_{sum} is the sum of the resistances i.e. resistance of the excitation coil R_{coil} and resistance of the connecting cables R_{cables}. So to have $E_L\cos(\omega t)$ over the inductance a magnetization signal of $E\cos(\omega t - \phi)$ needs to be generated (over the sum of the inductance and the resistances). To generate a magnetisation waveform with a higher harmonic component, (3.9) and (3.10) should be calculated separately for each harmonic and then added up. For instance, for the case

[5] In fact the magnetostriction strains depend on the magnetic flux density B induced in the material and not the magnetic field H.

of a sinusoidal magnetisation with a third harmonic, the final magnetisation waveform is the sum of the fundamental and the third harmonic.

On the other hand, when the inductance L_{coil} goes to saturation the magnetic field H and thus the magnetising current I are not sinusoidal any more (when the magnetic induction B is to remain sinusoidal). If H and I are not sinusoidal, the voltage drop over the resistances is not any more sinusoidal. Using a feedback of the observed shape of B, the sinusoidal character of B can be preserved. However, since we did not operate in the saturation region of the samples, the shape of the voltage waveform was not significantly affected.

A plot of the voltage-mode *LabVIEW* interface showing the measured magnetic induction B, magnetic field H and the magnetostriction strain $\lambda_{\parallel}$ is presented in Fig. 3.14. The B-H loop and the B-$\lambda_{\parallel}$ butterfly as well as the amplitude spectrum magnitude of the strains in the frequency domain are presented also.

The current-mode magnetisation

The magnetisation signal generation under the current-mode requires more steps than that of the voltage mode. In fact, the current signal I is proportional to the magnetic field H, based on the Ampère's law($\oint \bar{H} \cdot d\bar{L} = nI$). However, since the B-H relationship is nonlinear and shows hysteresis, the induced magnetic induction B in the sample thus differs from what the user has generated in the PC. Once again assuming purely sinusoidal magnetisation waveform, the measured magnetic induction B has a slightly different amplitude and form than that of the desired sinusoidal waveform. A feedback control algorithm is programmed in the *LabVIEW* software to iteratively correct the magnetisation waveform in order to obtain the correct magnetic induction, in both amplitude and shape [53]. A flow chart of the complete process to magnetise the sample and iteratively feedback control is shown in Fig. 3.18, and will be discussed after.

The software programmed in *LabVIEW* contains three sub-programs such as: a single measurement, amplitude and form control. We will describe it here with a purely sinusoidal magnetisation waveform, however, it works for every signal type.

1- **Single measurement:**
   - ▷ Start from a wanted magnetic induction with a sinusoidal shape, so-called the B wanted (B_{w})
   - ▷ Based on the anhysteretic B-H curve of the material (e.g. Fig. 3.15) and the B_{w} defined by the user, generate the wanted magnetic field (H_{w})(e.g. Fig. 3.16)
   - ▷ According to the Ampère's law and knowing the magnetic path length and the number of the turns of the excitation coil, calculate the current signal I
   - ▷ Send the current I and measure the magnetic induction and magnetic field response of the material, so-called B measured (B_{m}) and the H measured (H_{m})

2- **Amplitude control:**

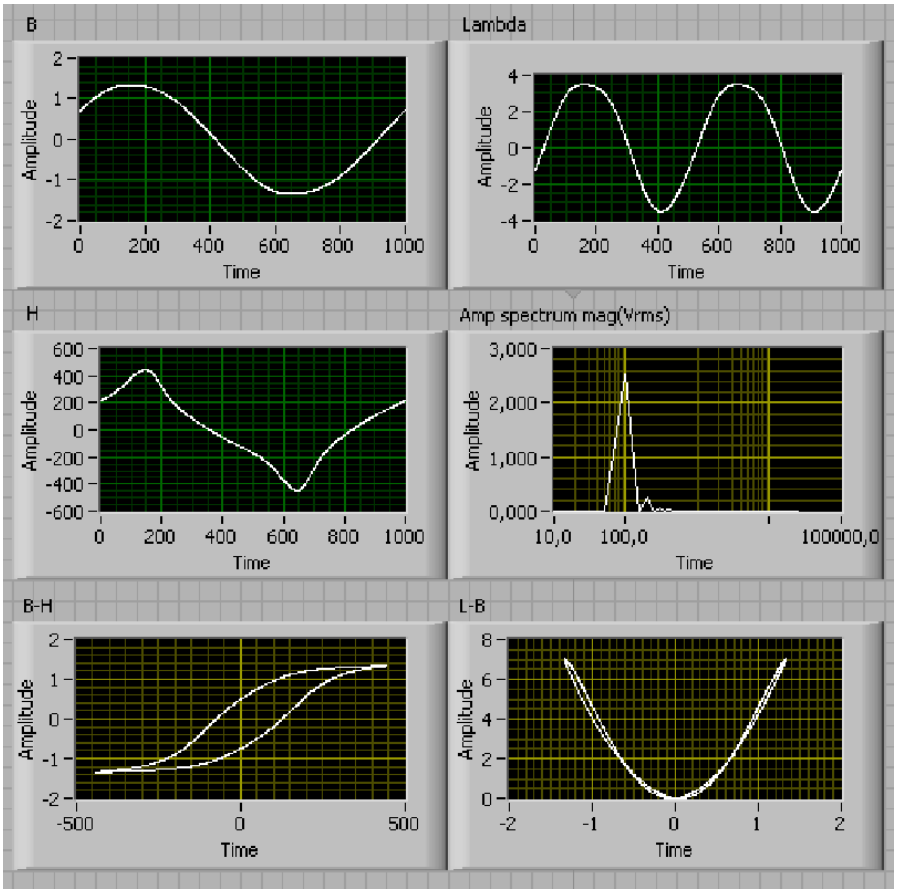

Figure 3.14: A plot of the voltage-mode *LabVIEW* window demonstrating: the measured magnetic induction B (top left), magnetostriction strain $\lambda_{\parallel}$ (top right), the magnetic field H (middle left), the amplitude spectrum of the strains in the frequency domain (middle right), the B-H loop (bottom left) and the B-$\lambda_{\parallel}$ butterfly loop (bottom right).

- ▷ Shift B_{m} and H_{m} to bring them in phase with the B_{w} which starts from a zero rising phase, as shown in Fig. 3.18
- ▷ Calculate the deviation of the peak value of the B_{w} with that of the B_{m}, so-called the amplitude deviation $\varepsilon_{\mathrm{amp}}$

$$\varepsilon_{\mathrm{amp}} = B_{\mathrm{w}_{\mathrm{peak}}} - B_{\mathrm{m}_{\mathrm{peak}}} \tag{3.11}$$

- ▷ If the $\varepsilon_{\mathrm{amp}}$ is smaller than an amplitude difference goal, selected by the user, then there is no need for the amplitude control. Otherwise, based on the previous magnetic field H_{w}, generate a new magnetic field signal $H_{\mathrm{w}_{\mathrm{new}}}$ according

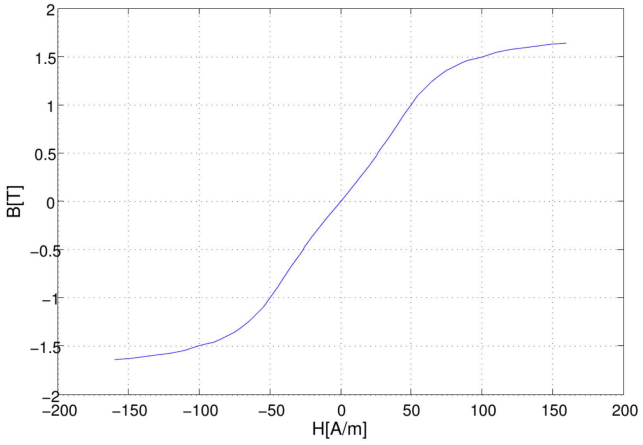

Figure 3.15: An anhysteretic B-H data of the material.

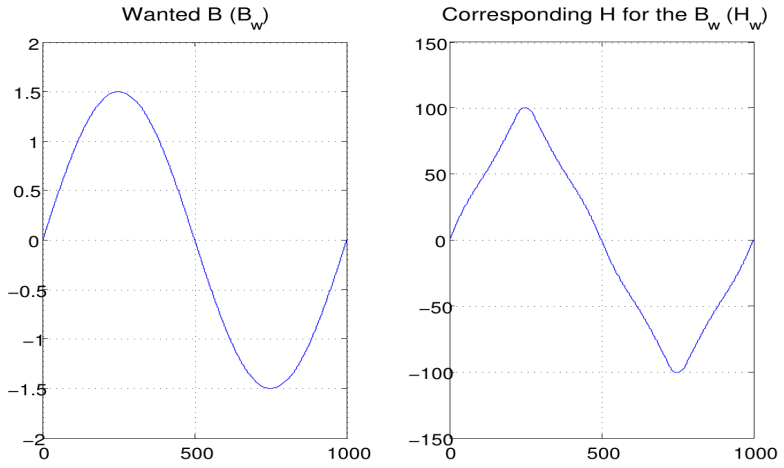

Figure 3.16: The magnetic induction B signal defined by the user and the corresponding magnetic field H which is generated based on the B and the anhysteretic B-H data of the material.

to

$$H_{\mathrm{w_{new}}} = (1 + K_{\mathrm{p}}\varepsilon_{\mathrm{amp}})H_{\mathrm{w}} \tag{3.12}$$

where K_{p} is a linear control variable defined by the user. Then, generate the corresponding magnetising current I and measure the response of the material (B_{m} and H_{m}) and go through the amplitude control again.

3- **Form control:**

- ▷ Generate a sub-array of the B_{m} and B_{w} which contains only the data of the falling branch of the waveforms from the positive peak to the negative peak. For a signal with 1000 samples per period, the sub-array has then 500 samples. Fig. 3.17 shows the complete waveform of a B_{m} (solid line) and B_{w} (dashed line) and the sub-arrays.
- ▷ Calculate the sum of the form deviations of each array element of the sub-array of the B_{m} compared to that of the sub-array of B_{w}, so-called the form deviation $\varepsilon_{\mathrm{form}}$

$$\varepsilon_{\mathrm{form}} = \sum_{i=1}^{500} |B_{\mathrm{w}}(i) - B_{\mathrm{m}}(i)| \tag{3.13}$$

- ▷ If the $\varepsilon_{\mathrm{form}}$ is smaller than the form difference goal, selected by the user, then there is no need for the form control. Otherwise, for every index i and the corresponding array element of the $B_{\mathrm{w,i}}$ find the array index x of the B_{m} for which its array element has the smallest difference, as

$$|B_{\mathrm{w}}(i) - B_{\mathrm{m}}(x)| = min \quad for\ i = 1:500 \tag{3.14}$$

- ▷ Re-arrange the sub-array of H_{m} waveforms according to the x indexes found in the previous step. Once again for a sub-array of 500 samples, the re-arranged H_{m^*} is as

$$H_{m^*}(i) = H_{\mathrm{m}}(x) \quad for\ i = 1:500 \tag{3.15}$$

- ▷ Construct a complete period of the re-arranged $H_{\mathrm{m}^*_{\mathrm{full}}}$ (array concatenation) where the first quadrant of the complete arrays are the negative of the second half of the sub-arrays. The second and the third quadrants of the complete arrays are the re-arranged sub-arrays. The last quadrant of the complete arrays are the negative of the first half of the sub-arrays.

$$H_{\mathrm{m}^*_{\mathrm{full}}} = [-H_{m^*}(250:500)]\mathrm{U}[H_{m^*}(1:500)]\mathrm{U}[-H_{m^*}(1:250)] \tag{3.16}$$

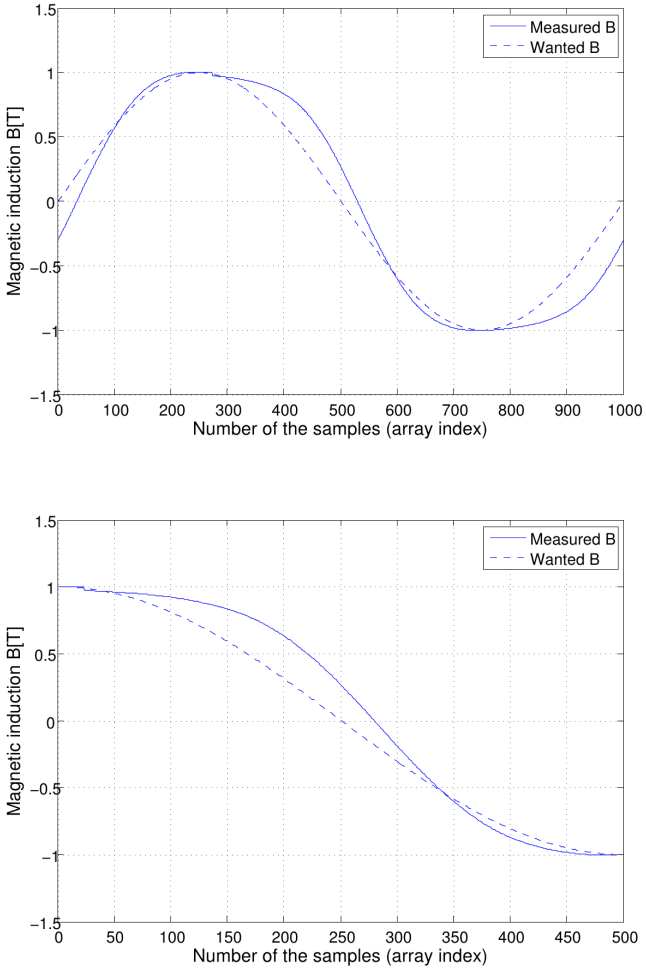

Figure 3.17: The plot of one period of the measured B (solid line) versus wanted B (dashed line) signals, as well as their sub-arrays of the falling branch (from positive peak to the negative peak) of the signals.

▷ Then, generate the corresponding magnetising current I and measure the response of the material (B_{m} and H_{m}) and go through the amplitude and form control again.

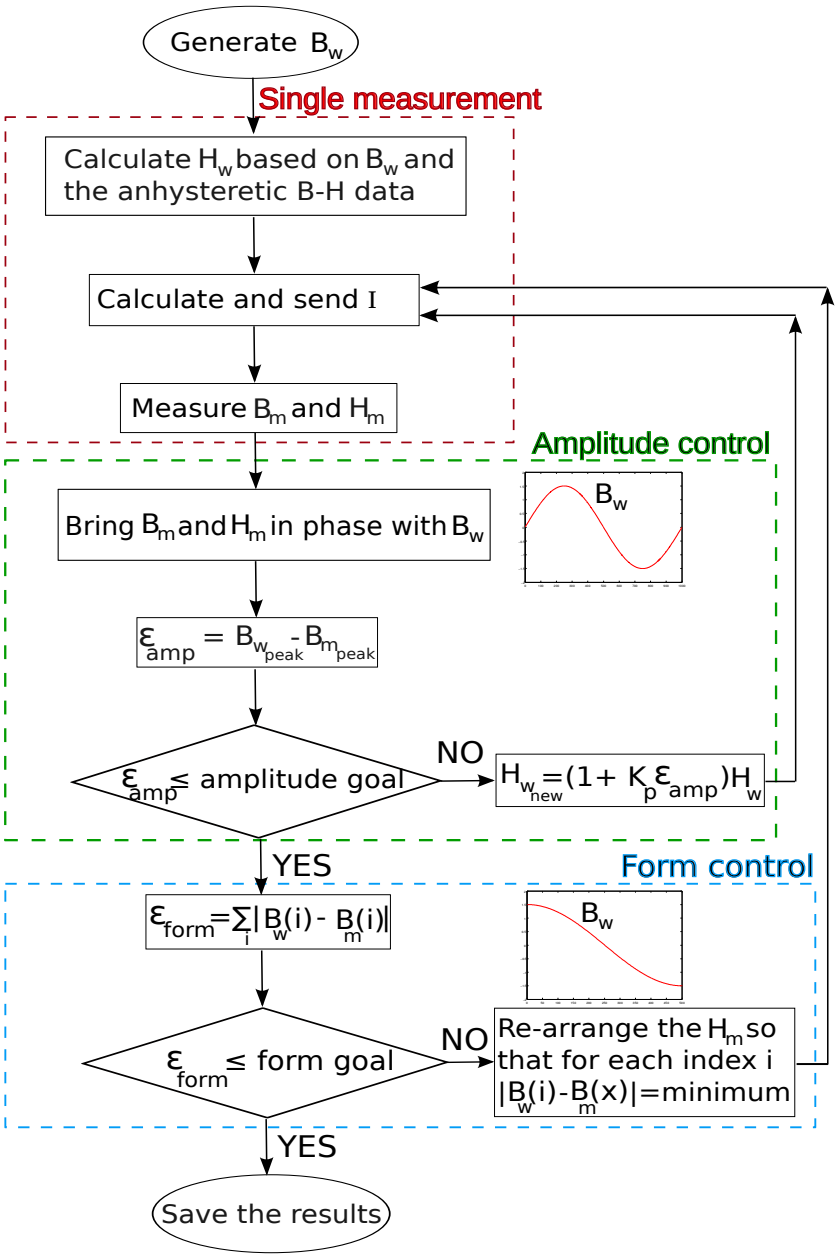

Figure 3.18: A flow chart of the current-mode magnetisation and the iterative feedback B control program which includes an amplitude and a form control algorithm.

3.6. Conclusion

In this chapter the measurement of the magnetostriction strain of electrical steel samples was discussed. The chapter started with an overview of the most often used strain measurement techniques and the conditions under which the measurements are performed.

Afterward the strain gauge setup developed in EELAB was presented. The advantages (e.g. high repeatability) and the limitations (e.g. the necessity of the coating removal of the samples to mount the strain gauges) of the setup were discussed. Then, the design of a new setup with a non-contact technique, based on heterodyne vibrometer, was presented in detail. The *LabVIEW* software program and the feedback controls to steer the setup were reported at the end.

The measurement results obtained by the laser setup and a comparison with that of the strain gauge setup will be presented in the next chapter.

CHAPTER 4

Measurement results

4.1. Introduction

In this chapter the measurement results obtained by the heterodyne laser setup on grain-oriented and nonoriented electrical steel samples will be presented. First, the results of different materials under a purely sinusoidal magnetisation will be presented. To make a comparison with the strain gauge setup, the behaviour of the non-coated samples are measured by the laser setup and then compared with the results obtained by the strain gauge setup. Next, the results of the coated samples are compared with those of the non-coated samples of the same material which are both measured by the laser setup. Based on the measurement results, the effect of the coating on the magnetostrictive deformations will be discussed for both grain-oriented and nonoriented electrical steel.

The focus of this PhD research is on the magnetostrictive deformation of transformer core materials. Since in reality there are always some higher harmonics present on the electricity grid, the effect of these harmonics on the magnetostriction should be studied. To this end, the magnetostrictive behaviours of some different materials are measured under a sinusoidal magnetisation with a third harmonic component, the results of which will be presented in this chapter. In the last section, the effect of the fifth harmonic on a grain-oriented material will be presented. Such results are applied to calculate the deformation of a three-phase test transformer core which will be presented in chapter 7.

4.2. Purely sinusoidal magnetisation

4.2.1 Non-coated samples

As a comparison between the two setups developed in EELAB, the strain gauge and the laser setups, the magnetostriction strains of samples of electrical steel have been

measured by both setups. Since with the strain gauge setup the coating of the sample was required to be locally removed, the coating of the samples with the laser setup were also removed. The magnetostriction strains $\lambda_{\parallel}$ versus the magnetic induction B, the butterfly loops, for a nonoriented electrical steel sample and a grain oriented sample have been measured. The nonoriented material is a material of which the laminations are coated only on one side. It has a thickness of 0.7mm. The grain-oriented material is a 3% Si-Fe cut from laminations of 0.9W/kg losses at 1.5T and 50Hz, hereafter called as GO-I. For the nonoriented material the measurements are performed under a magnetisation with peak magnetic induction of 1T and 0.6T and a frequency of 50Hz, as shown in Fig. 4.1 and Fig. 4.2, respectively. The behaviour of the GO-I material under a magnetisation with a peak magnetic induction of 1T and a frequency of 50Hz is shown in Fig. 4.3. The solid line shows the result obtained by the laser measurement and the dashed line shows the results of the strain gauge setup. As explained in the previous chapter, only even harmonics of the excitation frequency appear in the magnetostriction response. Therefore we removed the possible odd harmonics (arising due to noise).

Looking at the even harmonics, for a 50Hz excitation, the dominant frequency response is 100Hz which is twice the magnetisation frequency. In addition, for the measurement results by the strain gauge setup, the data in the frequency spectrum are filtered for harmonics higher than 40 times the base frequency before reconstructing the time pattern. Looking at the dashed line butterfly loops, still some noise can be observed. The noise influence is relatively larger for the measurements under magnetisation with peak amplitude smaller than 0.8T and thus these results are less accurate. In Fig. 4.2, the magnetostriction strains measured by using the strain gauge setup for a magnetic induction of 0.6T are highly influenced by noise even after filtering. Such filtering is not applied for the laser measurement and is not needed. The laser setup provides magnetostriction strain measurements under a magnetisation with peak amplitudes as low as 0.5T and shows a high accuracy. One of the advantages of this setup over the strain gauge setup is thus the significant reduction of noise in the measured data [54].

4.2.2 Coated samples

The measurement results on the coated samples show less deformation than those of non-coated samples. The coating is used to isolate the laminations and reduce losses. However, it also applies tension to the material, which as a result decreases the deformation. Fig. 4.4 shows the measurement results on a coated and non-coated sample of the same nonoriented material, both measured by using the laser setup. The coated sample shows around 20% less deformation, which proves that the coating tensile stress is beneficial in the reduction of the deformation.

A similar measurement for the GO-I material shows a significant difference between the results on the coated sample with those of the non-coated, as shown in

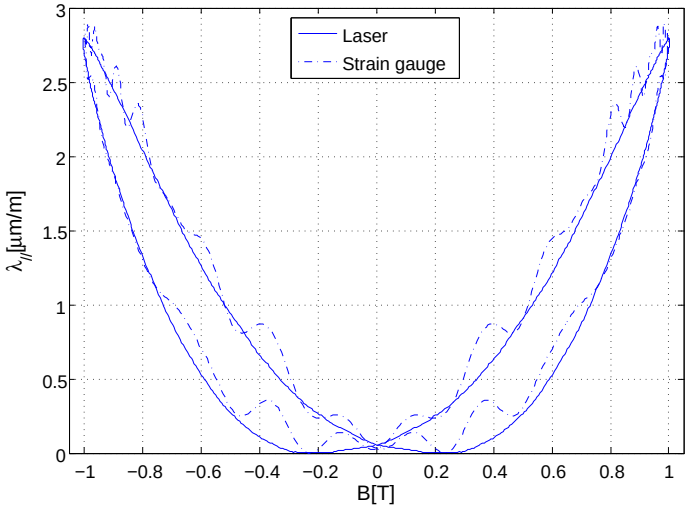

Figure 4.1: The magnetostriction strains of a non-coated sample of nonoriented electrical steel by using the strain gauge setup and the heterodyne laser vibrometer setup under a magnetic induction of B_{peak}=1T and f=50Hz.

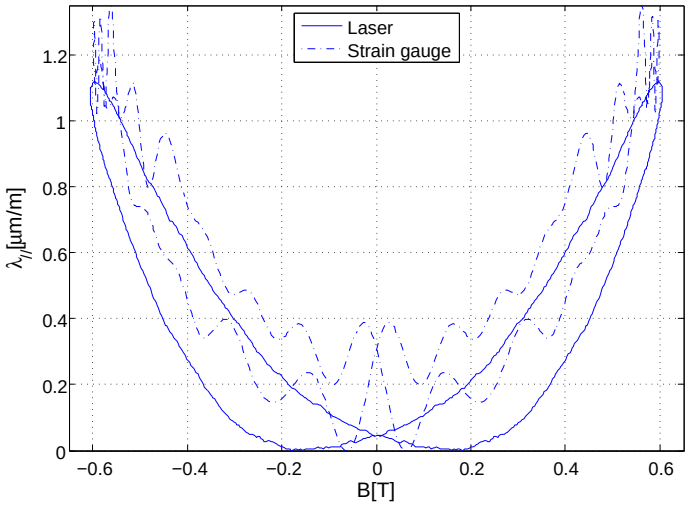

Figure 4.2: The magnetostriction strains of a non-coated sample of nonoriented electrical steel by using the strain gauge setup and the heterodyne laser vibrometer setup under a magnetic induction of B_{peak}=0.6T and f=50Hz.

Fig. 4.5. The results show that the magnitude of the deformations is much larger for the non-coated sample compared to the coated sample. In fact, as explained in 2.3.2,

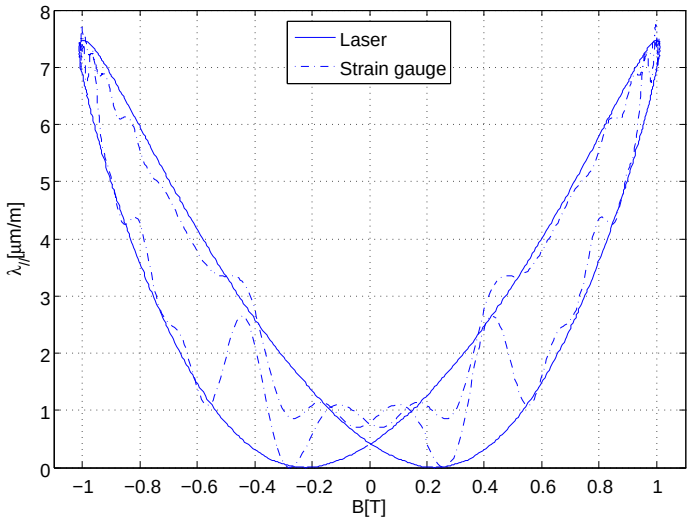

Figure 4.3: The magnetostriction strains of a non-coated sample of grain-oriented electrical steel by using the strain gauge setup and the heterodyne laser vibrometer setup under a magnetic induction of B_{peak}=0.6T and f=50Hz.

the coating tensile stress especially reduces the magnetostriction strains of the grain-oriented materials. The domain structure and the magnetostrictive behaviour of the grain-oriented materials have been studied in detail e.g. [7].

To further investigate the effect of the coating on the magnetostrictive behaviour of the nonoriented materials, the measurements were carried out on three other materials. The samples were cut from laminations of M800 with 1% Si, M470 with 1%-2% Si and M350 with 2%-3% Si, which have 8, 4.7 and 3.5W/kg losses at 1.5T and 50Hz, respectively. The thickness of the laminations of all three materials was 0.5mm. For each material type, two sets of samples were prepared. To the first type belong the samples with their length cut along the rolling direction of the material (to magnetise in the rolling direction). The second type were cut along the transverse direction (to magnetise in the transverse direction) of the material. In the sequel we indicate these as RD and TD respectively. The magnetostriction strains along the magnetisation direction $\lambda_{||}$ are measured under a magnetic induction of 1.2T, 1.1T and 1T and a frequency of 50Hz on both coated and non-coated samples. For each data point, the measurements are carried out on two samples and the average data are calculated, as shown in Table. 4.1. Table 4.2 shows the ratio of the magnetostriction strains of the non-coated to that of the coated samples of the data of Table. 4.1.

The results clearly demonstrate that the difference between the magnitude of the deformation for coated and non-coated samples is lower for nonoriented material than that of the GO-I material. Whereas the ratio of the magnitudes for the non-coated and coated samples can attain 15 for GO-I material, for the nonoriented materials this ratio

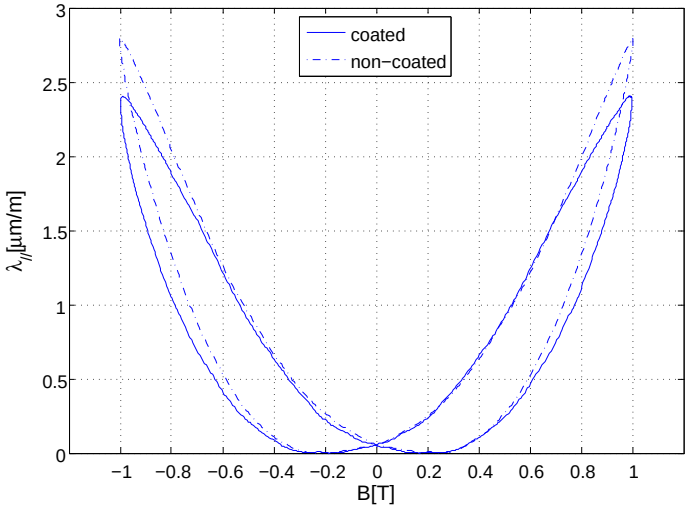

Figure 4.4: The magnetostriction strains of the sample of nonoriented electrical steel, coated and non-coated, measured with the heterodyne laser vibrometer setup under a magnetic induction of B_{peak}=1T and f=50Hz.

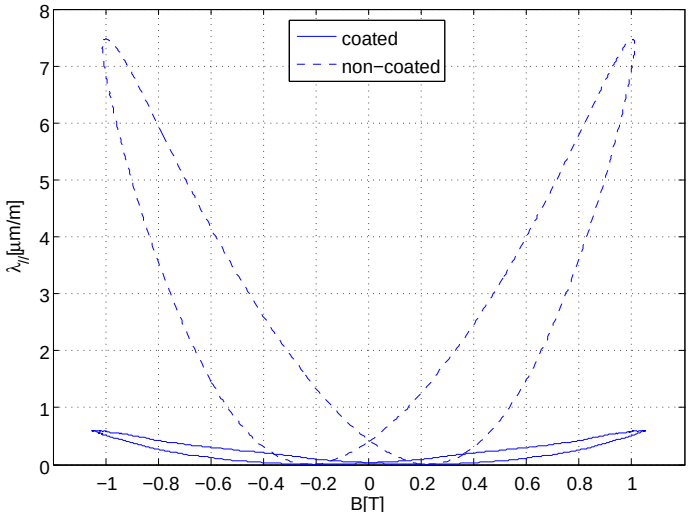

Figure 4.5: The magnetostriction strains of the same sample of grain-oriented electrical steel, coated and non-coated, measured with the heterodyne laser vibrometer setup under under a magnetic induction of B_{peak}=1T and f=50Hz.

is lower than two. The reason behind it is in fact the domain structure of the material and the closure domains with 90° domain walls which have been discussed in §2.3.2.

Table 4.1: The peak-to-peak magnetostriction strains of the three nonoriented materials along the RD and the TD directions on both coated and non-coated samples under the excitations of B=1.2T (first row), 1.1T (second row) and 1T (third row).

$\lambda_{\parallel}[\mu m/m]$	M800, 1%Si	M470, 1%Si-2%Si	M350, 2%Si-3%Si
RD, coated	1.17 0.91 0.78	0.82 0.83 0.57	1.36 1.03 0.83
RD, non-coated	1.73 1.38 1.07	1.53 1.3 1.08	2.79 2.18 1.65
TD, coated	6.45 5.48 4.44	5.21 4.36 3.69	5.67 4.83 3.92
TD, non-coated	6.48 5.48 4.86	6.01 5.02 4.26	7.22 6.22 5.23

Table 4.2: The ratio of the magnetostriction strains of the non-coated samples to that of the coated samples of the data of Table. 4.1.

$\lambda_{\parallel}$	M800, 1%Si	M470, 1%Si-2%Si	M350, 2%Si-3%Si
RD, non-coated/coated	1.48 1.52 1.37	1.87 1.57 1.89	2.05 2.12 1.99
TD, non-coated/coated	1.00 1.00 1.09	1.15 1.15 1.15	1.27 1.29 1.33

Another observation is that the measured strains for the non-coated grain-oriented material are significantly larger compared to the nonoriented material. Also, it can be concluded that the coating has more effect when we magnetise in RD than TD.

Although we expected to obtain a decrease of magnetostriction with the increase of percentage of Si [21], this has not been observed for the samples of M350. This might originate from the different production process of these samples. However, future studies are still needed for further understanding this difference.

4.3. Sinusoidal magnetisation with a higher harmonic component

Looking at the magnetostriction deformation in transformers, the studies so far have mostly focused on the behaviour under well known excitation waveforms, e.g. purely sinusoidal excitation [7], [8], [55], [18], and [36]. In practice, the voltage waveform of the electrical power grid is not purely sinusoidal. There are always some higher harmonics present, which are caused by nonlinear voltage-current characteristics of the loads connected to the grid. Looking at the industrial loads, power converters (rec-

tifiers) and variable speed drives are well known examples of nonlinear loads. Over the past years, an increase of nonlinear loads connected to the grid has consequently caused an increase of the harmonics in the grid [56].

Harmonic currents generated by nonlinear loads can cause overheating and failure of the transformers. To protect against overheating caused by harmonics, the transformer designers specify oversized transformers by a rating called K-factor. As a result, the transformers run at a fraction of their rated capacity and thus withstand harmonic contents. There have been several studies on the effect of the higher harmonics on the operation of transformers e.g. [57]. However, it is useful to identify how such higher harmonics contribute to the magnetostriction noise. In another word, to find the relationship between harmonics present in the magnetisation signal and those in the magnetostriction signal. Previously, some research on the effect of the higher harmonics on the magnetostrictive behaviour has been reported, where only harmonics in phase with the fundamental harmonic, under an external stress are studied [58]. However, the influence of the higher harmonics of the magnetic field with different phase delays with respect to the fundamental, on the magnetostrictive behaviour has not been well identified in the past.

The influence of the third and the fifth harmonics are studied in this work. To this end, for the generation of the magnetisation signal, the amplitude of the higher harmonic on the magnetic field is defined as a percentage of that of the fundamental component, e.g. 10%. To identify the phase delay θ_n between the fundamental and the higher harmonic, the zero crossing of the fundamental is taken as reference point, according to

$$B_1 \sin(2\pi f t) + B_n \sin(n(2\pi f t) + \theta_n) \tag{4.1}$$

where B_1 and B_n are the amplitude of the fundamental and the higher harmonic components, respectively. n is the number of the higher harmonic e.g. n=3 stands for the third harmonic. The fundamental frequency f, is assigned to be 50Hz, the grid frequency in Europe. Fig. 4.6 shows a sinusoidal signal with a fundamental component with an amplitude of 1.3T and a third harmonic with 8% amplitude of that of fundamental with a phase delay of 0° and 90° (with respect to the fundamental component) and the sum of the two. Thus, the sum is sent to magnetise the sample.

The obtained measurement results will be presented in the following sections and the resulting application for the calculation of the magnetostrictive deformation of a transformer core will be given in chapter 7.

4.3.1 Third harmonic

The magnetostrictive behaviour of samples of grain-oriented and nonoriented electrical steel was measured under both purely sinusoidal magnetic inductions and inductions with a third harmonic component. The nonoriented materials were M350 and M470, as has been previously presented. Two grain-oriented materials were mea-

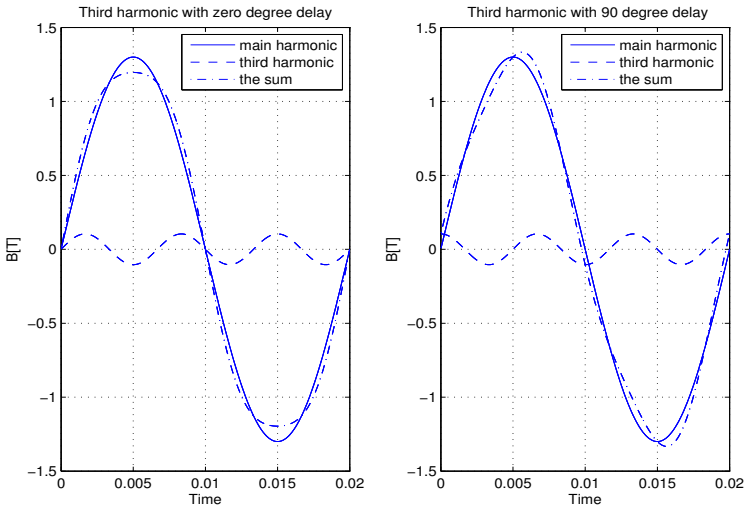

Figure 4.6: Magnetic induction with a fundamental component (1.3T) and the third harmonic (8%ratio) which has a delay of 0° and 90 °.

sured: GO-I (see §4.2.1) and samples cut from laminations with a loss of 1W/kg at 1.5T and 50Hz, which we will refer to as GO-II. Both grain-oriented materials had a thickness of 0.3mm. The amplitude of the fundamental harmonic of the magnetisation signal was varied between 1.1T, 1.2T and 1.3T. These magnetic induction levels correspond to the knee of the *B-H* hysteresis loop of the materials. Since the measurement results for each induction level have a similar behaviour, the data of the 1.3T fundamental for the different material types will be presented here. The amplitude of the third harmonic on the magnetic induction goes from 3% to 8% of that of the fundamental component, in steps of 1%. Such values are selected based on measurements by the European standards report [56]. The third harmonic has been delayed from 0° to 180° in steps of 30° with respect to the fundamental component.

For each magnetisation, the data of at least five measurements are averaged. The magnetostriction strains measurement results are post-processed in the frequency domain. Looking at the Fourier spectrum, harmonics with a frequency higher than five times the base frequency are very small and hence can be neglected. Since only the even harmonics are relevant, a database of only the second (100Hz) and the fourth harmonics (200Hz) of the magnetostriction strains in rms value is made [59].

Nonoriented M350 50A

The magnetostriction measurement results of the nonoriented sample of M350 under a purely sinusoidal excitation with a fundamental harmonic amplitude of 1.3T and

50Hz excitation show an amplitude of 0.284 and 0.048[μm/m] for the 100Hz and 200Hz components, respectively. The measured results under a magnetisation with the same fundamental harmonic and with a third harmonic are presented in Table 4.3. The 100Hz data are also illustrated in Fig. 4.7.

The results for the 100Hz component show that in general the magnitude increases with higher phase delay of the third harmonic from 0° to 180° phase delay. The reason for this can be attributed probably to the increase of the peak value of the magnetisation signal, as the phase variation from 0° to 180° between the main and the third harmonic of the magnetic induction changes the peak value of the magnetisation signal, which is sent to magnetise the sample. For the case of 0° delay, this peak value is lower than the fundamental component and so is the 100Hz component. Further increase of the phase delay up to 180°, causes the peak value of the magnetisation signal and as a result the 100Hz component to increase significantly, as seen in Fig.4.7. Other possible effects of harmonics aside, one might conclude that the magnetostriction mainly depends on the peak value of the excitation and thus both on the amplitude and phase of the harmonic with respect to the fundamental. To illustrate the variation of the 100 and 200Hz components, the percentual difference of the measured data of Table 4.3, compared with that of a purely sinusoidal excitation are presented in Table 4.4. We observe a significant variation of the 100Hz component when comparing the results of the 0° delay and the 180° delay. For the 3% third harmonic, this percentage variation across the measurement range is almost 24%. However, for the 8% third harmonic, it is almost 54%, which is substantial.

Table 4.3, b) shows the 200Hz components under a magnetisation with the third harmonic. These values are almost always larger than that of the purely sinusoidal magnetisation, except for 0° delay. For the third harmonic with 3% ratio, the percentage variation of the 200Hz component compared with that of a purely sinusoidal shows an increase of almost 70% going from 0° to 180° delay. For a third harmonic with a 8% ratio, this increase is more than 150%. Since the value of the 200Hz component is remarkably lower than the 100Hz component, it affects the magnetostriction behaviour less compared to the 100Hz component. As a result, mainly the variations of the 100Hz component should be considered to study the magnetostrictive behaviour.

Grain-oriented GO-II

The measurement results of the grain-oriented sample of GO-II under a purely sinusoidal excitation with a fundamental harmonic amplitude of 1.3T and 50Hz excitation show an amplitude of 0.213 [μm/m] for the 100Hz component and 0.013[μm/m] for the 200Hz component. The measured results under a magnetisation with the same fundamental harmonic and the third harmonic are presented in Table 4.5, and the 100Hz data are also illustrated in Fig. 4.8.

The measurement result of this material, shows a similar behaviour as that of the nonoriented sample of M350. The 100Hz component increases with a larger phase delay of the third harmonic from 0° to 180°, compared with the data of the purely

Table 4.3: The magnitude of the magnetostriction strains [μm/m] under sinusoidal excitations with a fundamental component amplitude of B=1.3T, 50Hz and the third harmonic (3% to 8% amplitude ratio and 0° to 180° phase delay) for the nonoriented sample of M350 a) 100Hz component, b) 200Hz component.

a) 100Hz component,
where the value under purely sinusoidal excitation is 0.284

	0°	30°	60°	90°	120°	150°	180°
3%	0.238	0.235	0.244	0.283	0.294	0.296	0.307
4%	0.220	0.234	0.245	0.287	0.289	0.310	0.330
5%	0.223	0.223	0.253	0.287	0.306	0.315	0.320
6%	0.221	0.211	0.235	0.288	0.306	0.313	0.332
7%	0.204	0.217	0.232	0.281	0.306	0.329	0.352
8%	0.198	0.213	0.223	0.290	0.311	0.327	0.351

b) 200Hz component,
where the value under purely sinusoidal excitation is 0.048

	0°	30°	60°	90°	120°	150°	180°
3%	0.036	0.045	0.059	0.065	0.074	0.069	0.069
4%	0.031	0.047	0.060	0.074	0.072	0.076	0.075
5%	0.033	0.050	0.071	0.079	0.085	0.088	0.086
6%	0.034	0.056	0.070	0.086	0.096	0.098	0.092
7%	0.041	0.059	0.077	0.088	0.098	0.105	0.102
8%	0.042	0.061	0.083	0.100	0.113	0.118	0.115

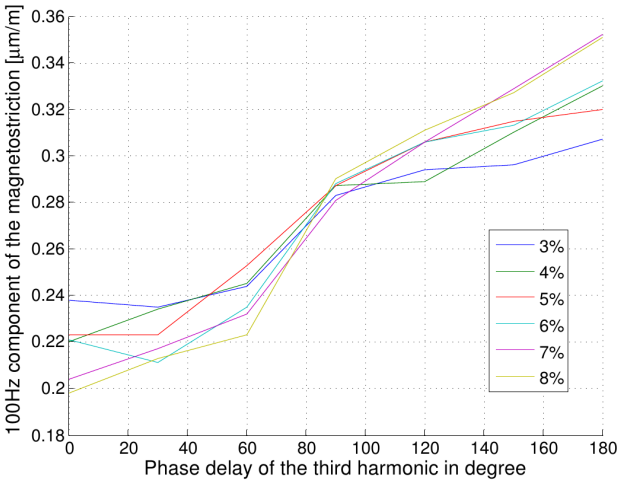

Figure 4.7: The magnitude of the 100Hz component of the magnetostriction strains [μm/m] under sinusoidal excitations with a fundamental component amplitude of B=1.3T, 50Hz and the third harmonic (3% to 8% amplitude ratio and 0° to 180° phase delay) for the nonoriented sample of M350.

Table 4.4: The percentual difference of the 100Hz and 200Hz components of the data of Table 4.3, a) and b) respectively compared with that of purely sinusoidal magnetisation.

a) 100Hz component,

	0°	30°	60°	90°	120°	150°	180°
3%	-16%	-17%	-14%	0%	4%	4%	8%
4%	-23%	-18%	-14%	1%	2%	9%	16%
5%	-21%	-21%	-11%	1%	8%	11%	13%
6%	-22%	-26%	-17%	1%	8%	10%	17%
7%	-28%	-24%	-18%	-1%	8%	16%	24%
8%	-30%	-25%	-21%	2%	10%	15%	24%

b) 200Hz component,

	0°	30°	60°	90°	120°	150°	180°
3%	-25%	-6%	23%	35%	54%	44%	44%
4%	-35%	-2%	25%	54%	50%	58%	56%
5%	-31%	4%	48%	65%	77%	83%	79%
6%	-29%	17%	46%	79%	100%	104%	92%
7%	-15%	23%	60%	83%	104%	119%	113%
8%	-13%	27%	73%	108%	135%	146%	140%

sinusoidal magnetisation. The percentage variation of the measured data (shown in Table 4.5) compared to those for a purely sinusoidal magnetisation are shown in Table 4.6. For a 0° delay of the third harmonic, the 100Hz component is lower than that under a purely sinusoidal magnetisation, whereas increasing the phase delay up to 180° shows an increase of the 100Hz component. For the 100Hz component, the variation of the delay from 0° to 180° results in a large magnetostriction increase. For the 3% third harmonic we observe an increase of 16%. For a 8% third harmonic however, the increase amounts to 50%.

The 200Hz components for a magnetisation with the third harmonic are shown in Table 4.5, b) and the percentage variation compared to those for a purely sinusoidal are shown in Table 4.6. In general, the effect on the 200Hz components is larger than for the 100Hz component. For the 3% third harmonic, we observe a variation of 70% for a phase delay variation from 0° to 180°. For a 8% third harmonic, this variation amounts to 85%.

Comparison of GO-II and M350 materials

Comparing the two material types of grain-oriented and nonoriented, the observations can be summarised as follows. As known, since magnetostriction is larger for the nonoriented materials, the 100Hz components of these samples are larger than those of grain-oriented materials. With both materials, the larger the phase delay of the third harmonic, the larger the value of the 100Hz component. This increase can be significantly large if the third harmonic ratio is high. However, the growth from 0° phase delay to 30° is rather small, especially if the relative value of the third har-

Table 4.5: The magnitude of the magnetostriction strains [μm/m] under sinusoidal excitations with a fundamental component amplitude of B=1.3T, 50Hz and the third harmonic (3% to 8% amplitude ratio and 0° to 180° phase delay) for a grain-oriented sample of GO-II a) 100Hz component, b) 200Hz component,

a) 100Hz component,
where the value under purely sinusoidal excitation is 0.213.

	0°	30°	60°	90°	120°	150°	180°
3%	0.200	0.200	0.210	0.219	0.222	0.230	0.235
4%	0.192	0.196	0.204	0.215	0.235	0.229	0.232
5%	0.180	0.180	0.198	0.217	0.231	0.222	0.250
6%	0.175	0.195	0.195	0.217	0.243	0.237	0.251
7%	0.173	0.182	0.199	0.217	0.230	0.251	0.257
8%	0.171	0.182	0.200	0.229	0.249	0.258	0.277

b) 200Hz component,
where the value under purely sinusoidal excitation is 0.013.

	0°	30°	60°	90°	120°	150°	180°
3%	0.011	0.006	0.013	0.015	0.019	0.023	0.020
4%	0.013	0.012	0.014	0.023	0.021	0.026	0.026
5%	0.016	0.018	0.019	0.025	0.033	0.030	0.034
6%	0.019	0.021	0.024	0.028	0.033	0.035	0.035
7%	0.025	0.025	0.030	0.039	0.040	0.040	0.043
8%	0.032	0.032	0.034	0.045	0.042	0.046	0.043

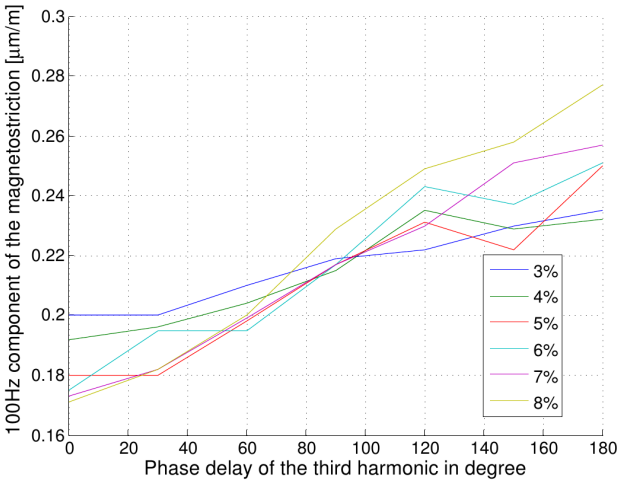

Figure 4.8: The magnitude of the 100Hz component of the magnetostriction strains [μm/m] under sinusoidal excitations with a fundamental component amplitude of B=1.3T, 50Hz and the third harmonic (3% to 8% amplitude ratio and 0° to 180° phase delay) for the grain-oriented sample of GO-II.

Table 4.6: The percentage variation of the 100Hz and 200Hz components of the data of Table 4.5, a) and b) respectively compared with that of purely sinusoidal magnetisation,

a) 100Hz component.

	0°	30°	60°	90°	120°	150°	180°
3%	-6%	-6%	-1%	3%	4%	8%	10%
4%	-10%	-8%	-4%	1%	10%	8%	9%
5%	-15%	-15%	-7%	2%	8%	4%	17%
6%	-18%	-8%	-8%	2%	14%	11%	18%
7%	-19%	-15%	-7%	-2%	8%	18%	21%
8%	-20%	-15%	-6%	8%	17%	21%	30%

b) 200Hz component.

	0°	30°	60°	90°	120°	150°	180°
3%	-15%	-54%	0%	15%	46%	77%	54%
4%	0%	-8%	8%	77%	62%	100%	100%
5%	23%	38%	46%	92%	154%	131%	162%
6%	46%	62%	85%	154%	154%	169%	169%
7%	92%	92%	131%	200%	208%	208%	231%
8%	146%	146%	162%	246%	223%	254%	231%

monic is low, e.g. lower than 6%. For the 200Hz component, the measured data of the grain-oriented sample with a third harmonic are relatively larger than those for the nonoriented samples. Of course, these magnetostriction effects of harmonics on the magnetisation signal might be quite material-dependent.

Comparison of GO-I, GO-II, M350 and M470 materials

In addition to the M350 nonoriented and GO-II grain-oriented material, the 100Hz component for the magnetostrictive behaviour of two other materials such as: the grain-oriented GO-I and the nonoriented M470 were investigated as well. Table 4.7, a), shows the data under the same magnetisation with a 8% third harmonic. For these materials, the same trend for the increase of the 100Hz component with the increase of the phase delay is observed, as well.

The main effect of the third harmonic turns out to be a change of the peak value of the magnetisation signal. And indeed, the measurement results for a sinusoidal magnetisation with 1.1T amplitude are similar to the results under magnetisation with 1T fundamental and a 10% third harmonic with 180° phase delay. The two magnetisation waveforms are shown in Fig. 4.10, which illustrate the same peak amplitudes. These results for the four materials are shown in Table 4.8.

4.3.2 Fifth harmonic

The magnetostrictive behaviour of the GO-I material was measured under a sinusoidal magnetisation with a fifth harmonic component. The strains along and perpendicular

Table 4.7: The magnitude of the 100Hz component of the Fourier spectrum of the magnetostriction strains for four different materials under a purely sinusoidal magnetisation (B=1.3T, f=50Hz) and with a third harmonic (8% amplitude ratio and 0° to 180° phase delay).

a) 8% third harmonic present

	0°	30°	60°	90°	120°	150°	180°
NO M350	0.198	0.213	0.223	0.290	0.311	0.327	0.351
NO M470	0.160	0.215	0.224	0.243	0.256	0.278	0.308
GO-II	0.171	0.182	0.200	0.229	0.249	0.258	0.277
GO-I	0.235	0.254	0.271	0.318	0.338	0.355	0.360

b) Purely sinusoidal magnetisation versus
a 8% third harmonic variations from 0° to 180° phase delay

	purely sinusoidal	third harmonic (180° - 0°)
NO M350	0.284	54%
NO M470	0.267	55%
GO-II	0.213	50%
GO-I	0.291	43%

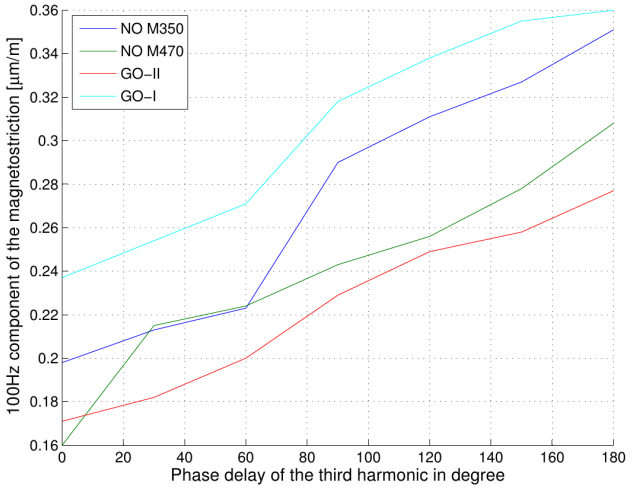

Figure 4.9: The magnitude [μm/m] of the 100Hz component of the Fourier spectrum of the magnetostriction strains for four different material under a sinusoidal magnetisation (B=1.3T, f=50Hz) with 8% third harmonic.

to the magnetisation direction are measured $\lambda_{\parallel}$ and $\lambda_{\perp}$, respectively. Similar to the measurements with the third harmonic, for the fifth harmonic measurements various combinations of amplitudes and phase delays of the fifth harmonic (with respect to the fundamental harmonic component) were considered. The frequency of the fundamental harmonic of the magnetisation signal is taken as a constant of 50Hz. The amplitude of the fundamental harmonic of the magnetic induction B is measured from 0.5T to

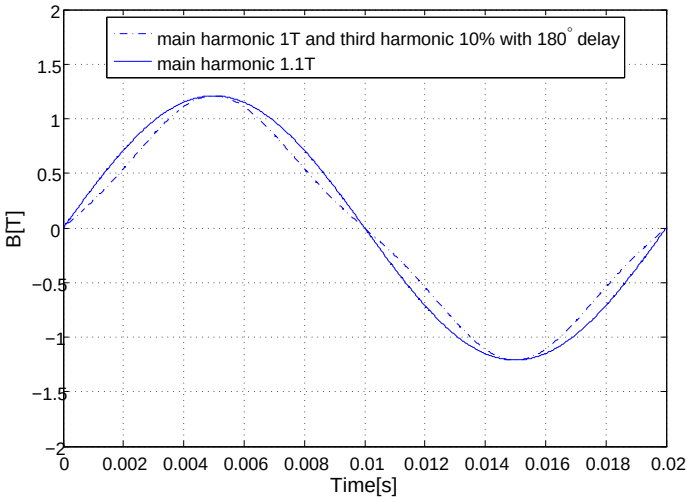

Figure 4.10: The magnetisation waveform for a sinusoidal waveform with a main harmonic of 1T and 10% third harmonic with 180° phase delay and a purely sinusoidal magnetisation with 1.1T.

Table 4.8: The magnitude of the 100Hz component of the Fourier spectrum of the magnetostriction strains for four different materials under a purely sinusoidal magnetisation (B=1.1T, f=50Hz) and with 1T fundamental and a third harmonic (10% amplitude ratio and 180° phase delay).

	purely sinusoidal	10% third harmonic (180°)
NO M350	0.179	0.191
NO M470	0.194	0.193
GO-II	0.107	0.116
GO-I	0.211	0.217

1.6T in steps of 0.1T. For each amplitude of the fundamental harmonic, the amplitude of the fifth harmonic has been varied from 1% to 10% of that of the fundamental in steps of 1% (in total 10 steps). The phase delay of the fifth harmonic has been changed from 0° delay to 360° delay in steps of 30° (in total 12 steps). This means that for each amplitude of the fundamental harmonic 120 different combinations of the fifth harmonic component were generated. For each of these combinations, five measurements were performed and the average data were calculated.

Fig. 4.11 shows the magnetostriction strains $\lambda_{\parallel}$ measured under a magnetic induction with a fundamental amplitude of 1.5T. The y ordinates show the magnitude and the phase of the 100Hz and 200Hz of the frequency spectrum of the strains. The abscissae are the number of the variations of the fifth harmonic (120) ordered as follows. The first twelve data points stand for 1% fifth harmonic with 0° to 330° delays, respectively. The second twelve data points correspond to fifth harmonic with 2% amplitude and 0° to 330° phase delays and so forth up to 10% fifth harmonic.

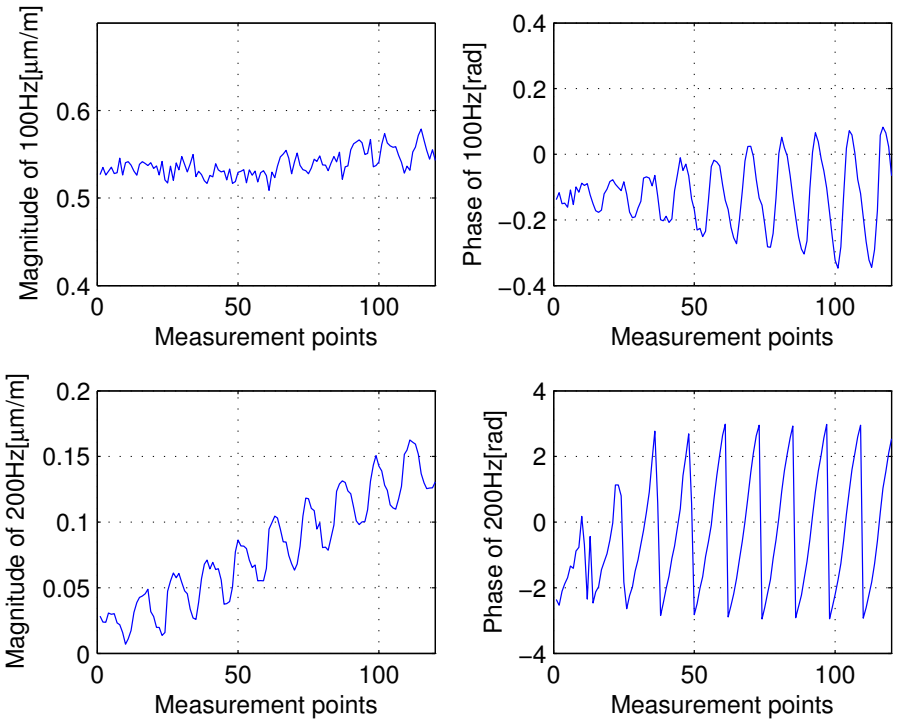

Figure 4.11: The magnitude and phase spectrum of the 100Hz and 200Hz harmonics of the magnetostriction strains ($\lambda_{\parallel}$) under a sinusoidal magnetisation with a fundamental amplitude of 1.5T and a fifth harmonic component which varies from 1% to 10% amplitude of the fundamental (1.5T) with a phase delay of 0° to 330° (with respect to the fundamental harmonic component).

Looking at the results of the 100Hz magnitude, with higher percentage of the fifth harmonic a slow increase is observed. However, neither the increase of the percentage of the fifth harmonic nor the variation of the phase delay of the fifth harmonic show a periodic variation of the magnitude of the 100Hz harmonic of the magnetostriction strains. The phase of the 100Hz harmonic of the magnetostriction strain shows a cyclic variation: more with the increase of the percentage of the fifth harmonic. In fact, for each percentage the phase of the 100Hz goes first to a negative peak and then a positive peak in a shape of a (negative) sinusoidal waveform in function of the phase delay from 0° to 330°.

Regarding the 200Hz harmonic of the magnetostriction strains, with an increase of the percentage of the fifth harmonic of the magnetisation signal an increase of the 200Hz harmonic magnitude is observed. Moreover, both the magnitude and the phase show clear periodic variations as a function of the phase delay. For each percentage of the fifth harmonic, with the variation of the phase delay of the fifth harmonic from 0° to 330° delay a cyclic variation of the magnitude of the 200Hz is observed, which

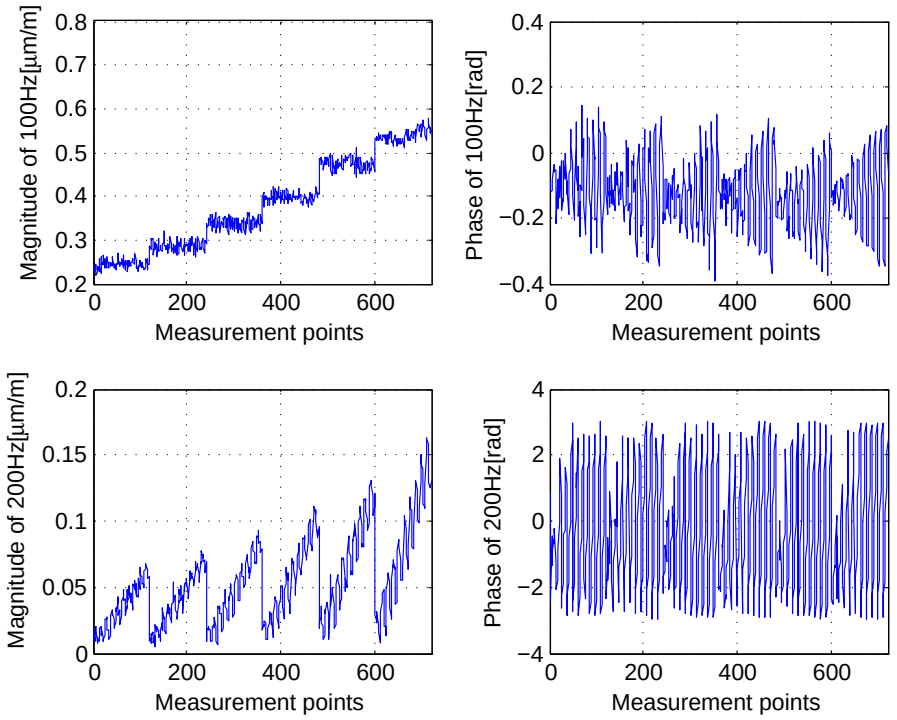

Figure 4.12: The magnitude and phase spectrum of the 100Hz and 200Hz harmonics of the magnetostriction strains ($\lambda_{\parallel}$) under a sinusoidal magnetisation with a fundamental amplitude of 1.1T to 1.6T and a fifth harmonic component which varies from 1% to 10% amplitude of the fundamental with a phase delay of 0° to 330° (with respect to the fundamental harmonic component).

goes first to a positive peak and then a negative peak in a shape of a sinusoidal. The phase variation of the 200Hz is also periodic which compared with that of the 100Hz reaches much higher angles.

Fig. 4.12 shows the 100Hz and 200Hz harmonics of the magnetostriction strains under magnetisations with a fundamental harmonic amplitude of 1.1T to 1.6T and a fifth harmonic with 1% to 10% amplitude of the fundamental. The phase delay has been varied from 0° to 330° (with respect to the fundamental harmonic component). The abscissae data are as an extra step coming from Fig. 4.11 but for six different fundamental amplitudes. As observed, the variations are similar for every fundamental harmonic amplitude of the magnetic induction B. Moreover, the larger the amplitude of the fundamental harmonic, the more the variations of the 200Hz magnitude of the strains.

Data interpretation

In general, for the measurements with a third harmonic component on the magnetisation signal the 100Hz magnitude of the magnetostriction strains in function of the percentage and the phase delay of the higher harmonic were larger and more clear than those with the fifth harmonic component on the magnetisation signal. For both measurements with a third and fifth harmonic, the 200Hz magnitude shows a significant change in function of the phase delay which is relatively much larger than that of the 100Hz. In fact, the application of the higher harmonics on the magnetisation signal affects more the higher harmonics of the magnetostriction strains. This means that the influence on the 200Hz harmonic of the magnetostriction is more than that on the 100Hz.

Previously, for the measurements under a magnetisation with a third harmonic component, a phase delay from 0° to 180° (between the third and the fundamental harmonic) was considered. The sum of the fundamental and the third harmonic had the lowest peak value for the case of 0° delay. For a 180° delay, the third harmonic was added up into the fundamental and the largest amplitude was reached. Looking at the obtained magnetostriction strains, a direct relationship between the peak value of the magnetisation signal (the sum of the fundamental and the third harmonic) and the magnitude of the harmonics of the magnetostriction strains was found. A higher amplitude of the magnetisation signal resulted in a higher magnitude of the magnetostriction strains.

The amplitude variation of the magnetisation signal for a measurement with a fifth harmonic component is different than that with a third harmonic component. The fifth harmonic is added up into the fundamental for a delay of 0° where the peak value of the sum is the lowest for a 180° delay. The trend between the amplitude of the magnetisation and the magnitude of the harmonics of the magnetostriction is less clear for different phase delays. However, once the amplitude of the higher harmonic increases the magnitude of the strains also increases, specifically for the 200Hz harmonic.

4.4. Conclusion

The magnetostrictive deformation of several grain-oriented and nonoriented electrical steel samples are measured by using the dual hererodyne laser vibrometer setup. For a purely sinusoidal magnetisation waveform, a comparison between the measured results obtained by the laser setup and those with the strain gauge setup on a set of non-coated samples shows similar amplitudes of the magnetostriction strains. However, the results with the laser setup are more accurate (with less noise), especially under magnetisations with small amplitudes e.g 0.5T. The magnetostrictive behaviour of the coated and non-coated samples, which are measured by using the laser setup, showed that the coating limits the magnetostrictive deformations. For the case of the grain-oriented materials the difference is significantly larger.

The results under a sinusoidal magnetisation with a third and fifth harmonic proves that the 100Hz and 200Hz components of the magnetostriction strains do not only depend on the amplitude of the higher harmonic, but also on the phase delay of the higher harmonic with respect to the fundamental harmonic. Moreover, the variation of this phase delay can cause a significant increase of magnetostriction. The influence of the higher harmonic of the magnetisation signal on the magnitude of the 200Hz component of the magnetostriction is more than that on the 100Hz component.

CHAPTER 5

A computational method for the vibrations and deformation of magnetic cores

5.1. Introduction

In this chapter an overview of the method for the computation of the vibrations and deformation of a magnetic core as a result of the magnetic sources such as: magnetic forces and magnetostriction will be presented. While the magnetic forces refer to the forces applied on a material from an external field, magnetostriction is an outcome of the microscopic structure of the material. Therefore, as explained in chapter 2, the macroscopic deformation of the material is a contribution of both the magnetic forces and magnetostriction, and thus both are taken into account. The application of a commercial software e.g. *COMSOL* was not possible, since some of the equations required for the magnetostrictive calculations are not supported yet. To this end, an in-house method is applied.

This in-house technique is based on a 2D FE method to calculate the deformations of magnetic cores, e.g. a core of a transformer or an electrical machine. For the description of the deformation of the magnetoelastic material the Chu model formulations are considered, which were described in chapter 2.

For the calculation of the magnetostriction strain tensor $\overline{\overline{T}}_{\mathrm{ms}}$ of the Chu model, a model of the magnetostrictive behaviour of the material of the core is required. Such model is made by using ANN based on the magnetostriction strain measurement results of the samples of the core material. The principles of the ANN and how it is implemented in the FE calculations will be explained in this chapter. After that, the implementation of the model described in chapter 2 will be explained. Further on, the FE computation procedure will be described in steps.

5.2. Magnetostriction modelling

For the magnetostriction strain tensor $\bar{\bar{\varepsilon}}_{\mathrm{ms}}$, a 2D model of the magnetostriction strain behaviour of the core material is required. To this end, a model is made by using ANN in the parallel and perpendicular direction to the direction of the applied magnetic field as a function of the magnetic induction B, $B-\lambda_{\parallel}$ and $B-\lambda_{\perp}$ respectively. Further on, first an overview of the ANN will be given and then the magnetostrictive modelling will be explained.

5.2.1 Artificial neuron

Artificial neural networks are inspired from biological neurons where the networks are composed of inter-connecting neurons. Such models are known for applications such as modelling the human brain activities. However, they can be used in many other application areas. One of the advantages of the neural network is that it does not require a physical model or equivalent system for the modelling. It can link any inputs and outputs with no particular knowledge of the physical system. For our application Feed-Forward Neural Networks (FFNN) are suitable, for which the outputs can be calculated as explicit functions of the network inputs and the network parameters (without any feedback loops). For more information about neural networks we refer to [60].

An FFNN consists of neurons, where each neuron has one or more inputs and only one output. A simple neuron is shown in Fig. 5.1 with n inputs $(x_1, x_2, ..., x_n)$ and one output y. The inputs are first each multiplied by a weight factor $(w_1, w_2, ..., w_{\mathrm{n}})$ and then summed up. A bias is also added to each neuron which can be modeled as an extra input with the value of one. For the calculation of the neuron output y, the bias can be assigned as an extra input numbered zero (x_0). The sum of the inputs multiplied with their weight factor a goes through a transfer function f to form the output y, as follows

$$a = \sum_{i=0}^{n} w_{\mathrm{i}} x_{\mathrm{i}}, \tag{5.1}$$

$$y = f(a) = f(\sum_{i=0}^{n} w_{\mathrm{i}} x_{\mathrm{i}}). \tag{5.2}$$

5.2.2 ANN topology

The neurons in a network are arranged in so-called layers. An ANN normally has several layers where each layer consists of a different number of neurons. The neurons in each layer have the same inputs but multiplied by different weight factors. The inputs to the first layer of the network are the inputs to the network. Starting from the second layer, the inputs are the outputs of the previous layer, e.g. the inputs to the

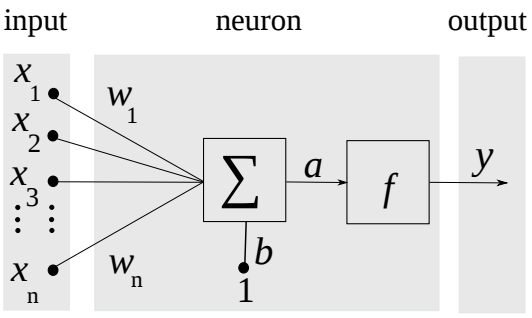

Figure 5.1: An artificial neuron with $x_1, x_2, ..., x_n$ inputs and y, where the $w_1, w_2, ..., w_n$ are the weight factor of each input, b is a bias and f is the transfer function.

second layer are the outputs of the first layer and so forth. The network outputs are then output of the last layer, so-called the output layer.

Each network has at least one layer, which is the output layer. The number of the neurons of the output layer is the same as the number of the outputs of the network. The layers between the input and the output layer, if there are any, are called the hidden layers. The neurons of each layer all go through the same transfer function f, and each layer can have a different transfer function. Fig. 5.2 shows a network with i hidden layers where only two of the hidden layers are displayed for the simplicity. The topology of this network can be described as follows

- There are n inputs to the network named as $x_1, x_2, ..., x_n$.
- There are m outputs of the network named as $y_1, y_2, ..., y_m$.
- Each layer has a bias represented as an input with the constant value of one.
- The first hidden layer has p amount of neurons where they all go through the same transfer function f_1. With the same approach all the other layers have different amount of neurons and different transfer functions. The $(i-1)$th hidden layer has g neurons with the transfer function f_{i-1} and the ith layer has q neurons with the transfer function f_i. The output layer has m neurons and f_{out} transfer function.
- In general, the weight factors of the ith layer are named as: $w^{(i)}_{\alpha,\beta}$ where α stands for the αth neuron in the layer and β stands for the βth weight factor of that neuron.

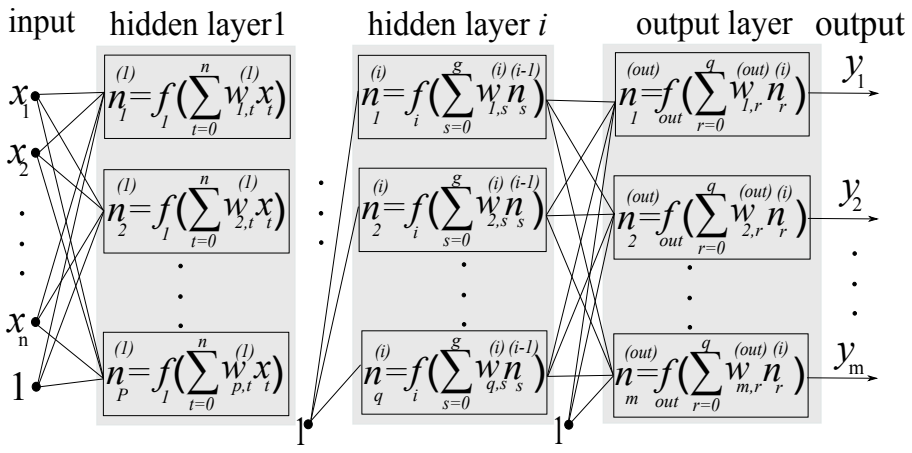

Figure 5.2: Topology of an ANN with i hidden layers, where there are n inputs to the network ($x_1, x_2, ..., x_n$) and m outputs ($y_1, y_2, ..., y_m$). The first hidden layer has p neurons and the ith hidden layer has q neurons and the output layer has m neurons which m equals the number of the network outputs.

- The transfer function of the hidden layers and the output layer f_{out} can be different e.g. linear or non-linear.

- The output of each neuron is the sum of the inputs and the bias which are multiplied with their weight factors and passed through the layer transfer function, e.g. as (5.2).

In fact, each network output is calculated based on the output of all the layers as follows

$$y_k = f_{\text{out}}\Big(\sum_{r=0}^{q} w_{k,r}^{(out)} \; f_i\Big(\sum_{\substack{s=0 \\ r\neq 0}}^{g} w_{r,s}^{(i)} \; \ldots \; f_1\Big(\sum_{\substack{t=0 \\ u\neq 0}}^{n} w_{u,t}^{(1)} x_t\Big)\Big)\Big) \tag{5.3}$$

for

$$k = 1, 2, ..., m$$

5.2.3 ANN modelling

To model the magnetostrictive behaviour of a material two ANN using FFNN are made, one for the strains in the parallel and one for the strains in the perpendicular direction to the direction of the applied magnetic field, $B - \lambda_{\parallel}$ and $B - \lambda_{\perp}$. The steps to design such networks for our application are explained below, as shown in Fig. 5.3.

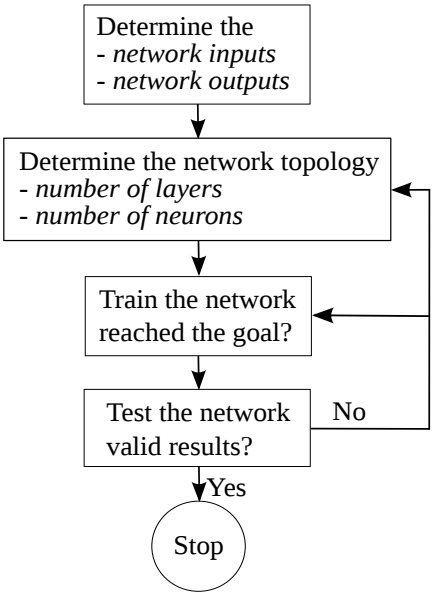

Figure 5.3: Flow chart of the iterative process to design an FFNN.

- **Network inputs**
  First the inputs to the network $x_1, x_2, ..., x_n$ should be defined. In the FE computation method the inputs and outputs of the NN should be in the frequency domain. Since the magnetostriction strain measurements are performed only as a function of the magnetic induction B, the input variables are then the parameters of B. For a purely sinusoidal magnetisation the inputs are the amplitude of the magnetic induction B and its frequency f. For the measurements under a sinusoidal magnetisation with a higher harmonic, e.g. fifth harmonic, the inputs are then the amplitude and the frequency of the both fundamental, B_1, f_1, and the higher harmonic component, e.g. the fifth harmonic B_5, f_5 and the phase delay of the higher harmonic, with respect to the fundamental.

- **Network outputs**
  The network outputs $y_1, y_2, ..., y_m$ should be defined as well. The network outputs should be in the frequency domain. To this end, the harmonics of the magnetostriction strains ($\lambda_{\parallel}$ and $\lambda_{\perp}$) in the frequency domain are assigned as the outputs. As explained in §3.5.3, looking at the frequency spectrum of the magnetostriction strains only the even harmonics of the magnetisation frequency are relevant to the magnetostriction. For instance for the measurements under a magnetisation with 50Hz frequency only even harmonics e.g. 100Hz, 200Hz of the measured strains are relevant to the magnetostriction. Thus, the outputs of the neural network are a number of such even harmonics of the strains which are of the same order of magnitudes as the first even harmonic component e.g. the 100Hz component. If we assign only the 100Hz and 200Hz of the strains, then the magnitude and the phase of such harmonics (in the frequency domain) are the outputs of the neural networks.

- **Network design**
  The network topology should be defined as follows: the number of layers, the number of neurons in each layer and the transfer function of each layer. Once we know the number of the network inputs and outputs, in fact we know the number of the neurons in the input and the output layers. There are no fixed rules for choosing the number of the hidden layers, the number of neurons in a hidden layer and the transfer function. A large number of networks should be designed to obtain an optimal network. To this end, there are two common strategies often applied: "expansion algorithm" and "reduction algorithm". With the expansion algorithm first a small network is designed with low number of layers and neurons per layer, If the results are not satisfactory, a larger network is designed with more number of layers and neurons per layer. With the reduction algorithm the opposite approach is taken. First we start with a large network with many layers and neurons per layer and if the results are not satisfactory a smaller network is designed [60].

  The approach taken in this work is based on the expansion algorithm. In general, if the relationship between the inputs and outputs is rather simple, the network has a low number of layers and neurons per layer and vice versa. For our application, for modelling the magnetostriction strains under a purely sinusoidal magnetisation a smaller network was designed compared with that for the measurements under a sinusoidal magnetisation with a fifth harmonic. The suitable transfer functions for such networks were a purely linear function and a hyperbolic tangent transfer function, purelin and tansig Matlab functions respectively.

- **Network training**
  Once the network is designed, it has to be trained based on a set of data of inputs and outputs, called the training data. In fact, the weight factor of the neurons and

the biases are defined by the network training. In our case, the network training has been performed based on the results obtained by the measurements. Different combinations of the inputs and their corresponding outputs, so-called the "target outputs", are applied to train the network.

The training is an iterative process in which the weight factor of the neurons are iteratively changed to reach the optimal values. Once the initial weight factors are assigned, there is a deviation between the output of the network $y_{(l)}$ to the input training data and the target outputs $t_{(l)}$, defined as follows

$$e_{(l)} = y_{(l)} - t_{(l)}, \tag{5.4}$$

where l=1,2,...,u. The aim of the training process is to minimize $e_{(l)}$ for each l by iteratively changing the weight factors. In another word, the network should be trained so that the network output to the input training data are the same as the target outputs. The "training fault" E_{train} can be calculated as follows

$$E_{\text{train}} = \frac{1}{um} \sum_{l=1}^{u} \sum_{k=1}^{m} e_{k,(l)}^2. \tag{5.5}$$

Different optimization algorithms can be used for the training process. The training algorithm used for the magnetostriction modelling is according to Levenberg-Marquardt optimization, which is often the fastest backpropagation algorithm. For more explanation of the training algorithms we refer to [60].

Fig. 5.4 shows a the magnitude of the 100Hz harmonic of the magnetostriction strain $\lambda_{\|}$ and the response of a trained network to the same input training data under a purely sinusoidal magnetisation.

As another example, for the measurements under a magnetisation with a fifth harmonic component, see §4.3.2, the target outputs and the response of the network to the input training data are presented in Fig. 5.5.

- **Network testing**
  Once the network is well trained, it is able to determine the correct network output for other inputs which were not in the training dataset. For testing the network, the test input data should not belong to the training dataset. Moreover, such input data should be within the range of the training dataset since the network is only trained in that range, Otherwise, the response of the network may not be correct. The test error can be calculated in the same manner as (5.5) for the test dataset. If the results are not satisfactory, the network should be re-trained and tested once again. If the latter is not successful, then a new network topology should be assigned.

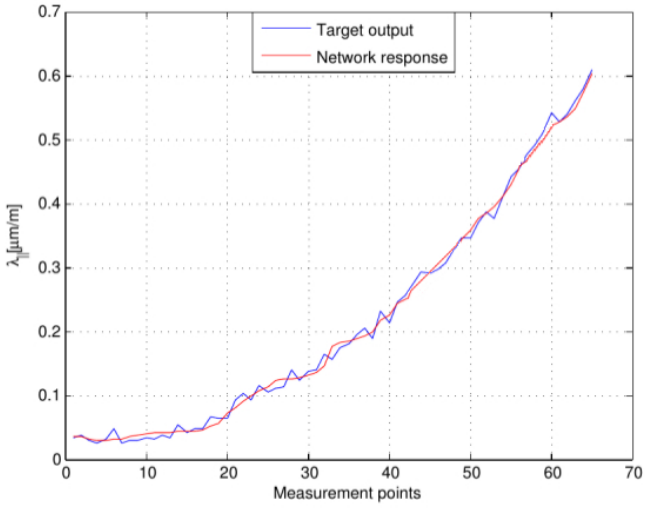

Figure 5.4: The target out and the network response to the input training data for a purely sinusoidal magnetisation.

5.2.4 FE Implementation

In the FE method the deformation of a magnetised material is calculated in two-dimensions. For the computation we apply a plane stress and assume that the sample can move freely in the third dimension. Once a mesh of the material is generated, the magnetic induction B and the magnetostriction strain tensor $\overline{\overline{\varepsilon}}_{\mathrm{ms}}$ are constant inside each mesh triangle[1]. Therefore, the equivalent stress tensor $\overline{\overline{T}}^{*}$ is constant such that the force distribution is reduced to singularities on the edges. The force $\overline{F}_{\mathrm{ij}}$[N/m] exerted on a mesh edge ij, shown in Fig. 5.6, can be computed based on the equivalent stress tensor $\overline{\overline{T}}^{*}$ in the adjacent triangles k and l is as follows

$$\overline{F}_{\mathrm{ij}} = l_{\mathrm{ij}}(\overline{n}_{\mathrm{ij}} \cdot \overline{\overline{T}}^{*}_{\mathrm{k}} - \overline{n}_{\mathrm{ij}} \cdot \overline{\overline{T}}^{*}_{\mathrm{l}}), \tag{5.6}$$

where l_{ij} is the length of the edge ij. The nodal forces $(\overline{F}_{\mathrm{i}}, \overline{F}_{\mathrm{j}})$ are then assigned as half of the forces exerted on the edges $(\frac{1}{2}\overline{F}_{\mathrm{ij}})$ to both node i and j. As a result, the forces at the nodes are a sum of the force contribution of all the neighbour edges of the neighbour mesh triangles.

The magnetic and mechanical computations are performed iteratively. performing a field computation for the displacement $\overline{u}$ and the strain tensor $\overline{\overline{\varepsilon}}$ of the previous step determines the geometry and the constitutive law for the magnetic field $\overline{H}$, see (2.42). Next, the nodal forces for the magnetic equivalent force distribution $\overline{f}^{*}$ are computed,

[1] A first-order mesh with triangular elements is generated.

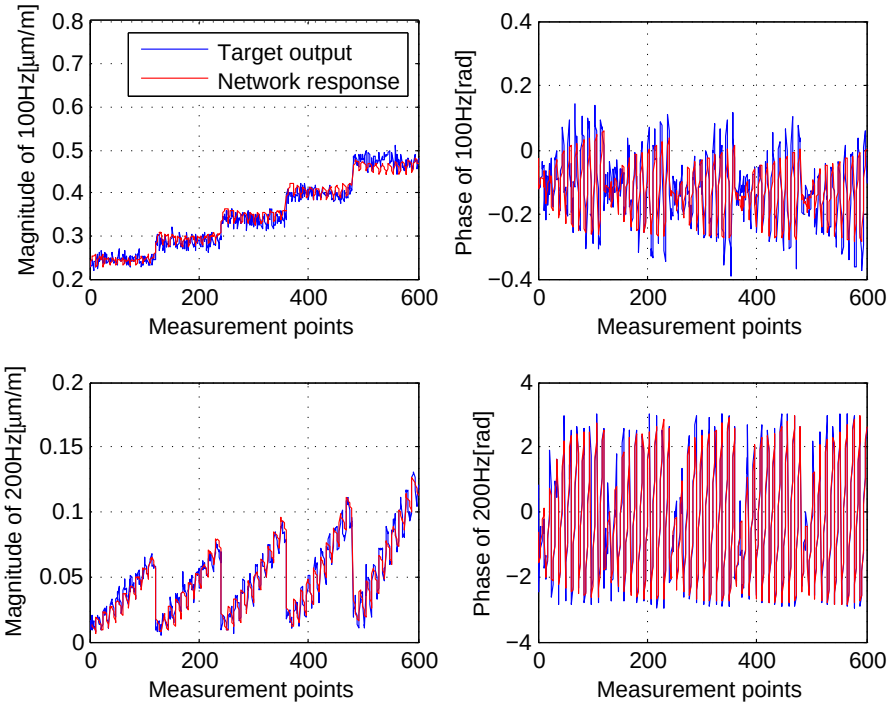

Figure 5.5: The target out and the network response to the input training data for a sinusoidal magnetisation with a fifth harmonic component.

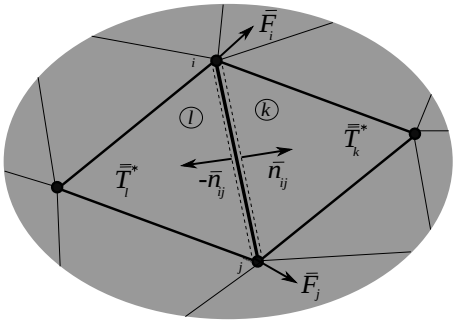

Figure 5.6: Computation of the nodal forces $(\overline{F}_{\mathrm{i}}, \overline{F}_{\mathrm{j}})$ in the mesh triangles, for which half of the force exerted on the edges $(\frac{1}{2}\overline{F}_{\mathrm{ij}})$ are assigned to each node [28].

see (2.56). These forces are the input to the mechanical equations to compute the deformation, e.g. 2.58.

5.3. Modal analysis

A short description of the modal analysis will be given in this section [61].

5.3.1 Basic definition

In general, for vibration analysis of a structure three stages are followed, such as:

- **Spatial Model**
  Spatial model refers to the description of the structure's physical characteristics, usually its mass, stiffness and damping properties.
- **Modal model**
  Based on the spatial model of a structure, an analytical modal analysis gives us the description of the vibration modes i.e. the modal model. This model results in natural frequencies of the structure with their corresponding vibration mode shapes and modal damping factors[2].
- **Response model**
  The analysis of how the structure will respond under given excitation conditions is called the response model.

For a theoretical approach, the vibration analysis starts from spatial to modal and then response model. With an experimental approach, a reverse direction is followed i.e. starting from response model and then obtaining the modal and spatial models.

For the computation of the FE technique always an undamped system is considered. Thus, the spatial model only consists of mass M and stiffness K. For the modal model the system without external forces is considered, for which we have

$$[M]\{\ddot{x}\} + [K]\{x\} = 0. \tag{5.7}$$

Assuming a solution type of

$$\{x\} = \{X\}e^{j\omega t}, \tag{5.8}$$

(5.7) results in

$$(-\omega^2[M] + [K])\{X\}e^{j\omega t} = 0, \tag{5.9}$$

which is an eigenvalue problem. The solution of (5.9) results in N values of ω^2 ($\overline{\omega}_1^2$, $\overline{\omega}_2^2$, ..., $\overline{\omega}_N^2$), which are the undamped system's natural frequencies.

If we substitute any of these frequencies in (5.9), a relative value for the $\{X\}$, i.e. $\{\Psi_r\}$, the so-called mode shape is obtained for the corresponding natural frequency, as

$$(-\omega_i^2[M] + [K])\{\Psi_i\} = 0. \tag{5.10}$$

[2] By natural vibration, we mean the vibration of the structure without any external forces or excitations.

The complete solution can be expressed in two $N \times N$ matrices as

$$[\ddots \cdot \overline{\omega}_r^2 \ddots \cdot], [\Psi] \tag{5.11}$$

5.3.2 Orthogonality properties

The modal model is orthogonal which makes the analysis easier. The orthogonality can be stated as follows

$$\begin{aligned} [\Psi]^T [M][\Psi] &= [M_i] \\ [\Psi]^T [K][\Psi] &= [K_i], \end{aligned} \tag{5.12}$$

from which the following is valid

$$[\overline{\omega}_i^2] = [M_i]^{-1}[K_i], \tag{5.13}$$

where M_i and K_i are referred to as the modal mass and the modal stiffness of the mode i.
A proof of the orthogonality can be presented as follows. Starting with the equation of motion for free vibration we have

$$([K] - \overline{\omega}^2[M])\{X\}e^{j\omega t} = 0, \tag{5.14}$$

which for a particular mode is

$$([K] - \overline{\omega}_i^2[M])\{\Psi_i\} = 0. \tag{5.15}$$

We can then multiply (5.15) by a different eigenvector, transposed, as

$$\{\Psi_k\}^T([K] - \overline{\omega}_i^2[M])\{\Psi_i\} = 0. \tag{5.16}$$

For the second mode a similar relation as of (5.15) can be written

$$([K] - \overline{\omega}_k^2[M])\{\Psi_k\} = 0, \tag{5.17}$$

which we can transpose and then multiply by $\{\Psi_i\}$

$$\{\Psi_k\}^T([K]^T - \overline{\omega}_k^2[M]^T)\{\Psi_i\} = 0. \tag{5.18}$$

Knowing that $[M]$ and $[K]$ are symmetric, they are identical to their transpose. Thus, we can combine (5.16) and (5.18) which results in

$$(\overline{\omega}_i^2 - \overline{\omega}_k^2)\{\Psi_k\}^T[M]\{\Psi_i\} = 0. \tag{5.19}$$

If $\omega_i \neq \omega_k$, (5.19) can only be solved if

$$\{\Psi_k\}^T[M]\{\Psi_i\} = 0; i \neq k. \tag{5.20}$$

Based on (5.15) and (5.18), the following is valid

$$\{\Psi_k\}^T[K]\{\Psi_i\} = 0; i \neq k. \tag{5.21}$$

If $i = k$, or if $\overline{\omega}_i = \overline{\omega}_k$, (5.20) and (5.21) do not apply. However, from (5.15) the following results

$$(\{\Psi_i\}^T[K]\{\Psi_i\}) = \overline{\omega}_i^2(\{\Psi_i\}^T[M]\{\Psi_i\}). \tag{5.22}$$

Based on (5.12) and (5.13), we know that

$$\begin{aligned} \{\Psi_i\}^T[M]\{\Psi_i\} &= M_{\mathrm{i}} \\ \{\Psi_i\}^T[K]\{\Psi_i\} &= K_{\mathrm{i}} \\ \overline{\omega}_{\mathrm{i}}^2 &= \frac{K_i}{M_i}. \end{aligned} \tag{5.23}$$

Calculating all different combinations of i and k gives us the full matrix of M_i and K_i in (5.12) and (5.13).

5.4. FE computation steps

A short overview of the FE magnetostrictive deformation calculation steps will be given in this section. However, the calculation technique in detail is not within the scope of this work and we refer to [30], [28], [29], [62] and [26]. For the theory behind the finite element method, for which a two-dimensional approach is taken, we refer to [18] . In short, the method calculates the magnetic and magnetostriction forces and the mechanical deformations of a certain transformer core geometry. For the application of transformers, the inputs required for the calculations are the following

- The size and the shape of the core
- The magnetic characteristics of the core material determined by the measurements such as: the B-H loop and a model of the magnetostrictive behaviour ($\lambda_{\parallel}$, $\lambda_{\perp}$ as function of the magnetic induction B)
- The mechanical properties of the core e.g. Young's modulus E (see §2.5) and Poisson's modulus ν
- The windings with their number of turns and the current I
- The source voltage parameters such as: the single-phase or three-phase voltage, its amplitude and frequency and the presence of higher harmonics if any

Having the inputs, for the computation of the magnetostriction deformation a series of steps are followed. These steps are shortly presented here and in Fig. 5.7.

- A 2D drawing of the geometry is required, in which the properties of the core and the windings are included.
- An electrical diagram showing the winding connections and the source power supply needs to be made.
- A mesh is generated on the basis of the 2D drawing.
- Having the generated mesh, the electrical diagram and the material properties (e.g. the B-H characteristic) a dynamic time-stepping magnetic FE calculation is performed.
- As a result of the previous step, the values of the magnetic induction B and the magnetic field H are calculated for triangle of the mesh and for each time step.
- Based on the B and H, the magnetic stress tensor $\overline{\overline{T}}_{\mathrm{mf}}$ and the magnetostriction stress tensor $\overline{\overline{T}}_{\mathrm{ms}}$ are calculated for every triangle of the mesh and for each time step. In this step the neural network is used to create the the magnetostriction stress tensor $\overline{\overline{T}}_{\mathrm{ms}}$ based on the calculated magnetic induction B. The inputs and outputs of the neural network should be in the frequency domain. Thus, to get the inputs of the neural network we need to do an FFT and once the outputs of the neural network are calculated an IFFT is performed.
- Knowing the calculated magnetic stress tensor $\overline{\overline{T}}_{\mathrm{mf}}$ and the magnetostriction stress tensor $\overline{\overline{T}}_{\mathrm{ms}}$, the total force in every node of the mesh is calculated at every point in time. This is done on the way as explained in §5.2.4.
- According to the mechanical material properties, and the total forces in the nodes of the mesh, a dynamic mechanical FE method is performed with a solution through modal analysis. For the mechanical FE calculations the same mesh as that of the magnetic calculations is used.
- From the mechanical FE computation we get the displacement results, which are in time (frequency domain) and in space (eigen modes). These modal vibrations are calculated in the frequency domain for every deformation mode and for every frequency[3]
- In the last step, the deformation of the nodes can be calculated, which can be performed in the time domain.

5.5. Conclusion

In this chapter, an existing method for the computation of the deformations of a magnetic core caused by the magnetic sources was presented. This method is based on the FE method and considers a 2D deformation of the core. For the description of the deformation of the magnetoelastic material the Chu model formulations were considered, which were described in chapter 2. The method requires a model of the magnetostrictive behaviour of the core material, which is made by using an FFNN.

[3] In fact, this method implies a weak-coupled approach, which means that the deformations are calculated after the complete calculation of all magnetic results [18].

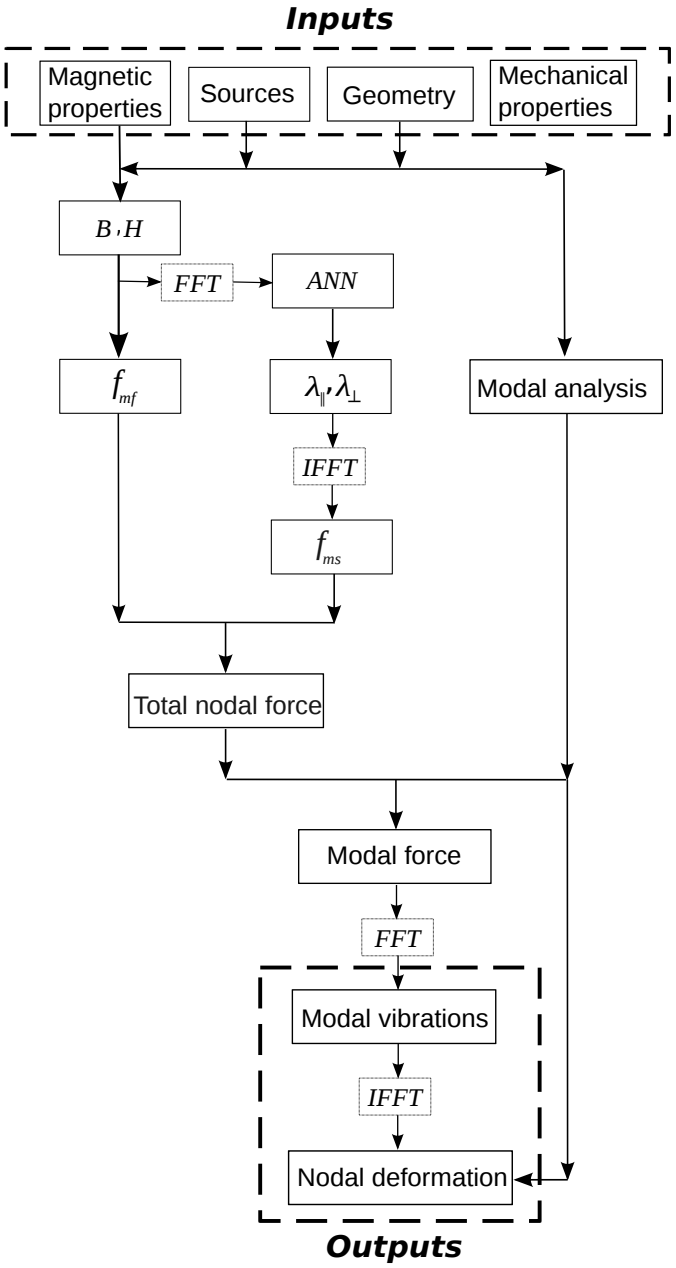

Figure 5.7: A flow chart of the FE computation technique for the calculation of the deformation of a magnetic core due to the magnetic forces and magnetostriction.

The method first calculates the magnetic induction B and the magnetic field H for every mesh triangle. Then, based on the NN models and knowing the B the total stress tensor is calculated. At the end, adding the mechanical properties of the core material, the modal analysis is performed and the vibrations of the core are calculated. A short description of the modal analysis has been presented in this chapter. A validation of this technique will be presented in the next chapter for a single-phase transformer core.

CHAPTER 6

Validation

6.1. Introduction

In this chapter a validation of the magnetostrictive deformation calculation technique, which was described in the previous chapter, will be presented. In the past, the deformations of a three-phase test transformer core and an induction machine core were computed by using this technique [18]. The magnetostrictive models of the core material were then made based on the measurement results of the samples of the core material obtained by the strain gauge setup. For the three-phase transformer core, vibration measurements were performed on the core in order to validate the computation results. However, the comparison between the two, the computed and the measured results, was not valid mainly due to the presence of other vibration sources in the vibration measurements. A discussion of these results will be presented further on.

In this PhD work, a new validation of the FE technique has been performed for a single-phase test transformer core. This test transformer core design will be explained further on. For the FE computations, the magnetostriction model of the core material was made based on the magnetostriction strain measurement results of the samples of the core material measured by the laser measurement setup. To validate the FE results, the vibrations of the test transformer core were measured by using a non-contact laser scanning vibrometer. The FE calculation results and the vibration measurement results showed rather good agreement which will be discussed in more details.

6.2. A validation of the FE technique on a three-phase transformer core

6.2.1 Background

In the past, the deformation of a three-phase transformer core was calculated by a FE magnetostrictive deformation computation technique. As a validation of the FE tech-

nique, the vibrations of the same core were measured and the results were compared with each other [18]. The three-phase transformer core material was a grain-oriented electrical steel type (3% Si-Fe). The magnetostriction measurements of the samples of the core material were performed by using the strain gauge setup.

For the validation, the vibration measurements were carried out on the same test transformer core by using an accelerometer product of Multichannel Analysis Systems, type 3550. Such a device is suitable for vibration measurement applications. It has a sensor to measures the local vibration. Based on the application, a two or three-dimensional acceleration signal can be measured and analysed. Since the FE calculation is a two-dimensional technique, for the three-phase test transformer, two-dimensional vibration measurements were performed.

Fig. 6.1 shows a picture of the three-phase test transformer core. For both the FE calculation and the vibration measurements a purely sinusoidal magnetisation with a frequency of 50Hz was applied. The amplitude of the magnetic induction B was assigned to be at the knee of the B-H characteristic of the core material. The comparison of the results showed that the results of the vibration measurements were larger than those of the FE (a factor of three to four times).

One of the possible reasons for such a difference was the assembly of this test transformer. The transformer core had a lap joint assembly, which is a common assembly considering the grain-oriented core material. However, the lap joint adds some extra vibrations and deformation to the magnetostrictive deformation of the core. Since only the magnetostriction deformation was modelled in the FE computation technique, the deformation contribution of the lap joints was not taken into account for the calculations. Thus, as the FE results did not correlate with the results of the vibration measurements and the FE technique was not really validated. The assembly of the three-phase test transformer and the result discussion will be further explained in the following sections.

6.2.2 Transformer assembly

Transformer cores consists of a stack of laminations in most cases of grain-oriented electrical steel. Compared with nonoriented electrical steels, grain-oriented materials have a higher magnetic permeability and lower hysteresis losses, in addition to a lower magnetostriction strain along the rolling direction of the material. This means that in the case of grain-oriented material, the induced magnetic induction B (along the rolling direction) is higher for the same applied magnetic field H compared with the case of nonoriented materials. However, the magnetic properties of the grain-oriented electrical steel are significantly different in the other directions than the rolling direction of the material. Therefore, the application of grain-oriented electrical steel is beneficial in transformer cores if the transformer assembly allows the magnetic flux to pass along the rolling direction of the material. To this end, a lap joint assembly, over-

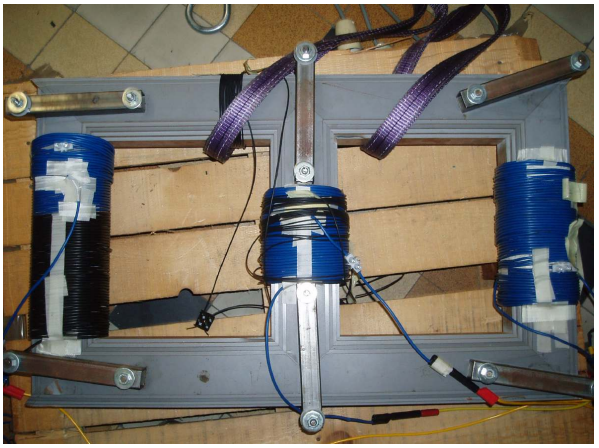

Figure 6.1: The three-phase test transformer core setup used for the validation.

lapping the laminations in the corners, is often applied as it allows the flux to always follow the rolling direction of the material[1].

Fig. 6.2 shows the assembly of a transformer and a single-step and multi-step lap assemblies. In the single-step lap assembly the sheets are in packets of two and in the multi-step lap assembly the sheets are in packets of five. Each packet has a joint displaced relative to the adjacent packet. With such design assemblies, the flux passes along the rolling direction all over the core except at the corners.

However, the flux path that goes from one lamination to another one inevitably passes through the very small air gaps between the two laminations, which creates an attractive interlaminar force. Therefore, in addition to the magnetostrictive vibrations, vibrations due to the clamping of the joint regions of the laminations are generated as well [3], [5], [8] and [63].

6.2.3 Results discussion

In the FE calculations of the three-phase test transformer core only the magnetostrictive deformation was modelled and calculated. However, for the validation of the FE results, the vibrations and deformation of the magnetised core due to the magnetostriction and the attractive interlaminar force of the lap corners were measured. Thus, the measured results were larger than the computed results as a result of the contribution of the corners. In fact, the computed and the measured results were incomparable since the conditions under which the comparison was made were not similar.

Moreover, the magnetostrictive model for the FE calculation was based on the measurement results obtained by the strain gauge setup. As mentioned in chapter 3,

[1] In the corners the flux pattern is not uni-directional anymore.

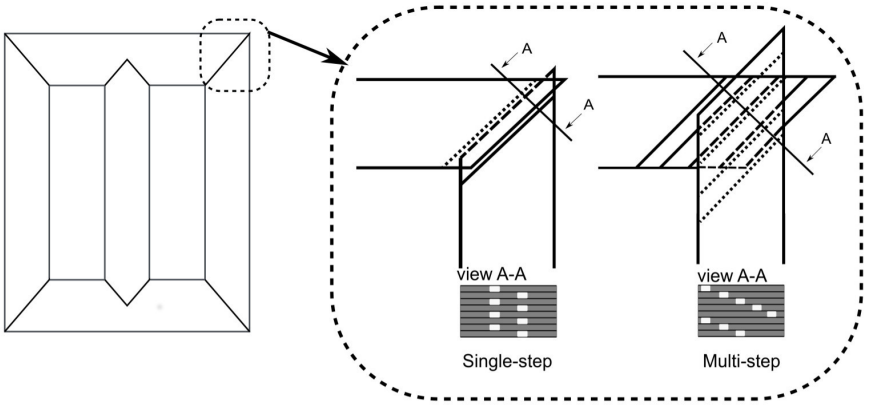

Figure 6.2: A transformer core with a single-step and multi-step lap joint assemblies in which the laminations are in packets of two and five, respectively. The air gaps, where once the flux passes cause an attractive interlaminar force, are shown with white color.

with the strain gauge setup the coating of the samples was partly removed for a proper attachment of the strain gauges. The material of the three-phase test transformer was grain oriented GO-I[2]. Regarding the measurement results obtained by the strain gauge setup and a comparison with those measured by the laser setup on this material type the coating effect was considerable, see §4.2.2. The magnetostriction strains of the coated samples were significantly smaller than those of the non-coated samples. Therefore, if the measurement results of the coated samples were applied for the FE calculation technique of the three-phase test transformer, the contribution of the noise of the corners compared with the magnetostriction noise, would be more than three to four times as was resulted in the past.

6.2.4 The motivations for a new test transformer

As reported in the previous chapters, the accuracy of the magnetostriction strain measurement results by using the laser setup is higher than those with the strain gauge setup. The possibility of the measurements of the coated samples is another advantage of the laser setup over the strain gauge setup. Therefore, a magnetostrictive model of a test setup based on the measurement results of the laser setup should better present the magnetostrictive behaviour of the test setup material.

Moreover, assuming that the FE calculation technique for the three-phase test transformer core could not be successfully validated because of the extra noise source,

[2] Lamination of 3% Si-Fe with 0.9W/kg losses at 1.5T and 50Hz which has been previously named as GO-I.

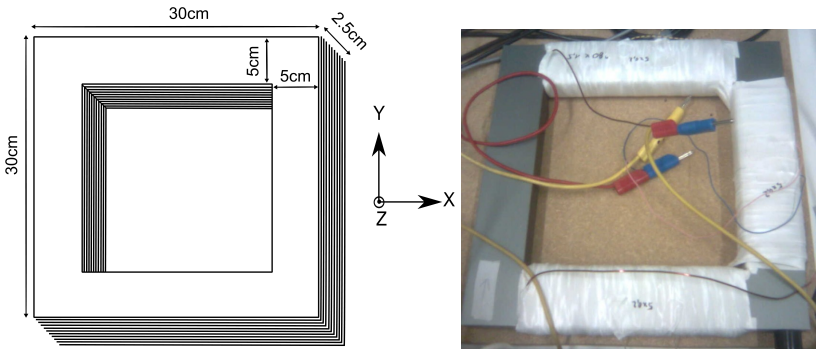

Figure 6.3: Schematic depiction of the single-phase test transformer core and the coordinate system (left); the core with only the primary magnetisation winding where one leg is left free for the vibration measurements (right).

another test setup which only resembles the magnetostrictive noise and deformation would thus be better.

On the one hand the advantages of the laser measurement setup and on the other hand a new test setup (representing only the magnetostrictive noise) motivated us for a new validation.

6.3. A validation of the FE technique on a single-phase transformer core

The test setup this time was a single-phase transformer core 30cm$\times$30cm with 5cm leg width, as shown in Fig. 6.3(left). The core consists of 50 laminations with a total thickness of 2.5cm where each lamination was 0.5mm thick. To resemble only the magnetostrictive deformation, a simple transformer assembly without any lap joint has been considered. To this end, the laminations were cut out of one piece, so that there is no air gap along the the flux path. Using a grain-oriented material for the test transformer with the described assembly was not a suitable choice, because of the strong anisotropy of the material. Applying a grain-oriented material would have resulted in a transformer with significantly different magnetic properties in each pair of the legs. To avoid this, a nonoriented material type with uniform magnetic properties in every direction was preferred. Such a test transformer is perhaps not a realistic design, however, the aim is to validate the FE magnetostrictive deformation prediction. The test transformer core is built out of nonoriented electrical steel type M350-50A[3].

[3] Such material has 3.5W/kg loss at 1.5T and 50Hz.

6.3.1 Spark erosion technique

The laminations were cut by using the spark erosion technique to avoid any harm to the magnetic properties of the material due to the cutting. The machine used for the cutting has an accuracy of $1\mu m$. Spark erosion is a manufacturing process to obtain a desired shape by using Electrical Discharges Machines (EDM). In this case, the sample is placed in a dielectric liquid between two electrodes. By connecting a voltage source to the electrodes, a series of rapidly recurring discharges (sparks) are generated. If the distance between the two electrodes is reduced, the electric field between them is stronger than the dielectric strength. As a result, a current flows between the two electrodes which is converted into heat. The surface of the sample is then strongly heated in the tiny area of discharge channel which forms a small crater. To obtain a certain shape of the sample, a series of the discharges is used, one next to the other. Thus, new craters are formed next to the previous ones.

6.3.2 Windings and connections

The magnetic core has only one winding, with 280 turns. The core is wound over three legs to spread the flux uniformly all over the core and avoid a local magnetisation [64]. The fourth leg is left free for the vibration measurements. We call this leg the "free leg". The wound test transformer core is shown in Fig. 6.3(right). For the vibration measurements, a magnetisation signal is generated in the PC and then amplified by a linear amplifier. A resistance is connected in series with the magnetisation winding to avoid a high inductive load. This resistance is only 7% of the total impedance and thus the magnetization voltage signal form is not disturbed. The voltage drop over the resistance is compensated in the *LabVIEW* program to obtain the desired voltage and the magnetic induction amplitudes over the core itself, as explained in §3.5.3.

6.4. Validation results under a purely sinusoidal magnetisation

In this section, the FE calculation results and the vibration measurement results of the single-phase transformer core will be presented and compared with each other.

6.4.1 FE calculation results

The magnetostriction strains of the samples of M350-50A laminations, which were used in the new test transformer core, were measured by using the laser measurement setup. Although nonoriented electrical steels are in general isotropic compared with the grain-oriented materials, still some degree of anisotropy exists in the magnetic properties of these materials. Since the core laminations of the single-phase test transformer are cut in one piece, the flux does not follow the same direction of the material along the four legs. In fact, the flux is parallel to the rolling direction for two legs and

perpendicular to the rolling direction for the other two legs. Therefore, the magnetostriction strains of two types of samples were measured, samples cut along with and samples cut transverse to the rolling direction of the material. For each sets of samples, the magnetostriction strains in the parallel and perpendicular directions to the applied magnetic fields were measured under purely sinusoidal magnetic inductions with amplitudes from 0.1T to 1.7T in steps of 0.1T at a 50Hz frequency.

As presented in §3.5.3, for a sinusoidal magnetisation of the samples, iterative form control and amplitude control were performed. The PC-generated magnetic induction signal was corrected in a feedback loop to acquire a sinusoidal form with the correct amplitude. For each magnetic induction amplitude B[T], five measurements were performed and the average data were post-processed in the frequency domain. Looking at the frequency spectrum, the harmonics higher than four times the base frequency were relatively small and thus were neglected. The 100Hz and 200Hz harmonics were used for the data modelling of the material for the FE calculations. Magnetostriction models in the parallel and perpendicular directions to the uni-directional magnetisation direction were designed by using ANNs for each sets of samples $B-\lambda_{\parallel}$ and $B-\lambda_{\perp}$, respectively. The NN modeling and the FE technique have been presented in chapter 5. The deformations of the core were then calculated for the nodes shown in Fig. 6.4 on the free leg of the core. The results obtained by the FE calculation in the frequency spectrum under a purely sinusoidal magnetisation with 1.2T amplitude and 50Hz are shown in Table. 6.1.

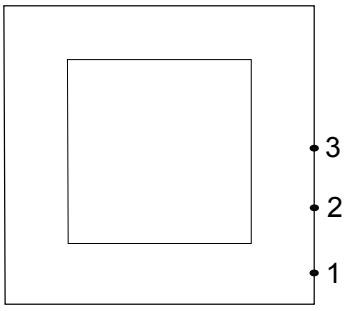

Figure 6.4: The three nodes along the free leg of the test transformer where the FE calculations and the vibrations measurements are performed.

6.4.2 Vibration measurement

To validate the FE calculation results, the vibrations of the test transformer core have been measured by using a laser scanning vibrometer. The principle of such a vibrometer has been presented in §3.4.2. The measurements have been performed at the department of Mechanical Engineering, Acoustics and Vibration research group at the

Free University of Brussels (VUB). The scanner was a PSV-400 vibrometer Polytec laser, which consists of a sensor head with an integrated scanning unit, a controller and a data acquisition and management system. A Polytec software package is designed for the device control, data processing and also the visualisation of the measurement results. The system works based on the Doppler effect, sensing the frequency shift of a back-scattered light from a moving object [65]. The scanner has multiple resolutions and can be adjusted as low as 0.2 mm/s/V. The suitable resolution range can be adjusted by the user, based on the measurement scale. For the transformer core vibration measurements, the highest sensitivity with 0.2 mm/s/V was used. The measurements can be made over a wide frequency bandwidth. Later on only the dominant frequencies can be chosen for post-processing.

To avoid any friction of the transformer core with the underlying surface, the core was hung from a frame in a horizontal plane parallel to the ground. In this way also the core weight is evenly distributed all over the plane. The laser head was pointed at the free leg of the transformer, as shown in Fig. 6.5. The laser measured the selected nodes of the core for preselected time intervals, based on the adjustment by the user, and then the average data of the measured velocities were saved. According to the average velocity signals, the deformation of the core was calculated in the same Polytec software. If the scanner laser beam is not well received, e.g. for the nodes between two laminations where the reflection of the laser beam is low, the scanner continues the measurements until a valid signal is received. In addition, the scanner can perform an automatic surface scan for a series of nodes in a grid pattern and display the results in a 3D animation. The density of the nodes in the grid is user defined. The scanner then probes the entire grid automatically using an interactive measurement grid.

The vibrations of the core were measured under a purely sinusoidal magnetisation with 1.2T amplitude and 50Hz at the same nodes where the FE calculation were performed. To this end, the *LabVIEW* program for the magnetic induction B control was applied, see §3.5.3, to make sure a purely sinusoidal applied voltage. The results are presented in Table 6.1.

Table 6.1: The 100Hz and 200Hz magnitude [m] and phase spectrum [rad] of the nodes shown in Fig. 6.4 calculated by the FE magnetostrictive deformation computation technique and measured by the PSV-400 scanning vibrometer.

	FE calculation results		vibration measurement results	
node	100Hz	200Hz	100Hz	200Hz
1	3.67E-7$\angle$0.06	1.88E-8$\angle-$2.18	3.81E-7$\angle-$0.23	4.59E-8$\angle-$2.61
2	3.59E-7$\angle$0.05	1.74E-8$\angle-$2.10	2.07E-7$\angle-$0.08	5.33E-8$\angle$1.97
3	3.59E-7$\angle$0.05	1.76E-8$\angle-$2.11	1.30E-7$\angle-$0.32	6.30E-8$\angle$1.58

As can be observed in Table. 6.1, the 100Hz harmonic component magnitude is relatively larger than that of the 200Hz and thus the former defines the deformation of the nodes. However, regarding the noise issue the 200Hz harmonic component effect

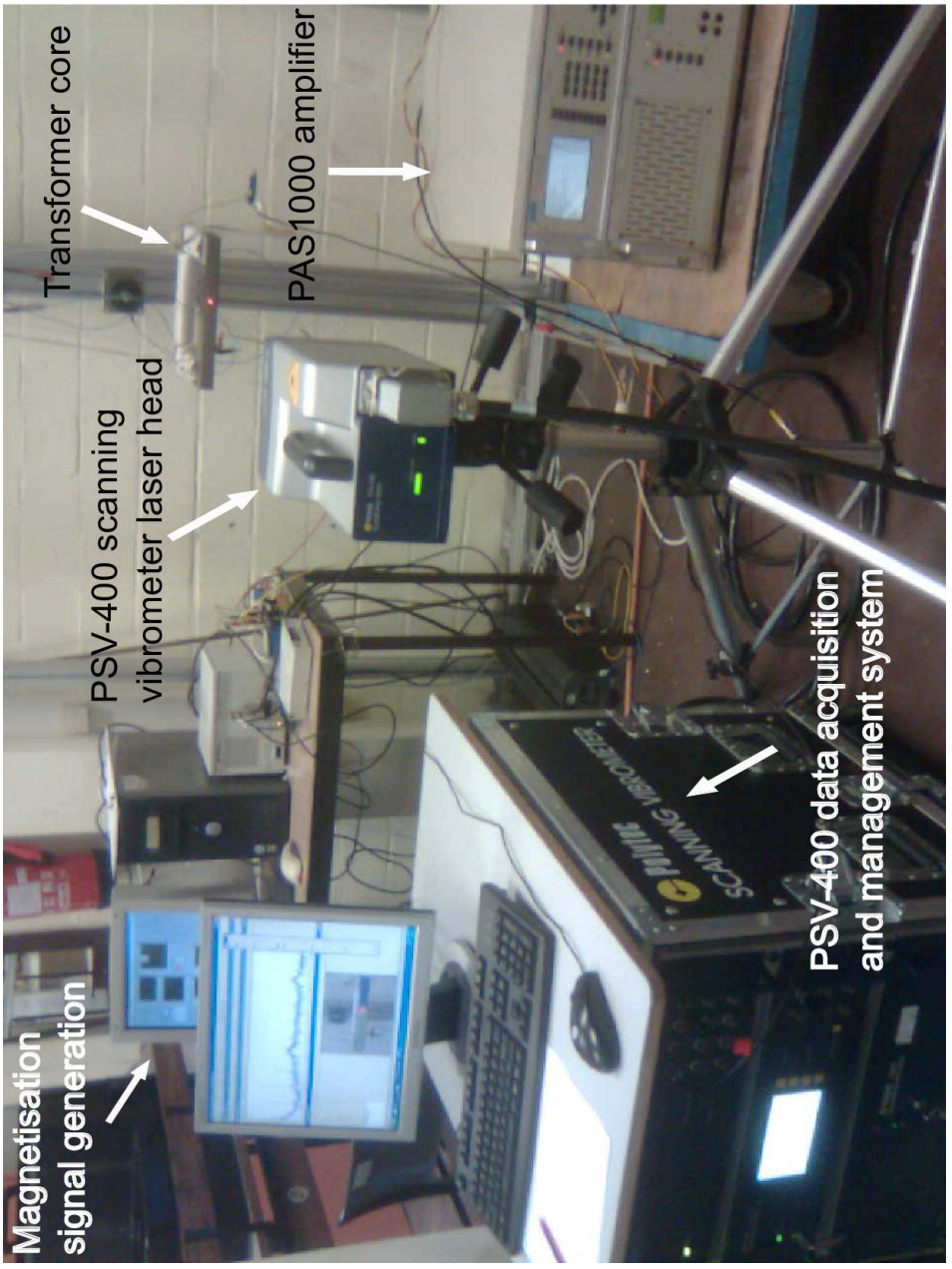

Figure 6.5: The PSV-400 scanning vibrometer laser beam pointed at the free leg of the transformer core. For the magnetisation of the core, the PC generated magnetisation signal is amplified.

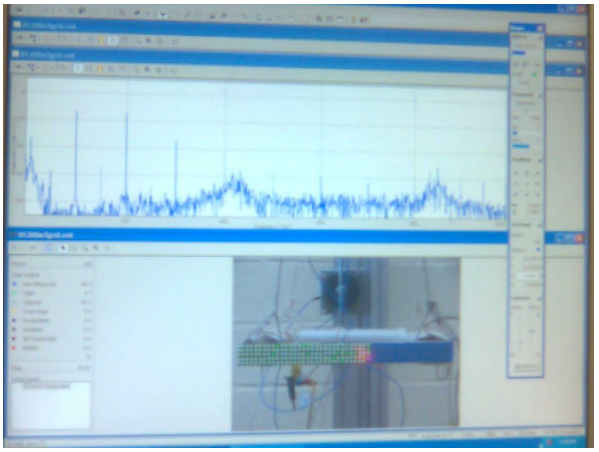

Figure 6.6: The test transformer free leg surface scan for a grid pattern of nodes. The nodes where the vibrations are measured are in green color, those being measured are in red and the ones where the vibrations are still to be measured are presented in blue color.

should not be neglected. The magnitudes of the 100Hz deformation for both the calculated and the measured results are of the same order. According to Fig. 6.4 node 1 is at the corner and 3 in the middle. Looking at the 100Hz data, the vibration measurement results show that it deforms indeed more at the corners, node 1 for example. However, the FE calculation results shows similar deformations along the whole leg.

To investigate the deformation of the magnetised test core a surface scan of the free leg has been performed and the results have been visualised in a three-dimensional animation. A picture of the interface software is presented in Fig. 6.6, which shows the grid pattern of the nodes. The nodes where the vibrations are measured are in green color, those being measured are in red and the ones where the vibrations are still to be measured are in blue. Fig. 6.7 shows two pictures of the animation, when the core free leg surface shows the maximum (the top picture) and the minimum (the bottom picture) magnetostrictive deformations. It is observed that in fact the core free leg does not deform uniformly all over the surface but more in the corners. The FE technique calculates the deformation in two-dimensions. Because of the two-dimensional approach of the computation method, the fact that the core in the z-direction is built up from a stack of laminations is not taken into account. As a result, neglecting the third dimension in the calculation can be a possible reason for the differences between the computation and the measurement results.

To summarize, the comparison between the measured and computed deformations shows a good agreement. Both the 100Hz and the 200Hz harmonic components are of the same order. For node 1 the 100Hz data are similar. Regarding the 200Hz harmonic component, the results are slightly different. The vibration eigen modes can also be

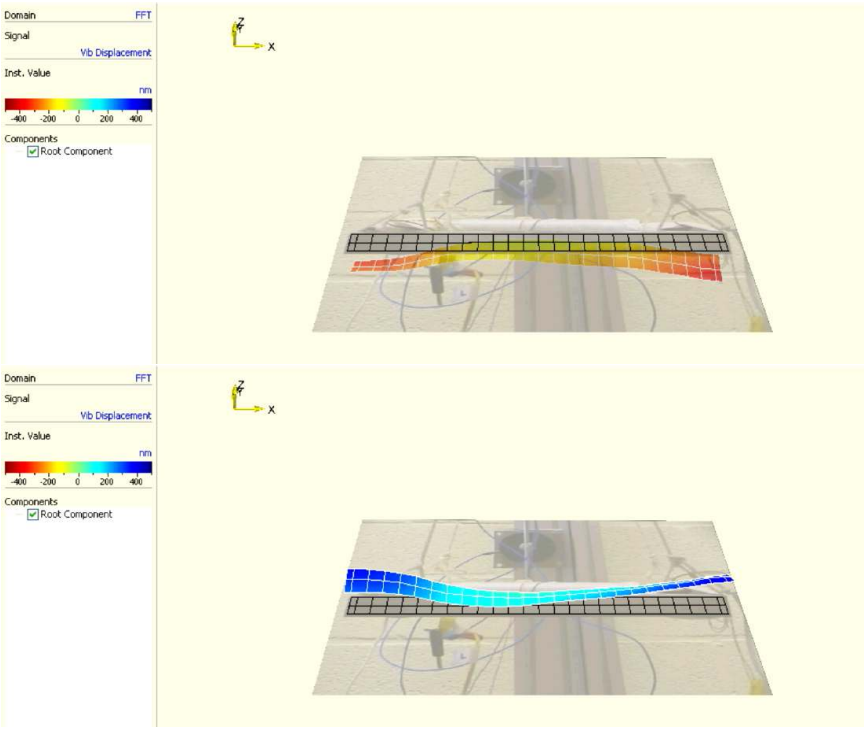

Figure 6.7: A 3D vibration measurement of the free leg of the single-phase test transformer core under a purely sinusoidal magnetic induction with 1.2T amplitude and 50Hz representing the maximum (inward) and the minimum (outward) deformations from the top to the bottom, respectively.

calculated by FE. As shown in Fig. 6.8 the shape of these eigen modes is rather complex and the deformation we measure is in fact the addition of these.

6.5. Vibration measurement under a sinusoidal magnetisation with a third harmonic component

In addition to the purely sinusoidal magnetisation, the deformation of the single phase test transformer core under a sinusoidal magnetisation with a third harmonic component was measured. Previously, the magnetostrictive behaviour of the core material, samples of the nonoriented M350-50A, under a sinusoidal magnetisation with a third harmonic was presented in §4.3.1. The results showed the significant influence of the amplitude and especially the phase delay of the third harmonic on the magnetostriction strain harmonics.

The surface of the free leg of the test transformer under a sinusoidal magnetic induction with a fundamental harmonic of 1.2T amplitude and 50Hz frequency and a

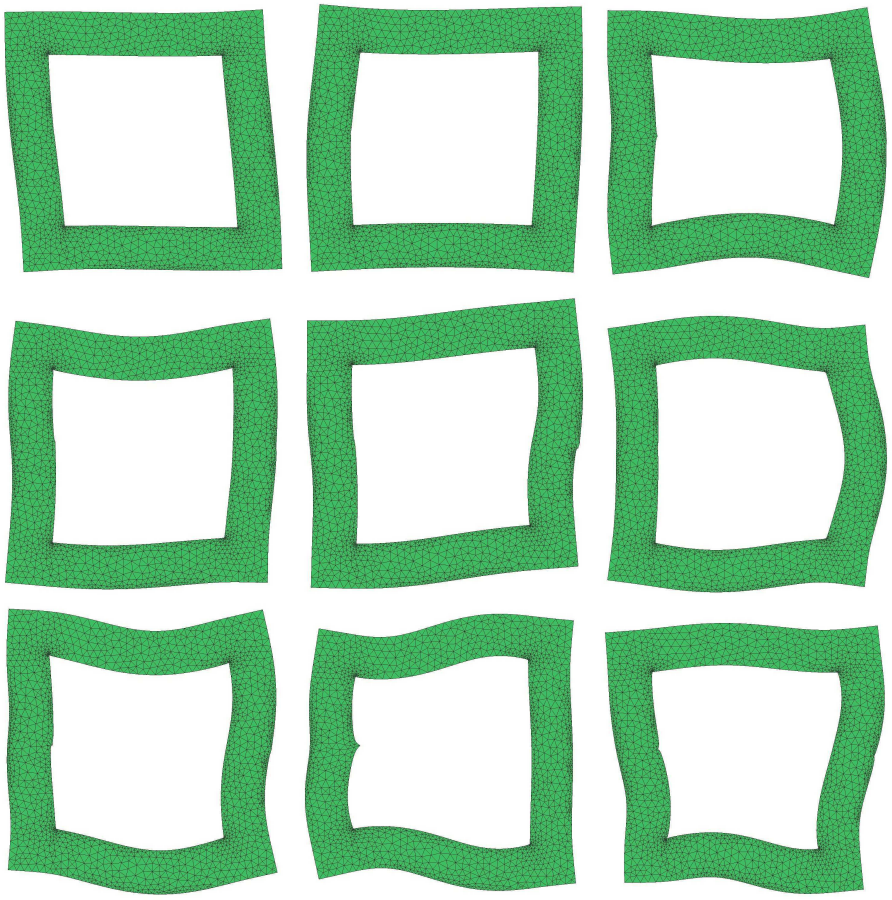

Figure 6.8: The first nine eigen eigen modes of the single-phase test transformer core calculated by the FE technique arranged from left to right from top to bottom.

third harmonic with 6% amplitude and 0°, 90° and 180° phase delays was scanned. Fig. 6.9 shows three pictures of the free leg deformation animations under the aforementioned phase delays from the top to the bottom corresponding to 0°, 90° and 180° phase delays, respectively. Based on Fig. 6.9 and Fig. 6.7, two main observations can be pointed out. All three measurements under a magnetisation with a third harmonic, compared with that under a purely sinusoidal, show a more wavy deformation of the free leg surface. In Fig. 6.7 the surface deformation deforms more or less in a quadratic shape. However, the surface deformation in Fig. 6.9 shows some fluctuations in a sinusoidal shape in addition to the main quadratic deformation. Moreover, we can observe in the same figure that the larger the phase delay of the third harmonic, the larger the fluctuations. For the case of the 0° phase delay the fluctuations are at the leg corners.

However, going to the 90° phase delay they grow more along the leg. In the case of the 180° phase delay the whole leg undergoes a sinusoidal deformation. Once again, we can conclude that to consider the influence of the higher harmonics in the grid on the magnetostrictive deformation of transformer core, both the amplitude and the phase delay of the higher harmonic, with respect to the fundamental, play a significant role.

6.6. Conclusion

The two-dimensional FE computation technique for the calculation of the magnetostrictive deformation of cores of transformers and electrical machines was presented in chapter 5. In this chapter the validation of this technique was studied. In the past, the FE calculated results for a three-phase transformer core were compared with vibration measurements of a similar core. However, mainly due to the step-lap assembly of the core the comparison of the results was not analogous and thus the technique was not validated.

In this PhD work, a new validation has been performed this time on a single-phase transformer core with an assembly without any lap joints. The vibrations of the core were measured by using PSV-400 scanning vibrometer. The FE results showed similar deformations for all three nodes. However, the vibration measurement results showed that the deformations are more significant in the leg corners. As a result, the comparison showed good agreement for one of the three selected node and less for the other two nodes.

The reason is that our calculation technique is 2D and thus does not account for the 3D effect of laminations. In fact, he FE computation technique calculates a 2D deformation, while the scanning vibrometer measured a 3D deformation. Thus, the eigen modes of the core may not have been calculated accurately which results in some differences. To conclude, the FE computation technique can still be improved by going from a 2D approach to a 3D approach.

In addition, a comparison between the deformation of the free leg of the test transformer core under a purely sinusoidal magnetisation and a magnetisation with a third harmonic component showed that the phase delay of the third harmonic can significantly affect the deformation form.

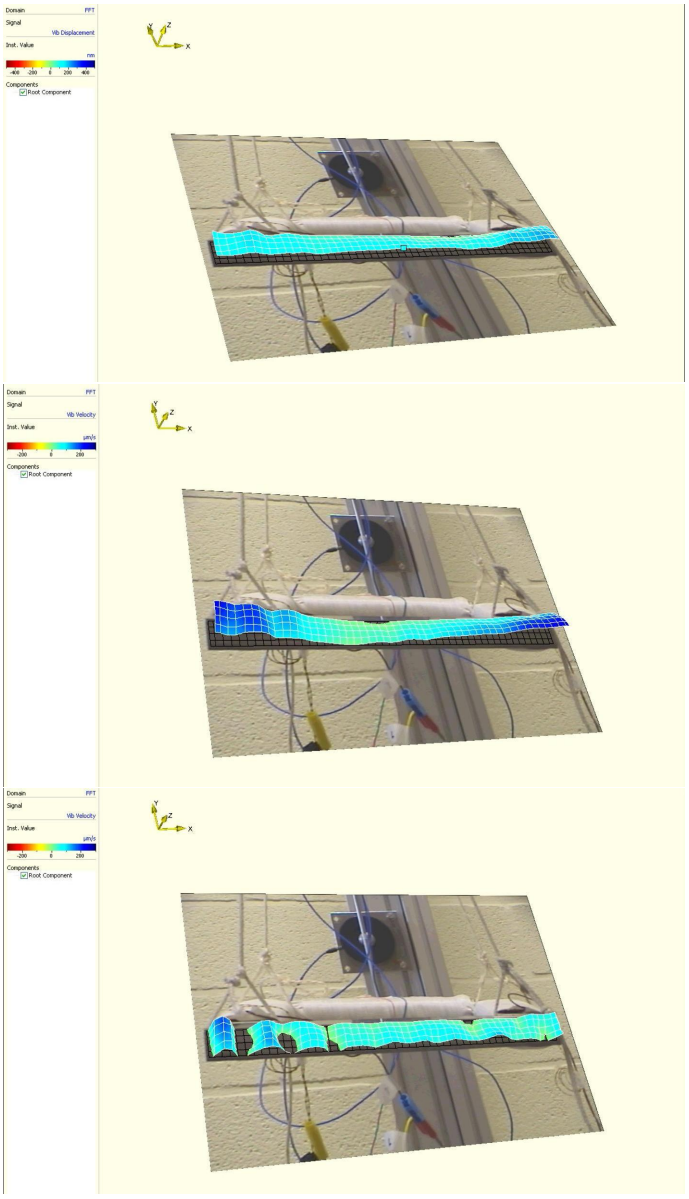

Figure 6.9: A 3D vibration measurement of the free leg of the single-phase test transformer core under a sinusoidal magnetic induction with a fundamental harmonic of 1.2T amplitude and 50Hz and a third harmonic with 6% amplitude and 0°, 90° and 180° phase delays from the top to the bottom, respectively.

CHAPTER 7

Application for a three-phase transformer core

7.1. Introduction

The magnetostrictive deformation computation technique and a validation on a single-phase test transformer core have been presented in chapter 5 and 6, respectively. Since the focus of this work is on the magnetostrictive deformation of transformers, as an application for the FE technique the vibrations of a three-phase transformer core are calculated.

The transformer core vibrations are computed under a sinusoidal magnetisation with a higher harmonic component. For the case of a three-phase transformer the presence of the fifth harmonic is relevant, since this harmonic has relatively the largest contribution in the European grid voltage [56]. To this end, the influence of the fifth harmonic with different amplitudes and phase delays with respect to the fundamental harmonic is considered for the FE calculations.

The chapter starts with a short overview on the effects of the higher harmonics on network equipments and especially on transformers. Further on, the FE computation results under a magnetisation with a fifth harmonic and a comparison with those under a purely sinusoidal magnetisation will be presented.

7.2. Three-phase transformer under a sinusoidal magnetisation with a fifth harmonic component

As mentioned in §4.3, the presence of higher harmonics on the grid voltage is unavoidable. They are mainly caused by non-linear loads connected to the grid, the ratio of which over linear loads has rapidly increased during the last years.

7.2.1 The importance of the study

To highlight the unwanted impacts of the higher harmonics of the grid on the network equipments and consumer appliances below some of the most common consequences are enumerated [56]:

- The electricity users may be subjected to voltages and currents at frequencies which they were not designed for.
- The cables and the overhead lines are derated as a result of the additional losses.
- The network equipments and the connecting devices age faster due to the ample harmonic currents.

Regarding power transformers, the main impact of the higher harmonics is an increase of the rated power losses, which results in a temperature rise inside the transformer. The heat build-up can have a negative effects on the insulation and eventually shorten the transformer lift time. In fact the K-factor ratio, which was mentioned in §4.3, is applied to make sure that transformers work within the design rated conditions to avoid unwanted consequences.

In this chapter the influence of the higher harmonics of the electricity grid on the magnetostrictive deformation of a three-phase transformer core (50kVA) is computed. The transformer core material is the grain-oriented electrical steel[1] the magnetostriction strains of which have been previously presented, see §4.2.1. The dimensions of the core laminations are 770×440mm and the core thickness is 90mm. For the calculation only a primary winding is applied to magnetise the core without any secondary windings since there are no loads assigned.

7.2.2 Magnetisation condition

The ANN models designed ($B-\lambda_{\parallel}$, $B-\lambda_{\perp}$) for the FE computations have been trained based on the measurement results of the samples of GO-I. The $B-\lambda$ measurements were performed under a sinusoidal magnetisation with a fifth harmonic component. Different amplitudes of the fundamental harmonic of the magnetic induction B have been applied, where for each the amplitude of the fifth harmonic on the induction has been varied from 1% to 10% of that of the fundamental. The phase delay of the fifth harmonic has been changed from 0° to 360°, with respect to the fundamental. These results were presented in §4.3.2.

7.3. FE computation results

The FE computations of a real three-phase transformer core have been performed under a magnetisation for which the amplitude of the fundamental harmonic of the voltage has been assigned to 340V, corresponding to an average magnetic induction

[1] Lamination of 3% Si-Fe with 0.9W/kg losses at 1.5T and 50Hz which has been previously named as GO-I.

with a fundamental harmonic amplitude of 1.3T. Three different amplitudes have been assigned to the fifth harmonic on the voltage 15%, 30% and 45% of that of the fundamental harmonic. For each of the fifth harmonic amplitudes, phase delays of 0°, 90°, 180° and 270° have been considered. The deformations have been all computed in the frequency domain and eigen modes have been calculated. The results for the first seven eigen modes for both 100Hz and 200Hz harmonics are presented in the following sections.

7.3.1 100Hz harmonic data

The magnitude of the first seven eigen modes for the 100Hz harmonic under a purely sinusoidal magnetisation and a sinusoidal magnetisation with a fifth harmonic with 15% amplitude ratio is shown in Fig. 7.1. The abscissa shows the fifth seven eigen modes under a purely sinusoidal magnetisation and those under a magnetisation with a fifth harmonic with 0°, 90°, 180° and 270° phase delays, respectively. Fig. 7.2 and Fig. 7.3 show similar data under a magnetisation with a fifth harmonic for which the amplitude percentage of the fifth harmonic has been assigned to 30% and 45% respectively of that of the fundamental.

Looking at these figures, the first eigen mode is always higher under a purely sinusoidal magnetisation. It decreases when there is a fifth harmonic with 0° delay, and even reduces for a 90° delay. An increase of the first eigen mode is observed for a fifth harmonic with 180° delay, compared with that for a 90° delay. Going from a fifth harmonic with 180° to 270° and 360° phase delay (similar to the case of 0° delay) the magnitude of the 100Hz harmonic of the first eigen mode decreases again. The variations of the second and third eigen modes are small. The fourth mode is always higher in the case of a purely sinusoidal magnetisation than for those under a sinusoidal magnetisation with a fifth harmonic component. Variations of the relative amplitude and the phase delays of the fifth harmonic do not show significant changes on the fourth eigen mode. The last three eigen modes, i.e. fifth, sixth and seventh, remain almost unaffected by the fifth harmonics.

7.3.2 200Hz harmonic data

Similar to the figures for the magnitude of the 100Hz harmonic, Fig. 7.4, Fig. 7.5 and Fig. 7.6 show the magnitude of the first seven eigen modes for the 200Hz harmonic under the same magnetisations. In the same manner, the abscissae are the first seven eigen modes under a purely sinusoidal magnetisation and those under a magnetisation with a fifth harmonic component with 0°, 90°, 180° and 270° phase delays, respectively.

In general, we can see that the 200Hz harmonic magnitude variations are relatively larger than those of 100Hz harmonic. In all three figures, the magnitudes of the first seven eigen modes for the 200Hz harmonic under a magnetisation with a fifth

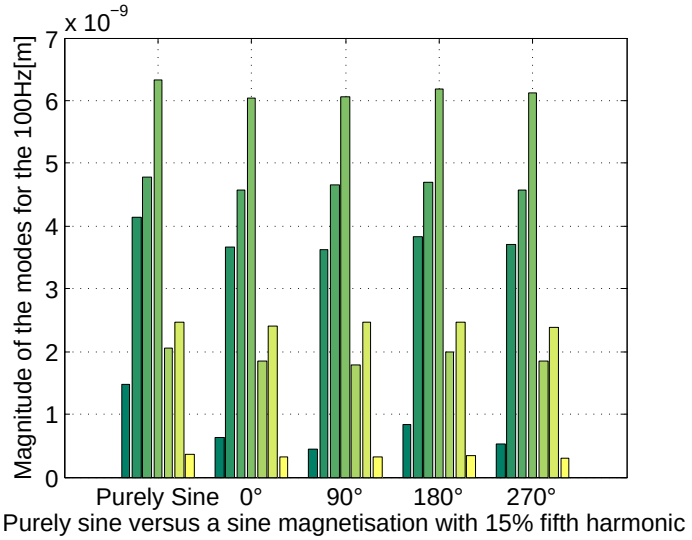

Figure 7.1: The magnitude of the first seven eigen modes for the 100Hz harmonic of a three-phase transformer core under a purely sinusoidal voltage and a sinusoidal voltage with a fifth harmonic with 15% amplitude ratio and 0°, 90°, 180° and 270° phase delays.

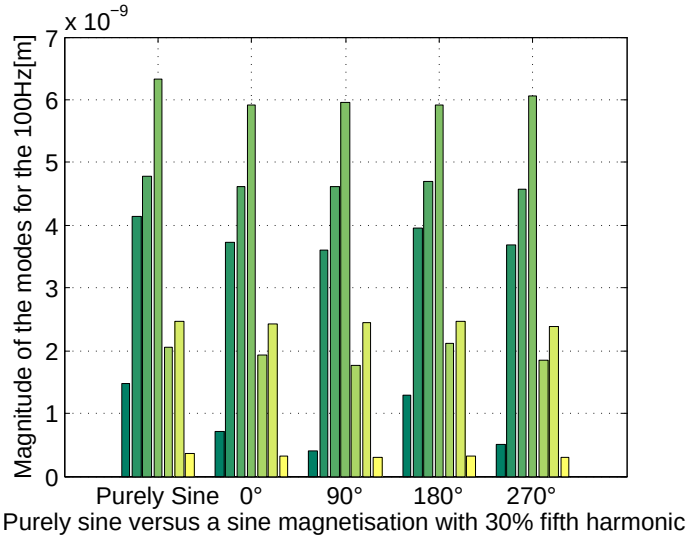

Figure 7.2: The magnitude of the first seven eigen modes for the 100Hz harmonic of a three-phase transformer core under a purely sinusoidal voltage and a sinusoidal voltage with a fifth harmonic with 30% amplitude ratio and 0°, 90°, 180° and 270° phase delays.

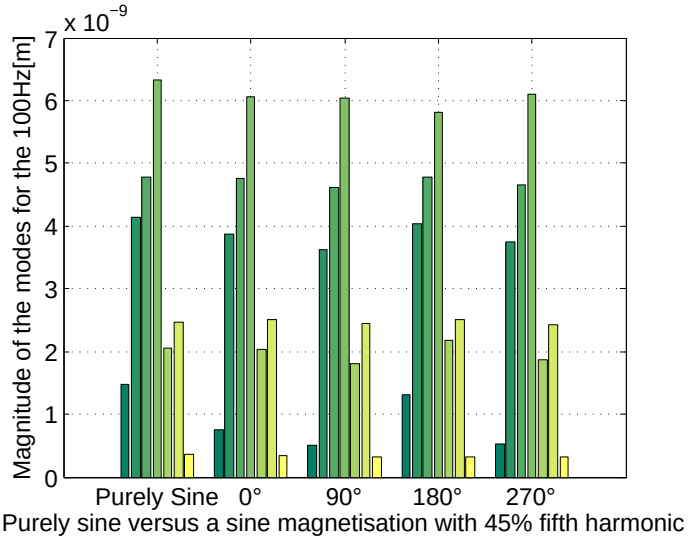

Figure 7.3: The magnitude of the first seven eigen modes for the 100Hz harmonic of a three-phase transformer core under a purely sinusoidal voltage and a sinusoidal voltage with a fifth harmonic with 45% amplitude ratio and 0°, 90°, 180° and 270° phase delays.

harmonic component on the voltage are larger than those under a purely sinusoidal magnetisation.

The reason for it can be presented based on the relation between the magnetostriction strain λ and the magnetic induction B. Previously, it has been explained that magnetostriction strains are proportional to the square of the magnetic induction, see §2.6.5. In this case, the magnetic induction contains a fundamental frequency f of 50Hz and a fifth harmonic. Neglecting the phase delay between the fundamental and the fifth harmonic, the total magnetic induction can be expressed as

$$B(t) = B_1 \cos(\omega t) + B_5 \cos(5\omega t),\ \omega = 2\pi f, \tag{7.1}$$

where B_1 and B_5 are the amplitude of the fundamental and the fifth harmonic components, respectively. Thus, magnetostriction strain λ is then proportional to the square of the total magnetic induction B as

$$\begin{aligned} \lambda &\propto (B_1 \cos(\omega t) + B_5 \cos(5\omega t))^2 \\ &= B_1^2 \cos^2(\omega t) + B_5^2 \cos^2(5\omega t) + B_1 B_5 \cos(\omega t + 5\omega t) \cos(\omega t - 5\omega t), \end{aligned} \tag{7.2}$$

where the first and the second terms contain 0 and 100Hz and 0 and 500Hz, respectively. The last term contains the sum and the subtract of the two frequencies, i.e. 200Hz and 300Hz frequencies. As a result we can see that the superposition of a

fundamental frequency of 50Hz and a fifth harmonic generates a 200Hz term and thus such harmonic component has a significant increase compared with that under a purely sinusoidal magnetisation.

Increasing the amplitude percentage of the fifth harmonic, from 15% to 30% and 45%, increases the magnitude of the 200Hz harmonic component clearly.
Regarding the phase delay of the fifth harmonic, with represent to the fundamental, an increase from 0° to 90° delay increases the magnitude of all the seven eigen modes for the 200Hz harmonic component. Going from 90° to 180° delay decreases the magnitude of the 200Hz harmonic of all the modes except the fourth one. With a further increase of the phase delay to 270° the 200Hz harmonic magnitude variations are very small but slightly different with different percentages of the fifth harmonic component. For the case of a 15% fifth harmonic, all the modes show a decrease. For the case of a 30% fifth harmonic some modes slightly increase and some decrease. For the case of a 45% fifth harmonic, some modes increase and some stay constant. Going from a 270° phase delay to 360° (similar to the case of 0° delay) the magnitude of the 200Hz harmonic of all the modes decrease. In general, the variations of the phase delay of the fifth harmonic on the voltage have more effect on the first four eigen modes than on the last three modes.

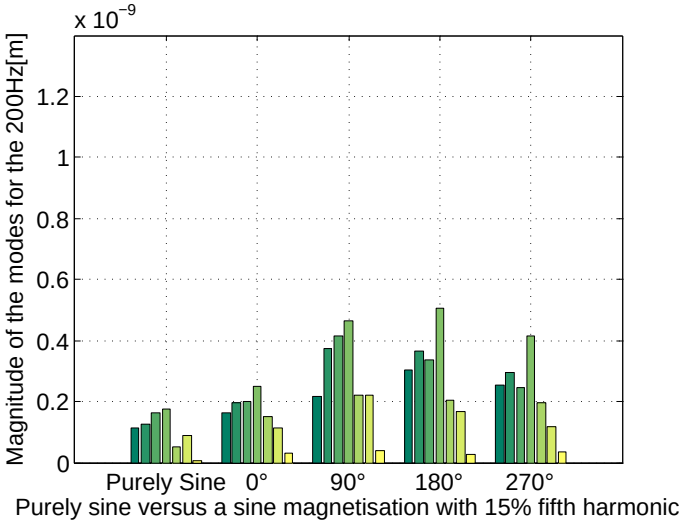

Figure 7.4: The magnitude of the first seven eigen modes for the 200Hz harmonic of a three-phase transformer core under a purely sinusoidal voltage and a sinusoidal voltage with a fifth harmonic with 15% amplitude ratio and 0°, 90°, 180° and 270° phase delays.

To clearly see the variations of the magnitude of the first seven modes for the 200Hz harmonic under a magnetisation with different percentages of the fifth harmonic Fig. 7.7, Fig. 7.8, Fig. 7.9 and Fig. 7.10 are plotted. The abscissa in Fig. 7.7

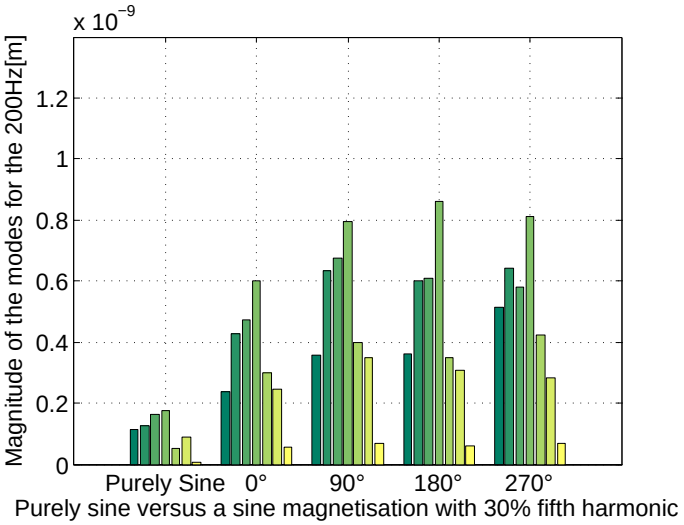

Figure 7.5: The magnitude of the first seven eigen modes for the 200Hz harmonic of a three-phase transformer core under a purely sinusoidal voltage and a sinusoidal voltage with a fifth harmonic with 30% amplitude ratio and 0°, 90°, 180° and 270° phase delays.

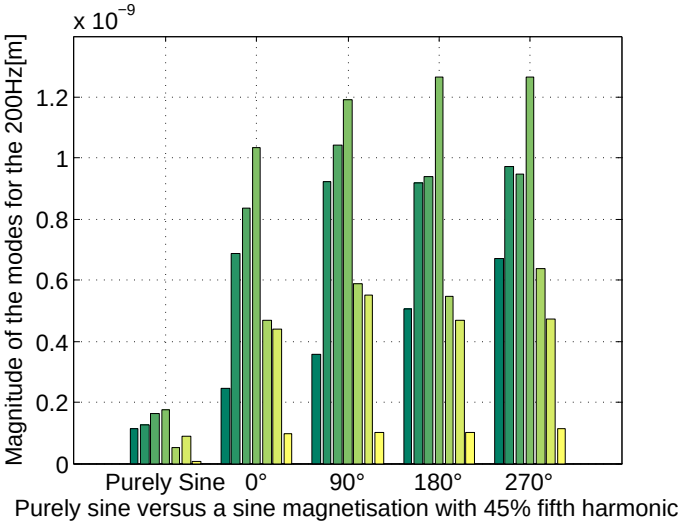

Figure 7.6: The magnitude of the first seven eigen modes for the 200Hz harmonic of a three-phase transformer core under a purely sinusoidal voltage and a sinusoidal voltage with a fifth harmonic with 45% amplitude ratio and 0°, 90°, 180° and 270° phase delays.

represents the first seven eigen modes with a fifth harmonic always with a 0° phase de-

lay and with 15%, 30% and 45% amplitude ratios, respectively. The abscissae in Fig. 7.8, Fig. 7.9 and Fig. 7.10 are similar to that of Fig. 7.7, but for the phase delays of 90°, 180° and 270°, respectively. We can clearly see that the magnitude of the 200Hz always increases with an increase of the amplitude percentage of the fifth harmonic on the applied voltage, regardless of its phase delay with respect to the fundamental harmonic component.

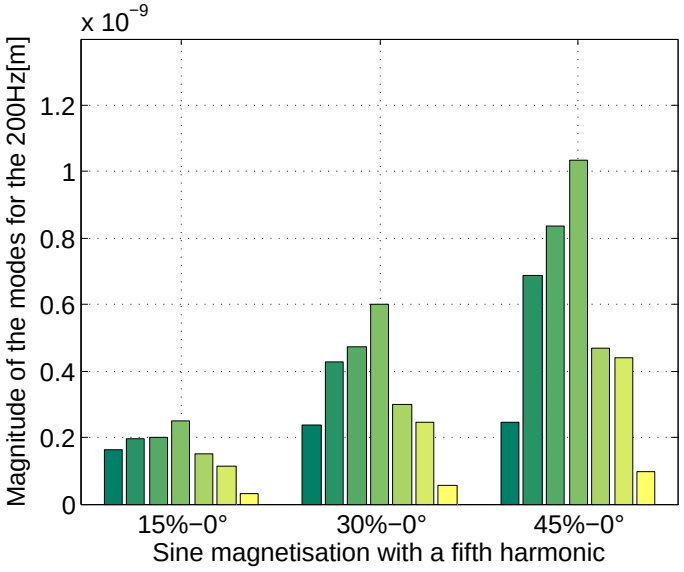

Figure 7.7: The magnitude of the first seven eigen modes for the 200Hz harmonic of a three-phase transformer core under a sinusoidal voltage with a fifth harmonic with 15%, 30% and 45% amplitude ratios with 0° phase delay.

The ratios of the magnitude of the 200Hz harmonic of the first four eigen modes under a magnetisation with a fifth harmonic component over those under a purely sinusoidal magnetisation are presented in Table 7.1. Once again, we can see how the increase of the relative amplitude and the phase delay of the fifth harmonic affects the magnitude of the 200Hz harmonic.

7.4. Results discussion

According to the presented results for the 100Hz and 200Hz harmonics of the first seven modes of the magnetostrictive vibrations of the three-phase transformer core the followings can be concluded.

- **100Hz data**
  In general, the magnitude of the first seven eigen modes for the 100Hz harmonic

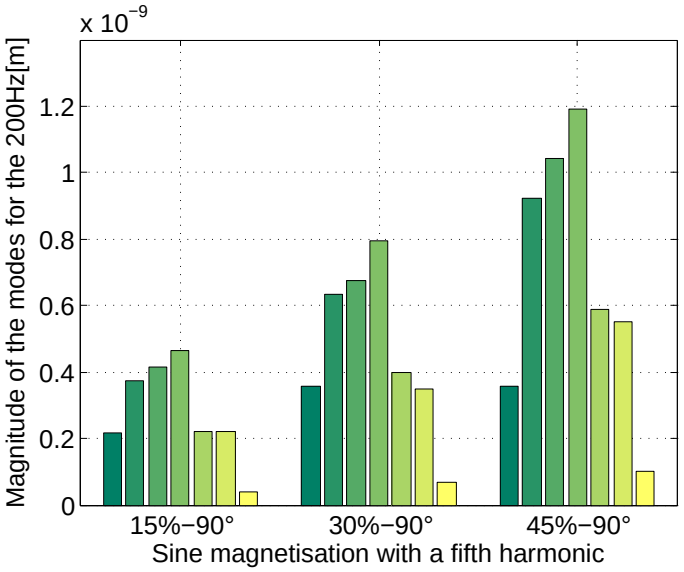

Figure 7.8: The magnitude of the first seven eigen modes for the 200Hz harmonic of a three-phase transformer core under a sinusoidal voltage with a fifth harmonic with 15%, 30% and 45% amplitude ratios with 90° phase delay.

stays almost the same. In another word, the magnitude of the 100Hz harmonic under a purely sinusoidal voltage is similar to those under a sinusoidal voltage with a fifth harmonic component. The variations of the amplitude percentages or the phase delays of the fifth harmonic, with respect to that of the fundamental, also do not result in significant changes of the 100Hz harmonic.

- **200Hz data**
  For the case of the magnitude of the first seven eigen modes for the 200Hz harmonic of the magnetostrictive vibrations of the three-phase transformer core significant variations are observed. Presence of a fifth harmonic on the applied voltage always causes an increase of the 200Hz magnitude, compared with the case of a purely sinusoidal applied voltage.

  In the case of a magnetisation with a fifth harmonic component, a higher percentage of the fifth harmonic clearly results in a higher 200Hz harmonic magnitude, see Fig. 7.7, Fig. 7.8, Fig. 7.9 and Fig. 7.10 and Table 7.1.

  The phase delay of the fifth harmonic on the applied voltage, also has an influence on the magnitude of the 200Hz harmonic components. In general, an increase of the phase delay from 0° to 90° and up to 180° increases the magnitude of the 200Hz harmonic. Further increase of the phase delay from 180° to 270° causes an increase in the cases of an applied voltage with a fifth harmonic with 30% and 45% amplitude ratios and a decrease in the case of a magnetisation with a fifth harmonic

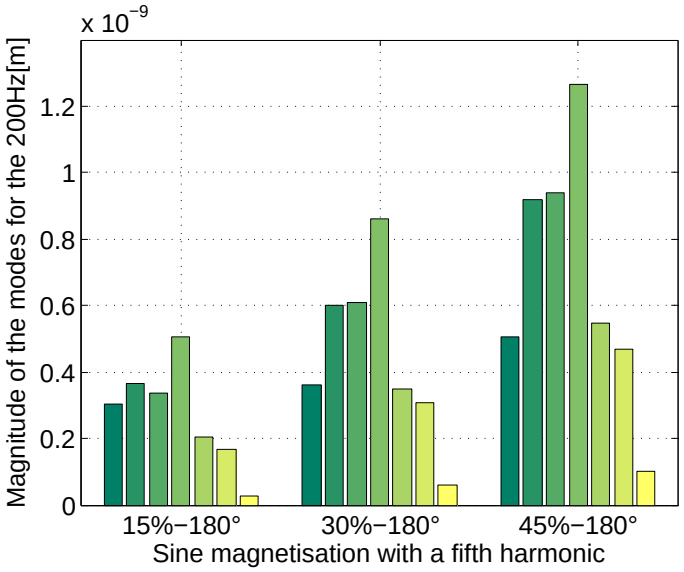

Figure 7.9: The magnitude of the first seven eigen modes for the 200Hz harmonic of a three-phase transformer core under a sinusoidal voltage with a fifth harmonic with 15%, 30% and 45% amplitude ratios with 180° phase delay.

with 15% amplitude ratio. Further increase of the phase delay up to 360° causes a decrease of the 200Hz harmonic magnitude.

So, we can say that among all the results, the lowest magnitude of the 200Hz is obtained under a purely sinusoidal magnetisation. The highest magnitude of the 200Hz is often for the case of a sinusoidal applied voltage with a fifth harmonic with 180° or 270° phase delays, see Fig. 7.4, Fig. 7.5, Fig. 7.6 and Table 7.1. For a fifth harmonic with 15% amplitude ratio and 180° phase delay, an increase with a factor of 2.641 results for the first eigen mode compared with the result under a purely sinusoidal magnetisation. If the ratio of the fifth harmonic increases to 30% and 45% of that of the fundamental with a phase delay of 270°, the 200Hz magnitude of the first eigen modes increases with a factor of 4.472 to 5.835. For the fourth eigen mode, which is the largest among the first seven modes, the differences between the magnitude of the 200Hz harmonic under a purely sinusoidal magnetisation and a sinusoidal magnetisation with 180° phase delay is even larger. For a 15%, 30% and 45% fifth harmonic ratio, an increase with a factor of 2.886, 4.929 and 7.242 are observed, respectively.

Three-phase transformer core deformation eigen modes

The three-phase transformer core deformation for the first seven eigen modes are shown in Fig. 7.11. Table. 7.2 show the core resonance frequencies.

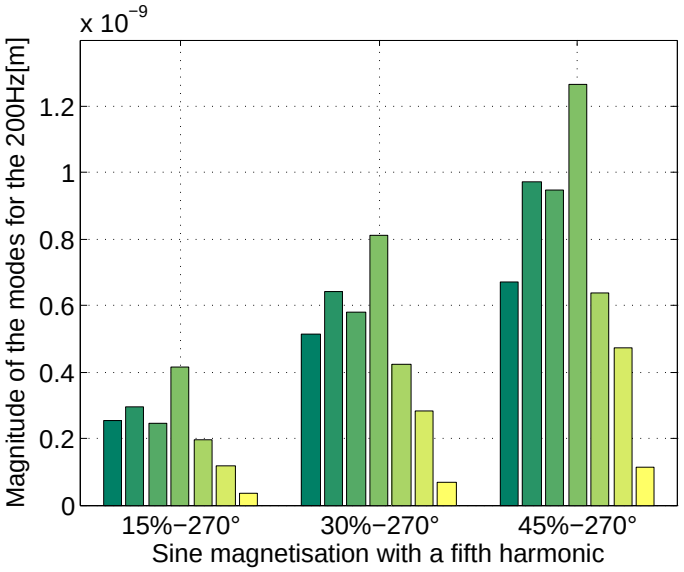

Figure 7.10: The magnitude of the first seven eigen modes for the 200Hz harmonic of a three-phase transformer core under a sinusoidal voltage with a fifth harmonic with 15%, 30% and 45% amplitude ratios with 270° phase delay.

7.5. Conclusion

Magnetostrictive vibration eigen modes of a three-phase transformer core under a sinusoidal magnetisation with a fifth harmonic component, which has been computed by the FE technique, were presented in this chapter. A comparison of the results with those under a purely sinusoidal magnetisation showed that in general the variations of the magnitude of the eigen modes for the 100Hz harmonic are small. However, the 200Hz harmonics show a significant increase when there is a fifth harmonic on the applied voltage.

A higher percentage amplitude ratio of the fifth harmonic on the voltage resulted in a higher magnitude of the 200Hz harmonic component. The variations of the phase delay of the fifth harmonic with respect to that of the fundamental harmonic of the applied voltage also caused significant variations of the 200Hz magnitude.

To conclude we can say that the influence of the presence of the higher harmonics in the grid voltage on the magnetostrictive deformation of transformer cores should not be under-estimated. To study such effect, considering only the amplitude percentage of such higher harmonics is not sufficient and their phase delays must be also taken into account.

Table 7.1: The ratio of the magnitude of the first four eigen modes for the 200Hz harmonic of the core vibration under a magnetisation with a fifth harmonic compared with that under a purely sinusoidal magnetisation,

a) fifth harmonic with 15% amplitude ratio and 0°, 90°, 180° and 270° phase delays, with respect to that of fundamental.

mode	15%-0°	15%-90°	15%-180°	15%-270°
1	1.407	1.897	2.641	2.216
2	1.567	3.002	2.939	2.373
3	1.214	2.527	2.050	1.491
4	1.4238	2.664	2.886	2.364

b) fifth harmonic with 30% amplitude ratio and 0°, 90°, 180° and 270° phase delays, with respect to that of fundamental.

mode	30%-0°	30%-90°	30%-180°	30%-270°
1	2.051	3.103	3.159	4.472
2	3.420	5.103	4.814	5.168
3	2.866	4.109	3.710	3.540
4	3.438	4.554	4.929	4.633

c) fifth harmonic with 45% amplitude ratio and 0°, 90°, 180° and 270° phase delays, with respect to that of fundamental

mode	45%-0°	45%-90°	45%-180°	45%-270°
1	2.136	3.119	4.412	5.835
2	5.533	7.405	7.366	7.824
3	5.076	6.353	5.719	5.776
4	5.919	6.803	7.242	7.244

Table 7.2: The resonance frequencies corresponding with the first eight eigen modes.

mode	Resonance frequency [kHz]
1	11.735
2	22.980
3	42.244
4	48.513
5	56.879
6	58.771
7	65.038

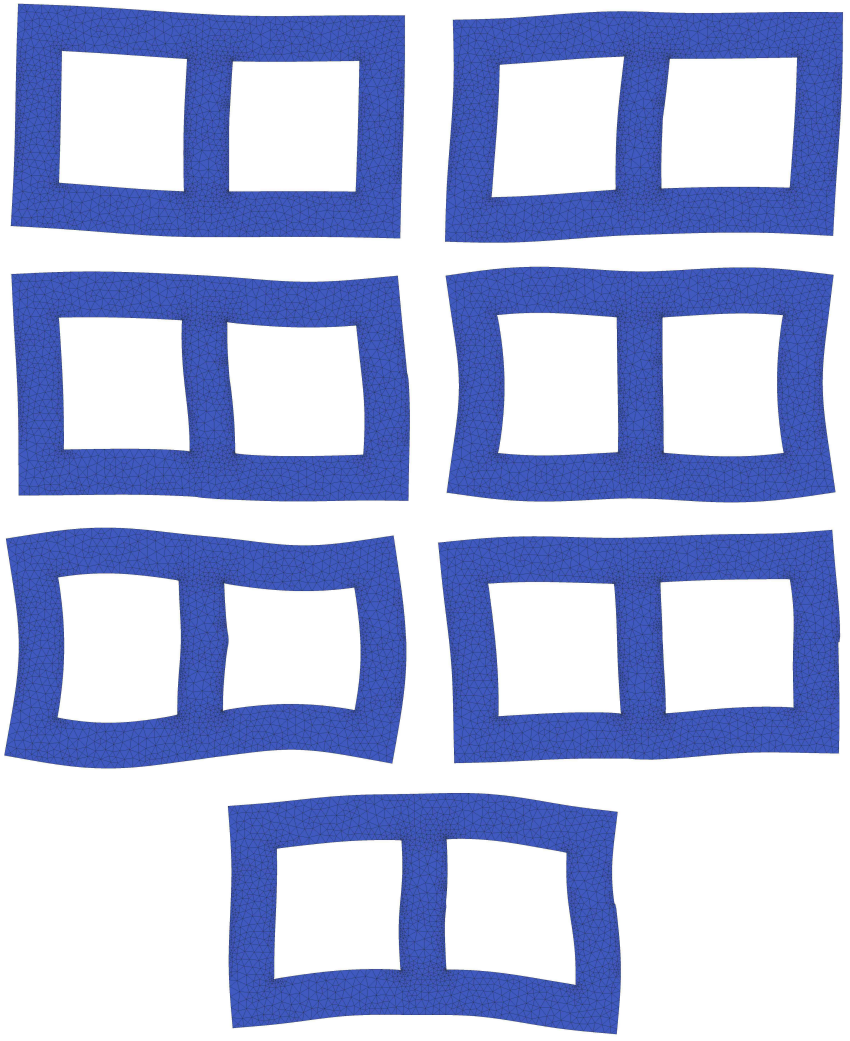

Figure 7.11: The first seven eigen mode of the magnetostrictive deformation of the three-phase transformer core.

CHAPTER 8

Conclusion and suggestions for future research

8.1. General conclusions

The ultimate goal of the research on magnetostriction is to reduce vibrations and noise of electrical machines and transformers. This research is in fact interdisciplinary and requires knowledge in different engineering disciplines e.g. mechanical, electrical and material research.

The aim of the research presented here is to study this subject from the electrical point of view with a focus on the magnetic sources of noise. Such noise is itself generated in the core of the device. To lower the magnetic noise an optimization method is required. Such a method should contain a sub-method to first calculate the vibrations of the core. This computation method has been developed in the past, which considers both the effects of the electromagnetic forces and magnetostriction. It computes the 2D deformation of the core based on the FE technique. The contribution of the electromagnetic forces can be analytically calculated. However, for the contribution of magnetostriction a model of the behaviour of the core material is necessary, which must be developed based on experimental data.

In general, magnetostriction is a complex magneto-mechanical phenomenon. It strongly depends on the material composition, the applied magnetic induction and the presence of any external forces. As a result, magnetostriction strain measurements are challenging and even though many setups have been developed so far, still a unique approach to thoroughly identify the magnetostrictive behaviour of different materials is missing.

A setup has been developed in the past in EELAB which was based on the strain gauge technique. This setup measures 2D magnetostriction strains under a unidirectional magnetisation. The magnetostriction strains are measured only as a func-

tion of an externally applied magnetic induction and any external pressure is avoided to the sample. The results obtained by this setup were accurate under magnetic inductions larger than 0.8T. However, this strain gauge setup could not measure the magnetostriction strains of coated samples and thus a new setup was built during this PhD work.

This new setup, which is based on laser technique, also measures 2D magnetostriction strains under a uni-directional magnetisation. Comparing the magnetostriction strain measurement results of non-coated samples of grain-oriented and nonoriented electrical steel obtained by the laser setup, with those obtained by the strain gauge setup, similar peak to peak amplitudes were observed. However, the accuracy of laser measurement results was relatively higher. Measuring the magnetostriction strains of the coated samples of the same materials by the laser setup was an achievement with this setup. The results clearly showed how the application of coating on electrical steel laminations is beneficial in lowering the magnetostrictive strains.

Magnetostriction strain measurement under a sinusoidal magnetisation with a higher harmonic component also was a new step in this work. The measured strains under a sinusoidal magnetisation with a third harmonic component showed that only knowing the amplitude of the higher harmonic is not sufficient to estimate the variations of the magnetostriction. The phase delay of such higher harmonic can significantly affect the magnetostriction strains. For a magnetisation with a third harmonic component, both the 100Hz and (in particular) the 200Hz harmonics of the magnetostriction strains change significantly. The measurement results under a sinusoidal magnetisation with a fifth harmonic on a grain-oriented electrical steel showed not much influence on the 100Hz harmonic of the magnetostriction strains. However, it showed a significant influence on the 200Hz harmonic of the magnetostriction strains. Similar to the measurements with a third harmonic, the results under a magnetisation with a fifth harmonic highly depend on the amplitude and phase delay of that of the fifth harmonic.

In the next step, the FE method for the deformation computation has been validated on a test transformer core, based on the measurement results obtained by the laser setup. The test transformer had a special design to only model the vibrations of the core due to magnetostriction. The modelling of magnetostriction strain results has been done by ANN. Such modelling has been previously proved to offer a high accuracy and short calculation time which is necessary for the optimization method.

After validating the FE technique, in the next step the method has been improved to consider the presence of the higher harmonics on the magnetisation signal. This is important for calculating the magnetostrictive vibrations of transformers, since the grid voltage is never purely sinusoidal.

In the end, the effect of the fifth harmonic of the grid on the magnetostrictive deformation of a three-phase transformer core is calculated by the FE method. The results showed the significant influence of the fifth harmonic especially on the 200Hz harmonic of the magnetostriction. Considering a fifth harmonic with 45% amplitude

percentage and 270° phase delay, with respect to the fundamental harmonic, the first eigen mode of the core increases more than five times compared to that under a purely sinusoidal magnetisation. Under the same magnetisation, the variation of the fourth eigen mode is higher than seven times compared to that under a purely sinusoidal magnetisation.

In this PhD only transformers are considered, however, the work can be easily applicable to other electrical machines, as well.

8.2. The novelty of this PhD work

The research contains some original and novel work which are listed below:

The magnetostriction strain measurement setup which has been developed during this PhD work is a novel setup. The application of the laser vibrometers for the strain measurements has been reported in the past. However, the developed setup does not require a calibration for every time use, which makes the measurements faster and lowers the errors. Moreover, since the lasers have a compact design, the setup can be easily used by people who do not have a background about laser techniques.

The magnetostriction strains reported in the literature, are often performed under a purely sinusoidal magnetisation. Some measurements are reported under a sinusoidal with a higher harmonic, however only the harmonics in phase with the fundamental harmonic are considered. In this work, measurements are performed under a sinusoidal magnetisation with a higher harmonic, for which different phase delays are taken into account. The results of such study showed that the phase delay of the higher harmonic of the magnetisation can significantly change the harmonics of the magnetostriction strains. Such study is especially useful for the identification of the magnetostrictive deformations of the transformer cores.

An FE technique has been developed in the past to calculate the deformation of the cores of transformers and electrical machines. This technique could not be validated on a three-phase transformer core because of the lap joint assembly of the transformer core.
In this work, a simple transformer core is designed for a single-phase transformer. Such core has a special design to resemble only the magnetostrictive deformation. The deformation of this core is computed and compared with the measurement results. The comparison between the computed and the measured results showed quite good agreement, which is also another step forward.

Previously, the FE computation technique could only calculate the deformations under a magnetisation only with a fundamental harmonic component. Considering the importance of the higher harmonics on the magnetostrictive behaviour, the technique

is improved to consider the presence of the higher harmonics on the magnetisation voltage as well.

To effect of the higher harmonics is studied on the deformation of transformer cores. To this end, the magnetostrictive deformation of a three-phase transformer core is calculated by the FE technique under a sinusoidal magnetisation with a fifth harmonic component.

8.3. Suggestions for future research

Of course, this PhD is only a modest contribution to the research on magnetostriction. There still remains a lot of research topics in this field. Some suggestions are:

Perhaps the first interesting idea is to measure magnetostriction strains in 3D. The setups developed during this PhD work and in the past are suitable for 2D measurements. However, measuring the magnetostriction strains in the third dimension, i.e. the out-of-plane strains which corresponds to the change of a sample in thickness, can be the next step. The strain gauge setup cannot be adapted to do so, however, the laser setup has the potential for it. Considering the small thickness of the electrical steel laminations the measurement accuracy will be a crucial task.

Another idea is measuring magnetostriction strains under an external pressure. Since magnetic cores of transformers often contain areas of increased stress, magnetostriction measurements under different pressures are necessary.

Once a 3D magnetostrictive behaviour of a material is obtained, it can be interesting to compute the core vibrations also in 3D. Even without a 3D magnetostrictive model a 3D computation is possible. In other words, the magnetic computation can be done in 2D and only the mechanical computation needs to be modelled in 3D. The challenge can be the modelling of the core geometry in 3D. For instance for the case of transformer cores, different lap joint assemblies and how the flux travels in such joints should be well identified. The clamping of the laminations in such lap joints needs to be considered. To this end, not only the magnetic but also the mechanical properties of the core should be well known.
As a validation of such 3D method for a transformer core, vibration measurements of the core are required. The vibration measurements presented in this work on a single-phase transformer core were limited to a special core design without any joints. However, this design was intended to validate the FE technique and is not realistic.

The next step toward the ultimate goal of this research is to apply the 3D core deformation in an optimization procedure to optimize transformer core design. The

aim of this optimization is in fact the reduction of vibrations and noise of transformer cores.

Bibliography

[1] W. Zawieska, "A power transformer as a source of noise," *International Journal of Occupational Safety and Ergonomics (JOSE)*, vol. 13, no. 4, 2007.

[2] L. Zhu, Q. Yang, R. Yan, Y. Li, X. Zhang, W. Yan, and J. Zhu, "Numerical computation for a new way to reduce vibration and noise due to magnetostriction and magnetic forces of transformer cores," *Journal of Applied Physics*, vol. 113, no. 17, 2013.

[3] B. Weiser, A. Hasenzagl, T. Booth, and H. Pfützner, "Mechanisms of noise generation of model transformer cores," *Journal of Magnetism and Magnetic Materials*, vol. 160, pp. 207–209, 1996.

[4] L. Lahn, C. Wang, A. Allwardt, T. Belgrand, and J. Blaszkowski, "Improved transformer noise behavior by optimized laser domain refinement at thyssenkrupp electrical steel," vol. 48, no. 4, pp. 1453–1456, 2012.

[5] ABB, "Transformer Handbook", Available online: http://dotorresg.files.wordpress.com/2011/12/abbtransformerhandbook.pdf.

[6] A. Moses, T. Phophongviwat, and S. Tabrizi, "Contribution of magnetostriction to transformer noise," *Universities Power Engineering Conference (UPEC)*, pp. 1–5, 2010.

[7] M. Yabumoto, S. Arai, R. Kawamata, M. Mizokami, and T. Kubota, "Recent development in grain-oriented electrical steel with low magnetostriction," *Journal of Material Engineering and Performance*, vol. 6, pp. 713–721, 1997.

[8] B. Weiser and H. Pfützner, "Relevance of magnetostriction and forces for the generation of audible noise of transformer cores," *IEEE Transactions on Magnetics*, vol. 36, no. 5, pp. 3759–3777, 2000.

[9] A. Belachen, "Vibrations of rotating electrical machines due to magnetomechanical coupling and magnetostriction," *IEEE Transactions on Magnetics*, vol. 42, pp. 971–974, 2006.

[10] H. Krönmuller and M. Fähnle, *Micromagnetism and the microstructure of ferromagnetic solids*. Max-Plank-Institut für Metallforschung, Stuttgart, Germany: Cambridge University Press, 1994.

[11] L. Vandenbossche, *Magnetic hysteretic characterization of ferromagnetic materials with objectives towards non-destructive evaluation of material degradation*. PhD thesis, Ghent University, Belgium, 2009.

[12] B. Van de Wiele, *Numerical study of magnetic processes: extending the Landau-Lifshitz-Gilbert approach from nanoscale to microscale*. PhD thesis, Ghent University, Belgium, 2010.

[13] G. Bertotti, *Hysteresis in magnetism: for physicists, materials scientists, and engineers*. San Diego, USA: Academic Press, 1998.

[14] J. P. Joule, "Sturgeons annals of electricity," vol. 8, p. 219, 1842.

[15] D. Jiles, *Introduction to magnetism and magnetic materials*. New York, USA: Chapman and Hall, 1991.

[16] R. Bozorth, *Ferromagnetism*. New York, USA: Wiley-IEEE Press, 1993.

[17] E. Lee, "Magnetostriction and magnetomechanical effects," *Reports on Progress in Physics*, vol. 18, no. 1, pp. 184–229, 1955.

[18] T. Hilgert, *Magnetische krachten en magnetostrictie in elektrisch staal en toepassingen op trillingen van elektrische machines en transformatoren*. PhD thesis, Ghent University, 2008.

[19] J. Shilling, "Domain structure during magnetisation of grain oriented 3% Si-Fe as a function of applied tensile stress," *Journal of Applied Physics*, vol. 42, no. 4, pp. 1787–1789, 1971.

[20] J. Shilling, "Magnetic properties and domain structure in grain-oriented 3% Si-Fe," *IEEE Transactions on Magnetics*, vol. 10, no. 2, pp. 195–223, 1971.

[21] J. Barros, T. Ros-Yanez, R. Colas, and Y. Houbaert, "Study of the workability and room temperature straining behaviour of highe silicon steel (4 wt% Si) by means of compression tests," *Revista De Metalurgia*, pp. 116–120, 2005.

[22] A. Moses, "Effects of applied stresses on the magnetic properties of high permeability silicon iron," *IEEE Transactions on Magnetics*, vol. MAG-15, no. 6, pp. 1575–1579, 1979.

[23] P. Anderson, A. Moses, and H. Sanbury, "Assessment of stress sensitivity of magnetostriction in grain-oriented silicon steel," *IEEE Transactions on Magnetics*, vol. 43, no. 8, pp. 3467–3476, 2007.

[24] L. Dupré, M. De Wulf, D. Makaveev, and J. Melkebeek, "Indirect identification of magnetostriction properties of sife alloys," *IEEE Transactions on Magnetics*, vol. 39, no. 5, pp. 3432–3434, 2003.

[25] A. Belachen, K. Fonteyn, R. Kouhia, P. Rasilo, and A. Arkkio, "Magnetomechanical coupled fe simulations of rotating electrical machines," *COMPEL: International Journal for Computation and Mathematics in Electrical and Electronics Engineering*, vol. 32, no. 5, pp. 1484–1498, 2013.

[26] L. Vandevelde, *Magnetische krachtwerking met toepassing op geluid en trillingen in inductiemachines*. PhD thesis, Ghent University, 1997.

[27] L. Vandevelde and J. Melkebeek, "A survey of magnetic force distributions based on different magnetization models and on the virtual work principle," *IEEE Transactions on Magnetics*, vol. 37, no. 5, pp. 3405–3409, 2001.

[28] L. Vandevelde and J. Melkebeek, "Modeling of magnetoelastic material," *IEEE Transactions on Magnetics*, vol. 38, no. 2, pp. 993–996, 2002.

[29] L. Vandevelde and J. Melkebeek, "Magnetic forces and magnetostriction in electrical machines and transformer cores," *IEEE Transactions on Magnetics*, vol. 39, no. 3, pp. 1618–1621, 2003.

[30] L. Vandevelde and J. Melkebeek, "Magnetic forces and magnetostriction in ferromagnetic material," *COMPEL: International Journal for Computation and Mathematics in Electrical and Electronics Engineering*, vol. 20, no. 1, pp. 32–50, 2001.

[31] P. Anderson, A. Moses, and H. Sanbury, "An automated system for the measurement of magnetostriction in electrical steel sheet under applied stress," *Journal of Magnetism and Magnetic Materials*, vol. 215-216, pp. 714–716, 2000.

[32] A. Moses and D. Davies, "Influence of compressive stress on magnetic properties of commercial," *IEEE Transactions on Magnetics*, vol. 16, no. 2, pp. 454–460, 1980.

[33] M. Javorski, J. Slavic, and M. Boltezar, "Frequency characteristics of magnetostriction in electrical steel related to the structural vibrations," *IEEE Transactions on Magnetics*, vol. 48, no. 12, pp. 4727–4734, 2012.

[34] D. Wakabayashi, T. Todaka, and M. Enokizono, "Measurement of three-dimensional magnetostriction on grain-oriented electrical steel sheet," *Journal of Electrical Engineering*, vol. 62, pp. 153–157, 2011.

[35] S. Somkun, A. Moses, P. Anderson, and P. Klimczyk, "Magnetostriction anisotropy and rotational magnetostriction of a nonoriented electrical steel," *IEEE Transactions on Magnetics*, vol. 46, no. 2, pp. 302–305, 2010.

[36] S. Somkun, A. Moses, and P. Anderson, "Measurement and modelling of 2-D magnetostriction of nonoriented electrical steel," *IEEE Transactions on Magnetics*, vol. 48, pp. 711–714, 2012.

[37] K. A. Fonteyn, *Energy-based magneto-mechanical model for electrical steel sheets*. PhD thesis, Alto University, Finland, 2010.

[38] T. Nakata, N. Takahashi, M. Nakano, k. Muramatsu, and M. Miyake, "Magnetostriction measurements with a laser doppler velocimeter," *IEEE Transactions on Magnetics*, vol. 30, no. 6, pp. 4563–4565, 1994.

[39] T. Nakase, M. Nakano, k. , Fujiwara, and N. Takahashi, "Measuring system for magnetostriction of silicon steel sheet under ac excitation using optical methods," *IEEE Transactions on Magnetics*, vol. 34, pp. 2072–2074, 1998.

[40] T. Nakase, M. Nakano, k. Fujiwara, and N. Takahashi, "Single sheet tester having open magnetic path for measurement of magnetostriction of electrical steel sheet," *IEEE Transactions on Magnetics*, vol. 35, no. 5, pp. 3956–3958, 1999.

[41] M. Hirano, Y. Ishihara, k. Harada, and T. Todaka, "A study on measurement of magnetostriction of silicon steel sheet by laser displacement meter," *Journal of Magnetism and Magnetic Materials*, vol. 254-255, pp. 43–46, 2003.

[42] G. Bán and F. Janosi, "Measuring system and evaluation method of dc and ac magnetostriction behaviour to investigate 3.2% Si-Fe GO electrical steels," *Journal of Magnetism and Magnetic Materials*, vol. 160, pp. 167–170, 1996.

[43] IEC Standard Publication TR 62581. "Methods of measurement of the magnetostriction characteristics by means of single sheet and Epstein test specimens". International Electrotechnical Commission, Geneva, Switzerland, 2010.

[44] IEC Standard Publication 60404-3. "Methods of measurement of the magnetic properties of electrical steel sheet and strip by means of a single sheet tester". International Electrotechnical Commission, Geneva, Switzerland, 2000.

[45] Polytec Inc. "Vibration Sensors", Available online: http://www.polytec.com/eu/products/vibration-sensors/.

[46] J. Aerts, *Optical Measurement of the Weak Non-linearity in the Eardrum Vibration Response to Auditory Stimuli*. PhD thesis, Antwerp University, Belgium, 2010.

[47] M. Bauer, F. Ritter, and G. Siegmund, "High-precision laser vibrometers based on digital doppler-signal processing," *Proceedings SPIE*, vol. 4827, pp. 50–61, 2002.

[48] Polytec Inc. "User Manual Laser Vibrometer IVS 200".

[49] S. Gorji Ghalamestani, T. Hilgert, S. Billiet, L. Vandevelde, J. Melkebeek, and J. Dirckx, "Measurement of magnetostriction using dual heterodyne interferometers: experimental challenges and preliminary results," *Optical Measurement Techniques for Systems & Structures*, pp. 171–180, 2009.

[50] S. Gorji Ghalamestani, T. Hilgert, L. Vandevelde, J. Dirckx, and J. Melkebeek, "Magnetostriction measurement by using dual heterodyne interferometers," *IEEE Transactions on Magnetics*, vol. 46, no. 2, pp. 505–508, 2010.

[51] S. Gorji Ghalamestani, L. Vandevelde, J. Dirckx, and J. Melkebeek, "Magnetostriction and the advantages of using noncontact measurements," *AIP conference proceesings*, vol. 1253, pp. 171–175, 2010.

[52] T. Hilgert, L. Vandevelde, and J. Melkebeek, "Magnetostriction measurements on electrical steels by means of strain gauges and numerical applications," *Przeglad Elektrotechniczny*, vol. 2005, no. 5, pp. 87–91, 2005.

[53] M. De Wulf, *Karakterisering en energieverliezen onder unidirectionele magnetisatie in relatie tot de microstructuur van zacht magnetische materialen*. PhD thesis, Ghent University, Belgium, 2002.

[54] S. Gorji Ghalamestani, L. Vandevelde, J. Dirckx, and J. Melkebeek, "Magnetostriction strain measurement: heterodyne laser interferometry versus strain gauge technique," *Optical Measurement Techniques for Systems & Structures*, pp. 167–174, 2013.

[55] T. Hilgert, L. Vandevelde, and J. Melkebeek, "Application of magnetostriction measurements for the computation of deformation in electrical steel," *Journal of Applied Physics*, vol. 97, no. 10, 2005.

[56] N. S. specialist group N-E EMC & Harmonics, "Power quality in European electricity supply networks-2nd edition," *Union of the Electricity Industry EURELECTRIC*, 2003.

[57] A. Kasprzak, M. Orlikowski, and B. D., "Operation of voltage transformer in grids with distorted signals," *Bulletin of the Polish academy of sciences-technical sciences*, vol. 59, no. 4, pp. 551–554, 2011.

[58] P. Anderson, "Measurement of the stress sensitivity of magnetostriction in electrical steels under distorted waveform conditions," *Journal of Magnetism and Magnetic Materials*, vol. 320, no. 20, pp. E583–E588, 2008.

[59] S. Gorji Ghalamestani, L. Vandevelde, J. Dirckx, and J. Melkebeek, "Magnetostriction and the influence of higher harmonics in the magnetic field," *IEEE Transactions on Magnetics*, vol. 48, no. 11, pp. 3981–3984, 2012.

[60] C. Bishop, *Neural networks for pattern recognition*. New York, USA: Oxford University Press, 1995.

[61] D. J. Ewins, *Modal Testing: Theory, Practice and Application*. New York, USA: John Wiley and Sons, 2000.

[62] L. Vandevelde, J. Gyselinck, M. De Wulf, and J. Melkebeek, "Finite element computation of the deformation of ferromagnetic material taking into account magnetic forces and magnetostriction," *IEEE Transactions on Magnetics*, vol. 40, no. 2, pp. 565–568, 2004.

[63] J. John and J. Winders, *Power Transformers Principles and Applications*. New York, USA and Basel, Switzerland: Marcel Dekker Inc., 2002.

[64] A. A. Abdallh, *An Inverse Problem Based Methodology with Uncertainty Analysis for the Identification of Magnetic Material Characteristics of Electromagnetic Devices*. PhD thesis, Ghent University, Belgium, 2012.

[65] Polytec Inc. "PSV-400 Scanning Vibrometer", Available online: http://www.polytec.com/eu/products/vibration-sensors/scanning-vibrometers/psv-400-scanning-vibrometer.